NTNU
Norwegian University of
Science and Technology

Transient Stability in Subsea PMSM with Damper Windings

Using Finite Element Method Simulations to
Identify the dq-circuit Parameters of a PMSM
with a Damper Winding Sleeve

Ole Bjørn Silset Warvik

Master of Energy and Environmental Engineering
Submission date: June 2016
Supervisor: Robert Nilssen, ELKRAFT

Norwegian University of Science and Technology
Department of Electric Power Engineering

Transient Stability in Subsea PMSM with Damper Windings

Ole Bjørn Silset Warvik
Department of Electric Power Engineering
Faculty of Information Technology, Mathematics and Electrical Engineering
Norwegian University of Science and Technology

There is a trend in the petroleum industry to introduce permanent magnet motors for subsea pumping applications. This is done in an effort to reduce costs. These applications require the machine to exert a satisfactory level of open-loop stability as control equipment drive up the costs. The transient behaviour of a special type of damper winding is to be investigated.

The student shall develop a finite element method simulation model, using a suitable software, to simulate the transient behaviour of a permanent magnet motor with a damper winding sleeve. The transient situation to be assessed is an abrupt change in load torque. The student shall assess whether the damper winding has the expected effect on the machines transient stability. A variety of rotor assemblies may be tested.

The student shall develop a comprehensive method for identifying the individual direct-quadrant axis parameters by use of results from finite element simulations.

Supervisor:
Professor Robert K. Nilssen
Norwegian University of Science and Technology

Co-supervisor:
Alexey Matveev
Rolls-Royce Marine AS

Summary:

Today, induction machines dominate the market for electrical machines in industrial pumping applications. This is also the case for subsea pumping applications. Permanent magnet machines are showing great promise for taking over this market, but in order for permanent magnet machines to succeed, their stability during load transients must be greatly improved.

In this project, the aim has been to analyze the behaviour of a Permanent Magnet Synchronous Motor with damper windings during transients. In addition to stability studies, a main topic if interest has been to develop a method to comprehensively determine the individual direct-quadrant axis parameters of the machine.

A particular special case of damper windings, where a metallic sleeve around the rotor does the job of both the damper winding and the magnetic retention sleeve, has been the main topic of investigation. The machine has been tested using three different materials in the damper winding.

To perform these simulations, a Finite Element Method software called Ansys Maxwell has been used.

A method for determining the dq-axis parameters has been developed, results using this method, in combination with the stability studies, suggest there is a direct relationship between the damper winding resistance and the damping abilities of the machine.

Samandrag:

Asynkronmaskiner, også kjent som Induksjonsmaskiner, dominerer marknaden for elektriske maskiner til drift av alle typar pumper i industrien. Dette er også tilfelle for elektriske maskiner tilpassa subseainstallasjonar. Ein annan type maskin som er særs lovande når det gjeld denne typen pumpedrifter, er permanentmagnetmaskinen. For at permanentmagnetmaskinen skal kunne brukast i denne typen installasjonar på havbotnen, må stabiliteten under lasttransientar bli betra kraftig.

I denne oppgåva har målet vore å analysera den transiente oppførselen til ein permanentmagnet-synkronmotor med dempevikling. I tillegg til stabilitetsstudier er hovudfokuset i denne oppgåva lagt til å finne ein pålitelig metode til å rekne ut kvar enkelt av to-akse parameterane til maskina. Dette inkluderer individuelle parameter for dempeviklinga.

Dempeviklinga som skal studerast i denne oppgåva er av ein eksperimentell type som enno ikkje er realisert i full skala. Den eksperimentelle dempeviklinga er ein metallsylinder som omringar rotoren. Maskinen har blitt testa med dempevikling av tre forskjellige metall.

Til å gjere berekningar er det blitt brukt programvare som nytter seg av elementmetoden til å løysa komplekse differensiallikningar. Programvaren som er blitt brukt, heiter Ansys Maxwell.

Ein metode for å finne dei individuelle to-akse parametra til maskinen er utvikla. Resultata frå denne metoden, kombinert med resultata frå stabilitetsstudia, viser at det kan vere ein direkte samanheng mellom motstanden i dempeviklingane og dempeeigenskapane til maskinen.

Transient Stability in Subsea PMSM with Damper Windings

Masters Thesis

—

Ole Bjørn Silset Warvik
Department of Electric Power Engineering
Faculty of Information Technology, Mathematics and Electrical Engineering
Norwegian University of Science and Technology

***Abstract* — Today, induction machines dominate the market for electrical machines in industrial pumping applications. This is also the case for subsea pumping applications. Permanent magnet machines are showing great promise for taking over this market, but in order for permanent magnet machines to succeed, their stability during load transients must be greatly improved. In this project, the aim has been to analyze the behaviour of a Permanent Magnet Synchronous Motor with damper windings during transients. In addition to stability studies, a main topic if interest has been to develop a method to comprehensively determine the individual direct-quadrant axis parameters of the machine. A particular special case of damper windings, where a metallic sleeve around the rotor does the job of both the damper winding and the magnetic retention sleeve, has been the main topic of investigation. The machine has been tested using three different materials in the damper winding. To perform these simulations, a Finite Element Method software called Ansys Maxwell has been used. A method for determining the dq-axis parameters has been developed, results using this method, in combination with the stability studies, suggest there is a direct relationship between the damper winding resistance and the damping abilities of the machine.**

This thesis is a continuation of the author's earlier work "Using Finite Elements Simulations to Determine the Transient Behaviour of a Permanent Magnet Motor with a Damper Winding Sleeve" from December 2015 [1].

I. Introduction and motivation

With recent times development in the prices of oil and gas, and the fact that the easily accessible resources are getting increasingly scarce, reducing the costs of production is increasingly important to the petroleum industry. Perhaps the most important factor for reducing the costs of offshore production is to move production equipment from floating installations to subsea installations placed on the seabed. Examples of such installations can be large pumps, compressors or valves. This would make the petroleum significantly less labour intensive which would enable the industry to turn profits on smaller, deeper and more remote fields. A consequence of these efforts is that large electrical machines must now be supplied via cables of a length of up to 50 km at deep waters from the topside platform. In the industry this is known as a long stepout. Solving the engineering challenges that go with this is an essential prerequisite for the industry to be able to cut costs.

As part of the long stepout, any control cables involved must also be long, leading to a significant time delay of the control signals, this will greatly influence the transient stability of the system at high frequencies. This, in combination with the added cost of installing control equipment at deep waters, means that any synchronous electric machines must exert a satisfactory level of open-loop stability to remain in synchronism during transients such as load fluctuations.

Traditionally the induction machine has been the machine of choice for pumping purposes, indeed for all kinds of industrial motor applications. This has mainly been attributed to their low cost and the fact that induction machines are extremely reliable. The drawbacks of these machines are their low power density and high startup currents. To date, induction machines have also been the machine of choice for subsea pumping applications. Studies show, however, that there is a considerable cost saving potential in moving towards the use of permanent magnet synchronous machines for such applications [2].

During the startup of a subsea pump, the motor has to overcome the mechanical stiction torque in the pump, under these circumstances, the induction machine will draw considerably larger start up currents than the permanent magnet machine will, even in the case of the machine being converter fed. This implies that, for the induction machine, the topside transformers must be over-sized in order to avoid saturation of the transformer core during startup. The permanent magnet machine, with its smaller startup currents, will not require the same level of over-sizing transformers [3].

Transformers are inherently big, heavy and expensive. Deck space and added support structure on a topside platform is also costly, therefore, reducing the size of the transformer offers great cost saving potential both in the topside platform as well as in the transformer itself. Therefore keeping the transformer relatively small would offer great advantages. Hence there is a strong incentive to use permanent magnet machines in such applications.

Over the last few decades, major developments in permanent magnet technology has made the permanent magnet motor a realistic competitor for the induction motor. In the past,

the magnets used in these machines were ferrite magnets, a type of magnets that has been consistently cheap and readily available. The drawbacks of ferrite magnets are their low remanent flux density and the fact that they are quite susceptible to flux weakening. In recent decades, however, the prices of rare earth magnets, such as neodymium ($Nd_3Fe_{14}B$) and samarium-cobalt ($SmCo_5$), has been significantly reduced. The biggest drawbacks of neodymium magnets are that they are more susceptible to flux weakening through heat and relatively poor price stability [4].

The optimal design and sizing of damper windings for synchronous machines is very difficult to determine analytically. As a result of this, the design of the damper windings is oftentimes done by empirical knowledge and by experience. In the existing literature on damper windings in permanent magnet synchronous motors, the emphases has, predominantly, been on direct online start and issues regarding the startup characteristics of the machine [5] [6].

As startup and transient stability are completely different issues, an optimal winding design for startup purposes, will not be optimal for transient stability. Existing literature is largely limited to damper bars. As this thesis will be focusing on combining the damper winding with the magnet retention sleeve, the existing design principles will not be valid. There is therefore a need to investigate this type of damper winding. This investigation shall be done by the use of finite element method software. These types of softwares are commonly used in industry and research and are very powerful tools for solving complex physical models. After several, largely failed, attempts at using Comsol Multiphysics to do the FEM analysis, the software that has been used is Ansys Maxwell 16.0. The reason for using Ansys Maxwell is it's excellent performance at transient analysis. The big drawback with these kinds of software tools is the amount of time it takes to get to know the software, its pitfalls and how to avoid these pitfalls. Other drawbacks are that these softwares take a lot of time to produce a solution, and that the solutions contain large amounts of data. The Maxwell Online Help [7] , and published tutorials [8] have been helpful.

II. Theory

A. Damping in oscillators

If we assume that the rotating body is a rigid body rotating about a set axis, the motion of rotating machinery can, according to [9], be described by the equation

$$T_{el} = T_{mech} + B\omega + J\alpha \tag{1}$$

where

$$\omega = \frac{\partial \theta}{\partial t} \tag{2}$$

and

$$\alpha = \frac{\partial \omega}{\partial t} = \frac{\partial^2 \theta}{\partial t^2} \tag{3}$$

T_{el} is the Electromagnetic torque delivered by the motor, T_{mech} is the load torque, B is the damping of the system, J is the moment of inertia of the system and θ is the angle of the rotor relative to the stator field. This makes ω the rotational velocity of the rotor, and α the rotational acceleration of the rotor.

If the system is undamped, and hence B = 0, equation 1 becomes

$$T_{el} = T_{mech} + J\alpha \tag{4}$$

which, when rearranged, gives

$$\alpha = \frac{T_{el} - T_{mech}}{J} \tag{5}$$

According to [10], moment of inertia is given by the equation

$$J = \int_0^R r^2 \partial m = \int_0^R r^2 m \partial r \tag{6}$$

where r is the radial direction, R is the outer radius ∂m is a small mass element, and ∂r is a small step in radial direction.

Upon inspection of equation (5) it becomes evident that if the mechanical load torque was to change without a change in the torque developed by the machine, the machine would start accelerating. The machine would not stop accelerating before there was a balance between the load torque and the developed torque. Hence if there were any fluctuations in the load torque in the system, the system would change its rotational speed. If not controlled, the system would not be able to return to its nominal rotational speed [11].

Equation (4) is an example of a harmonic oscillator, I.e a system that will never stop oscillating. In reality though, any case of an electric machine will always exert damping properties to some extent. Equations like equation (1) are called damped oscillators. These equations differ from harmonic oscillators in the sense that they include damping. There are three different cases of systems described by these types of equations. The three cases are critically damped systems, underdamped systems and overdamped systems. What differs between the three cases is the magnitude of the damping coefficient. For a critically damped system, the damping coefficient B, is just big enough for the oscillation not to overshoot the zero point. A critically damped system will also reach zero amplitude very quickly. In the case of overdamped systems, B is larger than for the critically damped system, but the system takes longer to reach zero amplitude. If B is smaller than for the critically damped

case, the system is an underdamped system. In the case of an underdamped system the oscillation will overshoot the zero point, and may, depending on the magnitude of B, cross zero amplitude many times before stabilizing at zero amplitude. For a harmonic oscillator, the amplitude of the oscillation would, as one might expect, not abate. Fig. 1 shows the different categories of damping.

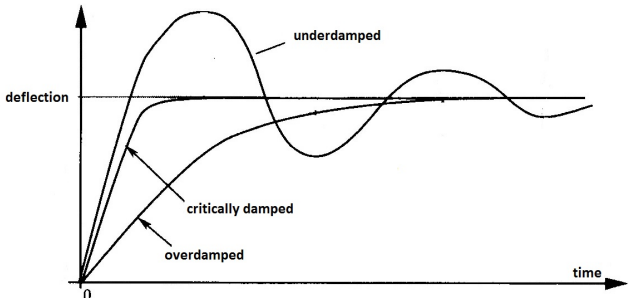

Figure 1. An example of the different cases of damping in a *damped oscillator. A critically damped oscillation, an overdamped oscillation* and an *underdamped* oscillation [12].

It has to be kept in mind that fig. 1 [13] illustrates a special case for a certain value of initial displacement and initial speed. It is, however, a good illustration of the general concepts.

B. Torque production

1) Torque produced by interacting fields

It is now evident that for the permanent magnet machine to remain in synchronism during transients, the machine must have the ability to sufficiently dampen mechanical oscillations during load transients. The question then becomes: How do you introduce this damping? In the case of an electrical machine, the only feasible way of introducing internal damping in the machine itself is to introduce another source of torque in the air-gap of the machine. This can only be done by adding an additional source of magnetic flux to interact with the fields already present in the machine. The way this is done in a permanent magnet machine is to introduce *damper windings*, oftentimes also called *amortisseur windings*. In doing so, what is actually done, is to add parts of the squirrel cage rotor, known from the induction machine, to the rotor of the permanent magnet machine. According to [14], the production of torque in the air-gap of an electrical machine can be described by the equation

$$T_{el} = K\boldsymbol{H_R} \times \boldsymbol{B_S} \tag{7}$$

where K is a machine constant, $\boldsymbol{H_R}$ is the magnetic field from the rotor and $\boldsymbol{B_S}$ is the flux density from the stator. If we assume the magnetic circuit to be linear, the concept of superposition of magnetic fields holds, and we can say that $\boldsymbol{H_R}$ is a superposition of the magnetic field from the permanent magnet and the magnetic field from the damper winding. This assumption does not, strictly speaking, hold, as magnetic circuits in electric machines aren't linear but have hysteresis curves. It does, however, provide a good visualization of the nature of torque production in electric machines with damper windings.

2) Torque production in squirrel cages

Figure 2 shows a typical configuration of a damper winding for a six pole salient pole motor.

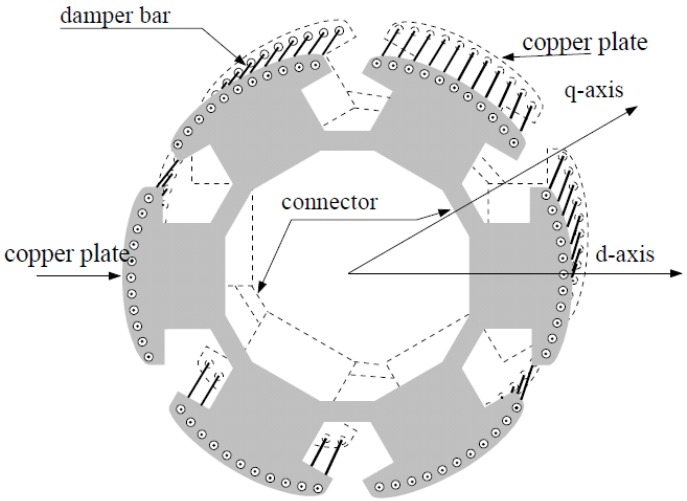

Figure 2. Example of a classical damper winding for a 6 pole salient pole machine [15].

It is clear that the damper shown in fig. 2 greatly resembles a squirrel cage rotor like it is known from the induction machine. In order for a squirrel cage rotor to produce torque, it must be rotating at a speed different from the rotational speed of the applied stator field. The induced voltage in a single closed loop is described by Faraday and Lenz's law, given in [14] by the equation

$$e_{ind} = -\frac{\partial \Phi}{\partial t} \tag{8}$$

where Φ is the flux flowing through the closed loop. Hence, the induced voltage in a closed loop is proportional to the rate of change of the flux flowing through the loop. The induced voltage leads to a current flowing in the loop. Which, in turn, produces a magnetic field. The field production can be described by Amperes law [16]

$$\oint_C \boldsymbol{B}\partial\boldsymbol{l} = \mu_0 \iint_S \boldsymbol{J} \cdot \partial\boldsymbol{S} = \mu_0 I_{enc} \tag{9}$$

where C is the closed loop, $\boldsymbol{B}$ is flux density, $\partial\boldsymbol{l}$ is a

small section of the closed loop. μ_0 is the permeability of vacuum, S is the area enclosed by the closed loop C, $\boldsymbol{J}$ is current density, $\partial \boldsymbol{S}$ is a small section of the area S and I_{enc} is the current in the enclosing loop.

To understand this, the concept of machine slip must be understood. According to [14] slip is given by

$$s = \frac{n_s - n_m}{n_s} \tag{10}$$

where n_m is the mechanical rotational speed of the rotor and n_s is the rotational speed of the stator field. Slip is simply a per unit measure of the lag in the rotors rotation with respect to the stator field.

Since, at synchronous speed, the stator field and the rotor is rotating at the same rate, equation (8) gives $e_{ind} = 0$ since $\frac{\partial \Phi}{\partial t} = 0$. This means no induced voltage in the squirrel cage. From this we can clearly see that without the machine operating at a slip, the squirrel cage winding cannot produce a magnetic field, and hence will not contribute to torque production in the machine.

From equation (10) we can see that if $0 < n_m < n_s$, the slip will be a positive number between 0 and 1, and hence $\frac{\partial \Phi}{\partial t}$ will be positive. As a result of this the induced currents in the squirrel cage will make a positive contribution to torque production through the direction of the magnetic flux they set up. In the same way if $n_s < n_m < 2n_s$ the slip will take a negative value between 0 and -1, this means that $\frac{\partial \Phi}{\partial t}$ is negative. This means that the induced currents in the squirrel cage will make a negative contribution to torque production through the direction of the magnetic flux they set up. This means that the squirrel cage will always give a torque contribution that pulls the rotational speed of the rotor towards the speed of the stator field. In short, the squirrel cage always pushes the machine towards synchronous speed. It must be mentioned that a synchronous machine rotor will also, to some extent, act like a squirrel cage winding, as there will be induced currents in the rotor steel and particularly in the permanent magnets. In reality however, this effect is not enough to provide the damping needed to dampen the oscillations and to force the machine to reach synchronous speed as quickly as required.

The fact that the squirrel cage pushes towards zero slip is the reason why its qualities are sought after in synchronous machines, as it provides the damping qualities needed for the machine to reach stability quickly. A synchronous machine is not a self starting machine, and therefore it will not be able to start when directly connected to 50 Hz. A well designed synchronous machine with damper windings on the other hand, will be able to perform a direct online start, this is another advantage of using damper windings. Although a damper winding optimized for transient stability will help during a direct online startup procedure, damper windings optimized for startup and for transient stability will have significantly different designs. Direct online startup characteristics will not be topic of discussion in this thesis as the machine being discussed is to be converter fed.

The damper winding assessed in this thesis is a special design that is not yet, to the best of the authors knowledge, in use in a commercial machine. The winding is a sheet of copper that has been rolled onto the rotor, making a sleeve to go over the surface mounted permanent magnets. The winding also doubles as a retention sleeve to protect the permanent magnets form mechanical stress at high speeds.

C. Magnetic reluctance and inductance

The magnetic reluctance $\mathscr{R}$ of an object as described by [17] is given by the equation

$$\mathscr{R} = \frac{l}{\mu_r \cdot A} \tag{11}$$

where l is the length, μ_r is the relative permeability and A is the cross sectional area. It can then be shown [18] that inductance has the following relation with reluctance

$$L \propto \frac{1}{\mathscr{R}} \tag{12}$$

which implies that a large reluctance will lead to a low inductance and vice versa.

D. The direct-quadrant reference frame

In order to effectively control electrical machines, the rotating two-axis direct-quadrant reference frame, often denoted dq-reference frame, is often applied. This machine will also be under a control regime that applies the dq-reference frame. Being able to comprehensively determine the machine's parameters is therefore essential in the design process of this, as any electrical machine.

The dq-reference is an electrically orthogonal frame of reference that, rather than referring to the classical three axis interpretation of a three phase system, transposes the excitations and circuit parameters to an equivalent two axis system which rotates with the rotor of the machine. The transformations presented here are valid for currents, voltages and flux linkages. The transform presented here is the power invariant transform.

To understand this, we first transform the three phase abc system to a two phase $\alpha\beta$ reference frame where the α axis is aligned with the a phase and the β axis is positioned 90° ahead of the α axis. See fig. 3. To perform this transformation, the Clarke transform is applied. According

to [19] this transform can be written as

$$\begin{bmatrix} f_\alpha \\ f_\beta \end{bmatrix} = \sqrt{\frac{2}{3}} \begin{bmatrix} 1 & -\frac{1}{2} & -\frac{1}{2} \\ 0 & \frac{\sqrt{3}}{2} & -\frac{\sqrt{3}}{2} \end{bmatrix} \begin{bmatrix} f_a \\ f_b \\ f_c \end{bmatrix} = T_{abc\to\alpha\beta} \begin{bmatrix} f_a \\ f_b \\ f_c \end{bmatrix} \quad (13)$$

This can also quite easily be derived by simple use of trigonometry and the assumption that the system is balanced. To go back to the three phase system one can apply the inverse Clarke transform, given by

$$\begin{bmatrix} f_a \\ f_b \\ f_c \end{bmatrix} = \sqrt{\frac{2}{3}} \begin{bmatrix} \frac{2}{3} & 0 \\ -\frac{1}{3} & -\frac{\sqrt{3}}{3} \\ -\frac{1}{3} & -\frac{\sqrt{3}}{3} \end{bmatrix} \begin{bmatrix} f_\alpha \\ f_\beta \end{bmatrix} = T^{-1}_{abc\to\alpha\beta} \begin{bmatrix} f_\alpha \\ f_\beta \end{bmatrix} \quad (14)$$

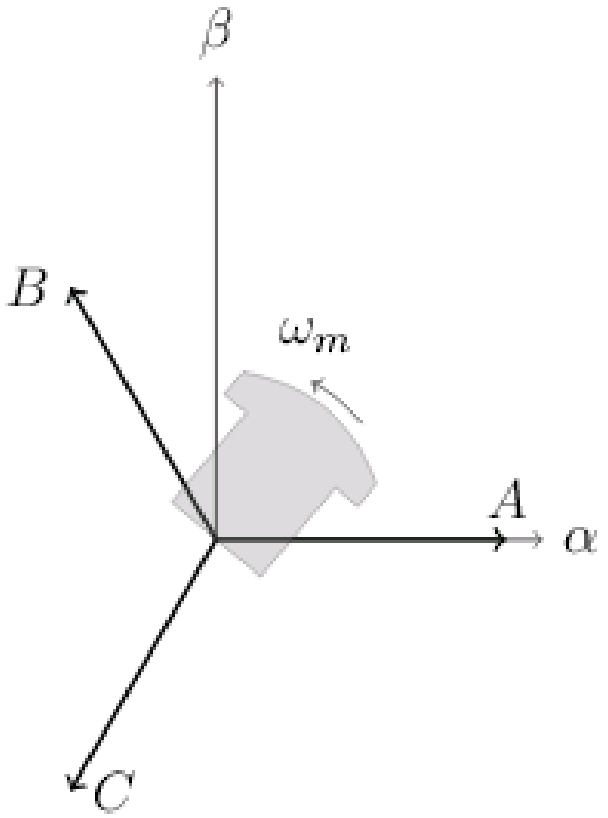

Figure 3. Visualization of the transformation from three phase abc reference frame to two phase $\alpha\beta$ reference frame [20].

We now have a two axis stationary reference frame, however, we still have a situation where the inductances are dependent on the rotor position. Therefore we want to transform the system into the dq frame of reference, where the reference frame rotates with the rotor. This can be done by applying the Park transform given in [19] by

$$\begin{bmatrix} f_d \\ f_q \end{bmatrix} = \begin{bmatrix} cos\,(\theta) & sin\,(\theta) \\ -sin\,(\theta) & cos\,(\theta) \end{bmatrix} \begin{bmatrix} f_\alpha \\ f_\beta \end{bmatrix} = T_{\alpha\beta\to dq} \begin{bmatrix} f_\alpha \\ f_\beta \end{bmatrix} \quad (15)$$

where the angle θ is the angle between the three phase a-axis and the north pole axis of the rotor. As for the former transformation, deriving this is a quite straightforward exercise when simple trigonometry is applied. To go back to the $\alpha\beta$ reference frame, we can use inverse Park transform

$$\begin{bmatrix} f_\alpha \\ f_\beta \end{bmatrix} = \begin{bmatrix} cos\,(\theta) & -sin\,(\theta) \\ sin\,(\theta) & cos\,(\theta) \end{bmatrix} \begin{bmatrix} f_d \\ f_q \end{bmatrix} = T^{-1}_{\alpha\beta\to dq} \begin{bmatrix} f_d \\ f_q \end{bmatrix} \quad (16)$$

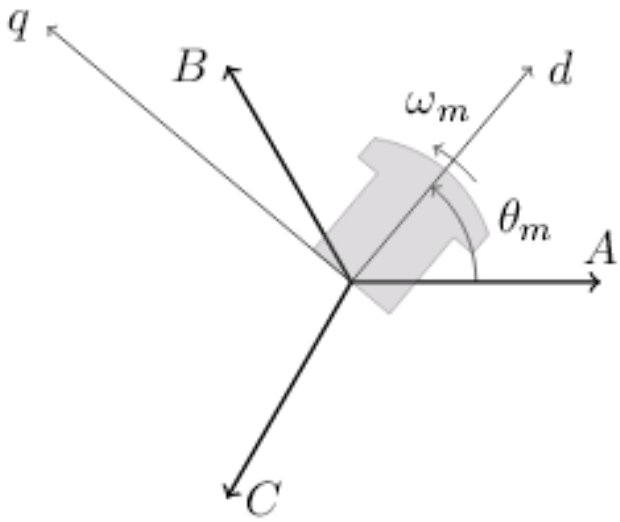

Figure 4. Visualization of the transformation from dq reference frame to two phase $\alpha\beta$ reference frame. [20].

Combining these transformations, we arrive at the direct transform from three phase to rotating, as described in [21], two phase given by

$$\begin{bmatrix} f_d \\ f_q \end{bmatrix} = T_{dq} \begin{bmatrix} f_a \\ f_b \\ f_c \end{bmatrix} \quad (17)$$

where

$$T_{dq} = \sqrt{\frac{2}{3}} \begin{bmatrix} cos\,(\theta) & cos\left(\theta - \frac{2\pi}{3}\right) & cos\left(\theta + \frac{2\pi}{3}\right) \\ -sin\,(\theta) & -sin\left(\theta - \frac{2\pi}{3}\right) & -sin\left(\theta + \frac{2\pi}{3}\right) \end{bmatrix} \quad (18)$$

Correspondingly, the inverse equation becomes

$$\begin{bmatrix} f_a \\ f_b \\ f_c \end{bmatrix} = T^{-1}_{dq} \begin{bmatrix} f_d \\ f_q \end{bmatrix} \quad (19)$$

where

$$T^{-1}_{dq} = \sqrt{\frac{2}{3}} \begin{bmatrix} cos\,(\theta) & -sin\,(\theta) \\ cos\left(\theta - \frac{2\pi}{3}\right) & sin\left(\theta - \frac{2\pi}{3}\right) \\ cos\left(\theta + \frac{2\pi}{3}\right) & -sin\left(\theta + \frac{2\pi}{3}\right) \end{bmatrix} \quad (20)$$

The greatest advantage of applying the dq-reference frame is the fact that, at steady state, we avoid the problem of inductances being position dependent and therefore time dependent. This makes it relatively straightforward to make equivalent circuits. The reason why they become position dependent is to be explained later on. Since the frame of reference itself rotates at synchronous speed, the currents and voltages in the dq axis will, at steady state, be perceived

as DC currents and voltages. It is here assumed that all currents, voltages and flux linkages are sinusoidal, including the air-gap MMF wave. An important observation that arises from the two axis theory is that when operating at nominal load, all flux will flow along the rotors quadrature axis, but when operating at no load, the flux is flowing along the machines direct axis, this means that when going from a steady state at no load to full load, or vice versa, the angle between the direct axis and the stator field δ, also known as the torque angle, must change by $90°$. The interested reader is urged to consult [22].

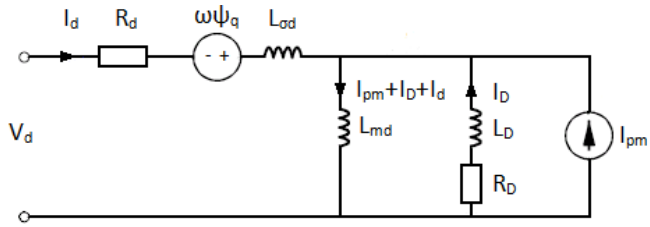

Figure 5. Direct axis equivalent circuit.

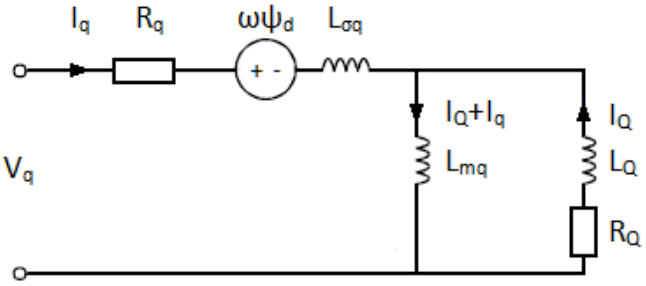

Figure 6. Quadrature axis equivalent circuit.

Figures 5 and 6 show equivalent circuits for the direct and quadrature axis respectively. As we can see, they greatly resemble the equivalent circuits for an induction machine.R_D, R_Q, L_D and L_Q are the damper winding parameters, L_{md} and L_{mq} are the magnetizing inductances, R_d and R_q are the stator resistances, $L_{\sigma d}$ and $L_{\sigma q}$ are the stator leakage inductances, and i_{pm} is a current equivalent of the permanent magnets. Due to symmetry, we can say $R_{sd} = R_{sq}, L_D = L_Q, R_D = R_Q, L_{md} = L_{mq}, L_{\sigma d} = L_{\sigma q}$. The $\omega\psi$ terms represent induced voltages due to flux linkage from the other axis, and the constant current i_{pm} represents the constant flux from the permanent magnet.

E. Rotor configurations

There are two basic types of rotors used in synchronous machines. Salient pole machines and non-salient pole machines [23]. From fig. 7 we can clearly see that for the salient pole machine, the reluctance in the quadrature axis is greater than the reluctance in the direct axis as the quadrature axis air-gap is longer. As a result the direct axis inductance is greater than that of the quadrature axis. This is not the case for the non-salient pole machine which has an even air-gap along the circumference of the rotor, notwithstanding the effect of the stator slots. This imbalance in direct and quadrature axis inductances fundamentally changes the control of the machine. The machine discussed in this thesis has a non-salient rotor configuration.

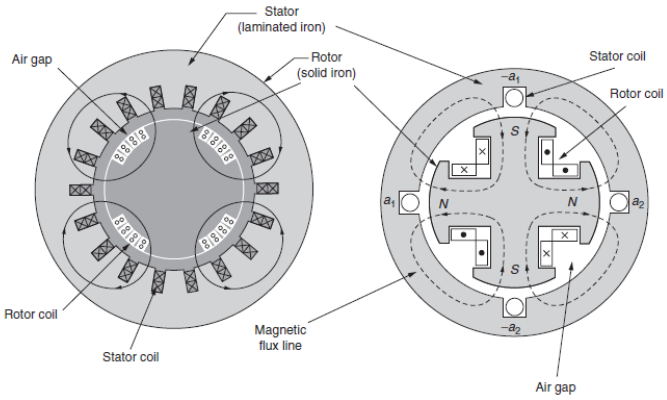

Figure 7. A non-salient pole machine and a salient pole machine [23].

There are several ways of placing the magnets in the rotor. Therefore the placement of the permanent magnets is also an important design aspect. The different ways of placing the magnets can be summed up in three categories:

- Surface mounted permanent magnets
- Inserted permanent magnets
- Interior permanent magnets

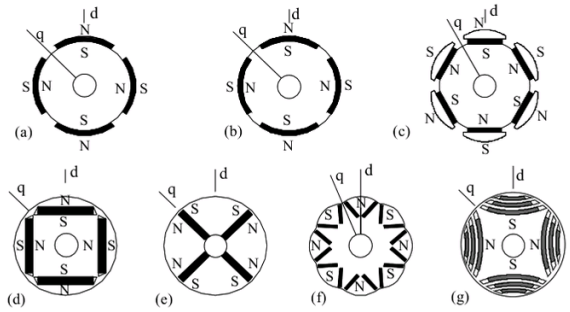

Figure 8. Examples of different rotor configurations in permanent magnet machines. a) shows an example surface mounted pm b) shows an example of inserted pm, c) d) e) f) and g) show various examples of interior pm [20].

For surface mounted permanent magnets, the magnets are mounted on the surface of the rotor. The advantage of doing so is that the inductances along the direct and quadrant axis take the same value since magnetic materials and air have very similar reluctances. This simplifies the control of the machine. The major drawback is the fact that the magnets are more exposed to high mechanical stress when rotating at a high speed and an increase of the air-gap length. These machines need a protective sleeve around the rotor in order

to withstand the mechanical stresses. The three categories of magnet placement are illustrated in fig. 8.

Inserted permanent magnets are quite similar to surface mounted. The difference being that the magnets are now placed in slots on the surface of the rotor. The major advantage is added mechanical strength while the biggest drawback is different inductances along the direct and quadrature axis, complicating the control of the machine. For interior permanent magnets, the magnets are completely buried in the rotor, resulting in great mechanical strength. The major drawback is, again, the difference in direct and quadrature axis inductances.

Another way of categorizing a permanent magnet material is by the direction in which it is magnetized. By far the most common of the two is called radial magnetization, where magnetic flux flows through the magnet in a radial direction in relation to the axis of the machine. The advantage of this method is that you can use cheap segmented magnets to make up your rotor, while the drawback is that it tends to give a very square shaped flux in the air-gap, which in turn will lead to overharmonic contents in the MMF wave. The other way is called linear or diametrical magnetization, where the the flux lines through the magnets are unidirectional. The advantage of this method is that it gives a far more sinusoidal shaped flux in the air-gap. The major drawback is the cost.

F. Cogging

Cogging is a parasitic torque component that arises from the fact that a slotted stator will have a varying reluctance as seen by an observer rotating along the rotor axis.

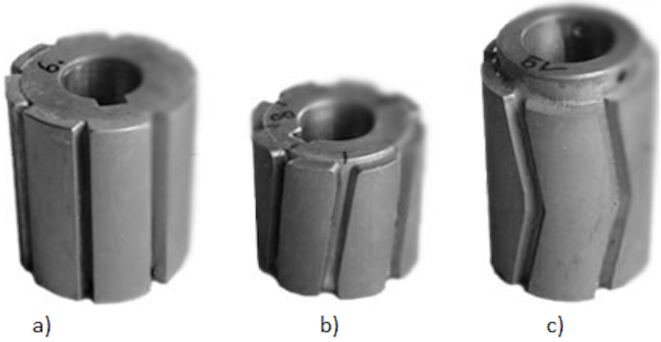

Figure 9. Different types of skewing. a) No skewing b) Unidirectional skew c) V skew [24].

This, in combination with a permanent magnet rotors, means that the rotor will feel a torque towards the position where the resulting reluctance is the lowest. This leads to losses and vibrations, which again leads to noise. These vibrations can in many cases be severe. There are many ways of reducing cogging, many of which are discussed in [25].

One of the most effective ways of reducing cogging is called skewing. By skewing, you reduce the cogging effect by turning the pole face of the rotor or the slots of the stator along the machines axis. The most common way of skewing is skewing the rotor. Examples of skewed rotors are shown in fig. 9.

G. Eddy currents

Eddy currents are parasitic currents that circulate in conducting materials within which time varying magnetic flux flows. This can be explained by inspection of equation (8). As flux varies, $\frac{\partial \Phi}{\partial t} > 0$, and a negative voltage is induced. The induced voltage sets up a current in the material that counteracts the change in magnetic flux. These induced currents are called eddy currents, and intrinsically lead to losses in the machine.

H. Laminations and stacking factor

A material is laminated when the material in question is stacked in layers with another material or materials in between the layers. The reason for doing this in the iron cores in an electrical machine is to prevent circulating eddy currents in the material. These eddy currents lead to losses and heat production, and must be prevented. The stacking factor k_s is defined by

$$k_s = \frac{\sum_{i=1}^{n} l_i}{l_{tot}} \tag{21}$$

where l_i is the length of the i^{th} lamination, n is the number of laminations and l_{tot} is the length of the material

I. Windings, winding factors and layout

The number of slots per pole per phase, often denoted as q, is a key figure for the design of an electric machine [17], and is given by the equation

$$q = \frac{S}{P \cdot Ph} \tag{22}$$

where S is the number of slots in the stator, P is the number of poles and Ph is the number of phases. In this machine $S = 24$, $P = 2$ and $Ph = 3$. When inserted into (22) This gives $q = 4$.

By [20] the winding factor in a machine is defined as

$$k_w = k_d k_p \tag{23}$$

where k_d is known as the distribution factor, and k_p is the pitch factor. In some versions of this equation a skewing factor k_s is also used to account for rotor skew. This is not included here, as this factor is less used and would equal 1

in this case as there is no skew. The distribution factor arises from the fact that there is a phase angle between the voltages induced in the coils of a spatially distributed winding, hence the resultant voltage does not reach the voltage amplitude it would have if the winding was concentrated. The pitch factor derived in [26] is given by

$$k_p = cos\left(\frac{\gamma}{2}\right) \tag{24}$$

where γ is the shortpitch angle. The winding factor of the fundamental is given by [20] as

$$k_{d1} = \frac{\text{geometric sum}}{\text{arithmetic sum}} = \frac{U_1}{qU_{v1}} \tag{25}$$

where U_1 is the resultant voltage and U_{v1} is the voltage induced in coil. In [26] it is derived that the distribution factor is

$$k_{d1} = \frac{sin\left(\frac{q\alpha_u}{2}\right)}{qsin\left(\frac{\alpha_u}{2}\right)} \tag{26}$$

where α is the angle between two adjacent slots. It is also derived that the winding factor of the fundamental harmonic is given by

$$k_w = cos\left(\frac{\gamma}{2}\right)\frac{sin\left(\frac{q\alpha_u}{2}\right)}{qsin\left(\frac{\alpha_u}{2}\right)} \tag{27}$$

and that the winding factor for the h^{th} harmonic is described by

$$k_{wh} = cos\left(\frac{h\gamma}{2}\right)\frac{sin\left(\frac{hq\alpha_u}{2}\right)}{qsin\left(\frac{h\alpha_u}{2}\right)} \tag{28}$$

J. Pole slipping

When a machine experiences an extreme transient, the torque required to keep the machine running normally could be higher than the torque the machine is able to produce. In such cases, the magnetic coupling between the rotor and the stator field will slip. This phenomenon is called pole slipping. Frequently a pole slip will lead to a collapse in torque production and loss of synchronism.

III. FEM MODEL AND MACHINE DESIGN

As mentioned earlier, the method used for attaining the field solutions for this machine is the Finite Element Method or in short FEM.

A. Finite Element Method and its implications on machine design

In many cases in engineering, it is difficult to find an accurate analytic solution to the problem at hand. The behaviour of electromagnetic fields in electrical machines, the flow of fluids in pipes and deformation of mechanical structures, are good examples of engineering applications where attaining analytic solutions is not only very laborious, but in many cases an impossible undertaking. Therefore it is oftentimes better, provided the error of the solution is acceptable and controllable, to find approximate solutions using well established numerical methods. This is the core of FEM analysis. Modern FEM analysis software can provide solutions for complex geometries with great precision. In FEM software, complex geometries are divided into smaller subsections. On the outer boundaries of these subsections, nodes are defined. The subsections are then put back together to form the original geometry by connecting the nodes of adjacent subsections. By doing this, a grid of nodes in space is created, for which very accurate numerical solutions are found. The solutions for parts of the geometry in between nodes are then found by means of linear interpolation.

It is now clear that the accuracy of the model is highly dependent on the number of subsections and nodes. In FEM tools this grid of nodes is known as the mesh. The finer the mesh, or higher the number of nodes, the higher the degrees of freedom in the model, and hence higher the number of calculations the software has to perform. This means that for a fine mesh, the software must perform a higher number of calculations. In addition to this the time steps and the simulation period also contributes to increasing the number of calculations necessary to solve the model. This is the fundamental drawback with using FEM tools, the higher the accuracy, the more demanding the computational requirements. Because of this, and he fact that transient analysis is needed, the machine in this project has been modelled in two dimensions only. To perform the simulations, a well known software named Ansys Maxwell has been used. In Ansys Maxwell, the a numerical method called Backward Euler is used. The interested reader is urged to consult [27].

B. General machine design

The machine being investigated is a permanent magnet machine designed for a motor application. The motor is fitted with an experimental damper winding design which is the main topic of investigation in this thesis. The design of the rest of the machine has therefore been carried out following simple design principles. The machine is a three-phase, two pole machine with 24 stator slots. The permanent magnets are non-segmented, radially magnetized and mounted on the surface of a non-salient rotor. The phase windings are double layer full pitch windings. If we insert the machines parameters into equation (27), we get $q = 4$. Table I shows data for the machine.

Table I
Machine data

Rated power	1.13 MW
Rated torque	3600 Nm
Rated current	227 A
Rated speed	3000 rpm
Frequency	50 Hz
Rated voltage	3.3 kV
Poles	2
Axial length	1 m

C. Winding design

The winding design parameters for the machine are given in Table II.

Table II
Design parameters

Parameter	Symbol	Value
Slot angle	α_u	15°
Pole pitch	ζ	180°
Pitch angle	β	180°
Shortpitch angle	γ	0°
Slots	s	24
Phases	ph	3
Poles	p	2
Slots pr pole and phase	q	4

With the parameters from the machine in question is inserted, we get from equation (26)

$$k_{d1} \simeq 0.9577 \tag{29}$$

From equation (24) we get

$$k_p = 1 \tag{30}$$

From equation (27) we then get

$$k_w \simeq 0.9577 \tag{31}$$

This winding layout yields voltage phasors as shown in fig. 11. As fig. 11 shows, there is not a big difference in the resultant phase voltages and the arithmetic sum of the individual voltage phasors, as illustrated by the winding factor. The windings are modelled with an end winding resistance $R_{EW} = 10m\Omega$ and an end winding inductance $L_{EW} = 10mH$ Fig. 10 shows how the windings are laid out and connected.

Slot #	1	2	3	4	5	6	7	8	9	10	11	12	13	14	15	16	17	18	19	20	21	22	23	24
Phase R	R	R	R	R									-R	-R	-R	-R								
Phase S									S	S	S	S									-S	-S	-S	-S
Phase T					-T	-T	-T	-T									T	T	T	T				
RST	R	R	R	R	-T	-T	-T	-T	S	S	S	S	-R	-R	-R	-R	T	T	T	T	-S	-S	-S	-S
Bottom	R	R	R	R	-T	-T	-T	-T	S	S	S	S	-R	-R	-R	-R	T	T	T	T	-S	-S	-S	-S
SingleP																								

Figure 10. Layout of the windings in the machine [28].

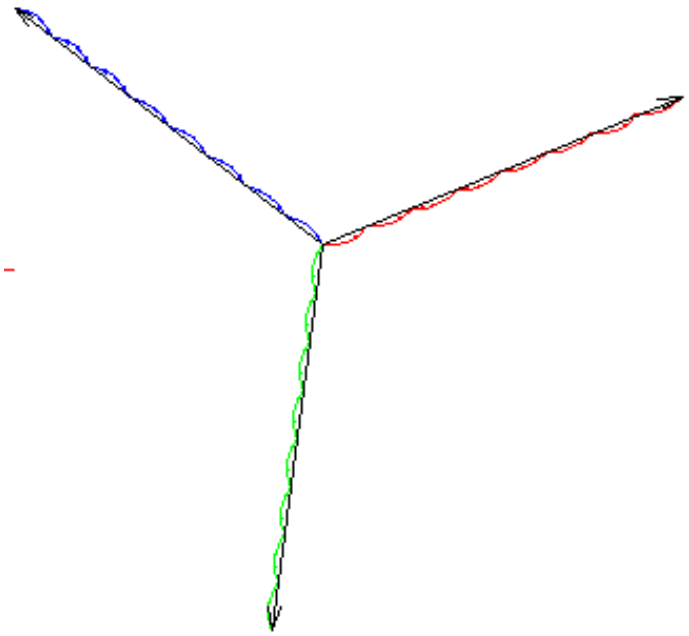

Figure 11. Resultant phase voltages in the stator [28].

D. Air-gap harmonics

The windings in this machine are made to be as simple as possible using full pitch windings, hence they are not in any way optimized to eliminate harmonics in the air-gap. The Fourier frequency spectrum of the lowest harmonics in the air-gap of the machine is shown in fig. 12.

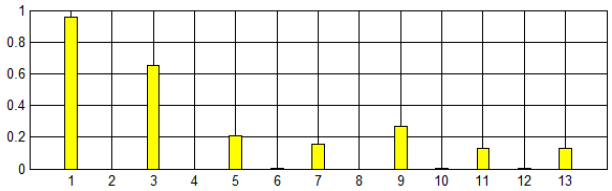

Figure 12. The harmonic content in the air-gap of the investigated machine [28].

As we can see, the 3^{rd} and 9^{th} harmonic are both quite prominent. If a winding with a short-pitch of 3 slots, corresponding to an angle of $45°$ was used, we would get the Fourier frequency spectrum shown in fig. 13.

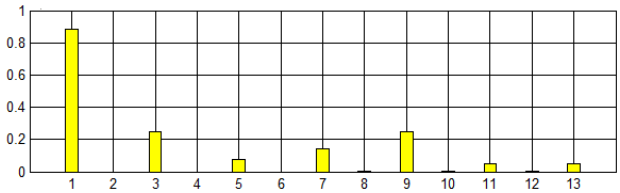

Figure 13. The harmonic content if the windings were short-pitched by $45°$ [28].

As we can see, the air-gap harmonics are lower in this case. We can also see that, as equation (27) suggests, the

fundamental harmonic has been reduced. Figures 14 and 15 show harmonics in magnetomotive force, MMF, in the air-gap of the machine model per phase and line respectively.

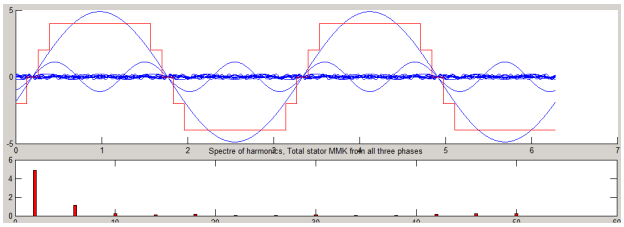

Figure 14. The harmonic MMF content in a phase in the machine [28].

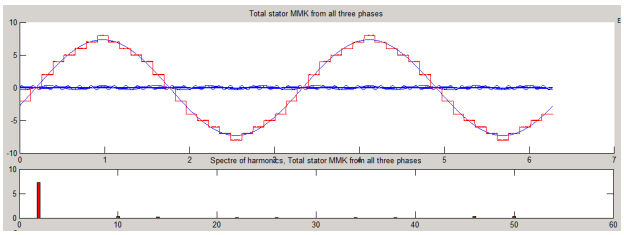

Figure 15. The harmonic MMF content in a line in the machine [28].

E. Rotor design

Figure 16 shows a quarter of the rotor design. The radius of the rotor assembly is 298mm. The shaft, shown in dark grey, is modelled as vacuum as the flux passing through it is negligible. The radius of the shaft, which is modelled as vacuum, is 150 mm. The rotor core is shown in light blue and is modelled as $D24-50$. $D24-50$ is a type of electrical steel with a hysteresis curve as shown in fig. 18. The rotor core has a thickness of 133 mm. The rotor has been modelled with laminations and has a stacking factor of 0.95. The permanent magnet, in dark grey, is modelled as a radially magnetized $NdFe_{35}$, which is a rare earth neodymium material.

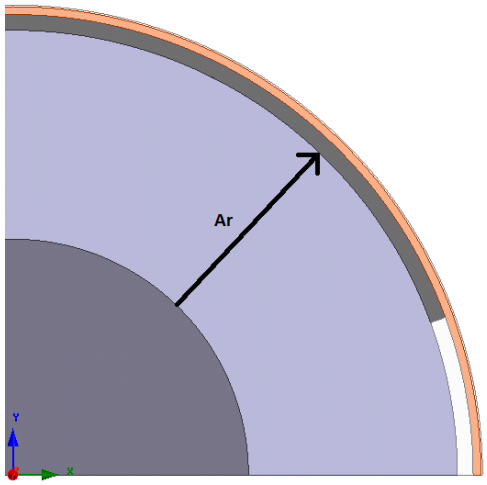

Figure 16. A quarter of the rotor design.

The magnet thickness is 10 mm, and sets up a field with a peak of about 0.42 T in the air-gap when stationary. The outer ring in orange is the damper winding, which is the main object of interest in this project. The damper has a thickness of 5 mm. The air-gap is 2 mm. One of the material used in the damper winding is a modified version of the standard copper material from the Ansys Maxwell library, the material has been modified in such a way that the conductivity has been reduced by half. This in order to increase the copper losses in the damper winding. This point is further discussed in appendix A. The other two damper winding materials investigated are aluminium and brass.

F. Stator design

Figure 17 shows a quarter of the stator design. The air-gap radius of the machine is 299mm. The outer radius of the machine is 560 mm. The outer diameter is determined by the design parameters As from figure 17 and Ar from figure 16, the criteria being that the distance As is equal to Ar in order to avoid saturation. Like the rotor, the stator core is modelled as $D24-50$. The slots are 126 mm deep and 40 mm wide. The machine has an unrealistically high fill factor, again because this is not the emphasis of this thesis. The stator has not been modelled with laminations, meaning eddy currents are likely to occur if eddy effects are included for the stator.

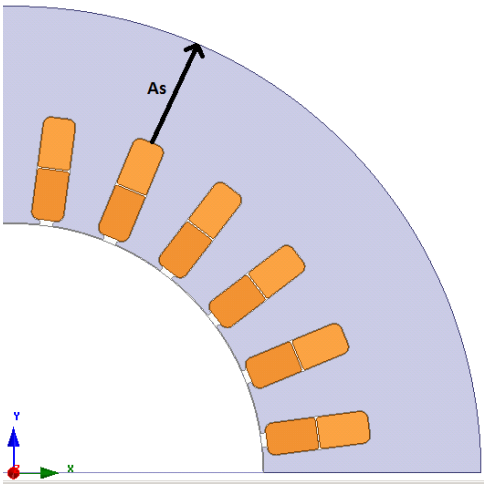

Figure 17. A quarter of the stator design.

As we can see from fig. 18, the material is fairly linear up to a flux density of 1.2 T. The remaining materials all have linear BH curves, meaning they are not subject to any magnetic saturation. The model depth is set to 1 m.

As any physical object, the rotor of the machine has a *Moment of inertia*, denoted as J. Moment of inertia is an objects resistance to change in rotational velocity. Using equation (6) and superposition the rotor of this machine has a moment of inertia becomes $J = 94.83\ kgm^2$. In simulations the moment of inertia is rounded to $J = 95\ kgm^2$.

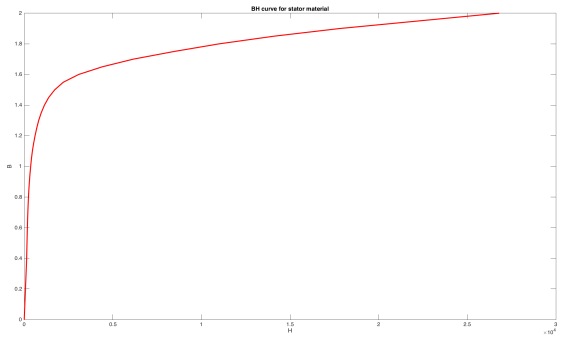

Figure 18. BH curve for the stator and rotor material.

As we can clearly see from equation (1), the inertia is a key element in the transient behavior of the machine. It must be pointed out that a weakness in this model is that only the inertia of the machines rotor itself has been taken into account. In reality, the pump or compressor that the motor is driving will also contribute to the total rotational inertia of the system. The reason why this is not included in the model is that the pump data is unknown. The consequence of this will be that the machine in this model will accelerate more quickly than the machine would do in reality. Therefore the case studied here can be viewed as a worst case scenario in terms of speed fluctuations.

G. Model settings

In order to simplify the model, the model has been reduced by half. Thus only one pole and one side of the windings of the machine is being simulated, the solution for the rest of the machine is then assumed to be symmetrical to the solution in the part that is solved. In Ansys Maxwell this is done by using so called *master* and *slave* boundaries where the boundary condition is $B_{slave} = -B_{master}$. Flux densities across the boundaries are shown in fig. 19 and fig. 20 respectively. This model reduction has proven effective in reducing simulation time.

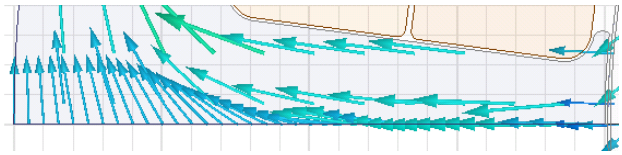

Figure 19. Flux density on master boundary.

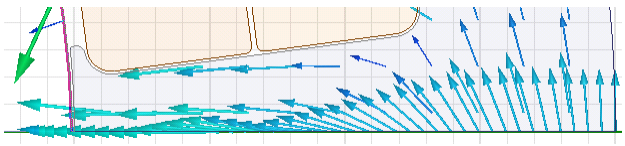

Figure 20. Flux density on the slave boundary.

The mesh that has been used in this model is shown in fig. 21 and fig. 22. There has been a lot of issues building the meshes in this model, as the Ansys Maxwell meshing tool has proved very unstable. Attempts were made to use another meshing method more suitable for curved geometries, but these attempts failed as the meshing tool crashed. Therefore this mesh has been used. The mesh is dense in the region around the air-gap, but rather sparse in the rotor core. This can potentially be a source of inaccuracy. In total the mesh consists of 43327 elements, among which 11704 elements in the air-gap and winding insulation. The number of elements in the damper winding is 1313. For the stability studies, time steps of 0.5 ms have been used, while for the parameter tests, time steps equal to 40 steps per period have been used. These time steps are very fine, and should not reduce the accuracy of the model.

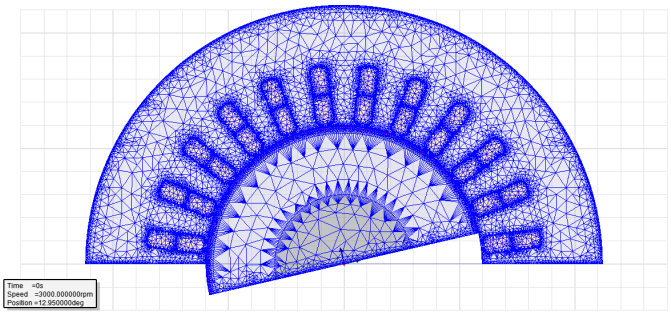

Figure 21. An overview of the mesh in the machine.

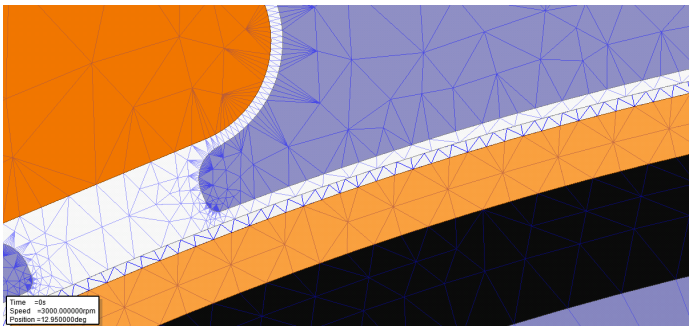

Figure 22. Closeup of the mesh in the air-gap and damper winding of the machine.

IV. Stability analysis of the machine

In all test cases it has been assumed that the machine is fed from a stiff grid, meaning the applied voltages are not depending on what is happening in the machine. The applied voltages are equal in each stability test, and are shown in fig. 23. In order to test the machine's ability to remain synchronism, the machine model must undergo a series of tests where the machine is tested under extreme circumstances. The presented machine is tested using several different materials in the damper winding.

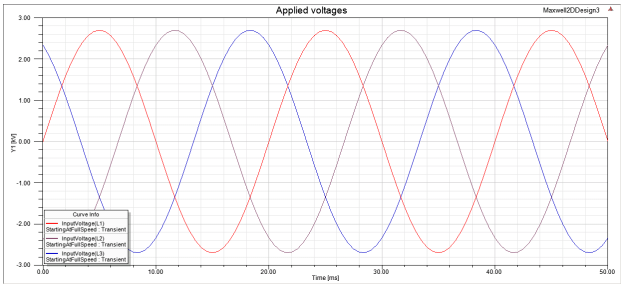

Figure 23. The phase voltages applied in all stability test cases.

A. Test scenario

In this test the machine undergoes abrupt changes in load, since it is also important to establish the machine's behaviour for a sudden rise back up to nominal torque. The test procedure goes as follows:

Table III Torque pulsations test	
Time $[s]$	Load torque $[Nm]$
0 - 1	3600
1 - 3	0
3 - 5	3600

This test represents a worst case scenario both in terms of abrupt loss of load and abrupt rise in load, and will show whether or not the machine is able to remain in synchronism in extreme conditions.

As we know from synchronous machine theory [21] when the load changes, the internal torque angle δ, which represents the angle between the rotors direct axis and the rotating stator field, must also change given that there is no advanced control mechanism in place. This means that when a change in load occurs, it is inevitable that there must be a temporary change in relative speed between the rotor and stator field. This temporary change in relative speed will be observed by a speed transient, the amplitude, frequency and duration of which is determined by equation (1), and therefore by the machine's damping qualities.

B. Testing for different materials

1) Case A: Only permanent magnets provide damping

In this case, the damper winding has been disabled, and all damping torque will be produced by induced currents in the machines permanent magnets. This case is included mostly to provide reference, and it is expected that this will not provide enough damping during extreme transients.

2) Case B: Damper sleeve made of reduced copper

In this case, the damper winding is made from a modified copper material, where the conductivity is set to half of its nominal value. Earlier studies suggest that this gives better damping qualities than a normal copper material does.

3) Case C: Damper sleeve made of aluminium

Aluminium damper windings have been used successfully before, particularly in axial flux machines [20]. Therefore is it of interest to test this material.

4) Case D: Damper sleeve made of brass

Damper windings are often made from brass, partly because its higher resistivity gives a higher starting torque.

Table IV Damper winding materials summary	
Case	Damper winding materials
Case A	Only permanent magnets
Case B	Reduced copper
Case C	Aluminium
Case D	Brass

Table IV Material properties	
Material	Conductivity $[M\frac{S}{m}]$
PM	0.625
Reduced copper	29
Aluminium	38
Brass	15

V. Method for determining machine parameters

The following tests have been designed to find the machine parameters:

A. Induced voltage parameter $\omega\psi$

The $\omega\psi$ parameter arises from the fact that flux in the direct axis induces a voltage in the quadrature axis and vice versa. This is a dynamic parameter that is easily obtained by measuring flux linkages in the dq plane and the angular velocity of the machine. The fact that angular velocity ω is part of the equation, means that this term goes to zero in the locked rotor test.

B. Determining stator parameters

This first procedure only has to be carried out once, as it only deals with stator parameters. The equivalent circuit for this test procedure is shown in fig. 24. The machine is to be tested with a locked rotor and with damper winding and permanent magnets disabled, hence the parameters $\omega\psi$, L_D, R_D, I_D and I_{pm} all fall out of the equivalent circuit. There are several ways of determining the parameters for the stator. One way is to apply a DC step voltage to the machine and measure the step response of the stator current. From this measurement one can then simply find the time constant and the steady state current.

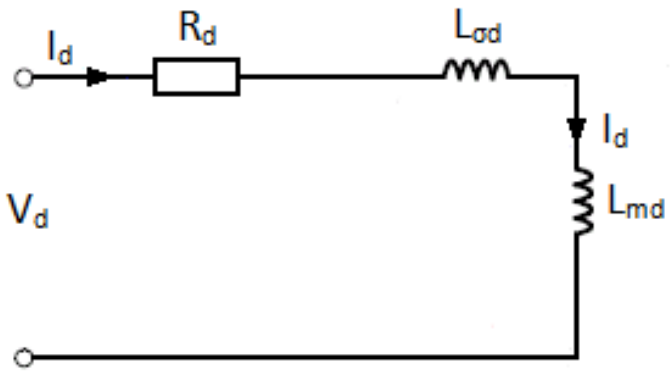

Figure 24. Equivalent circuit for the stator parameter test.

The parameters can then be found using Ohms law and the definition of the time constant in an RL circuit

$$R_{DC} = \frac{V_{DC}}{I_{DC}} \tag{32}$$

$$\tau_{RL} = \frac{L}{R} \rightarrow L = \tau_{RL} R \tag{33}$$

Where τ_{RL} is the time it takes for the current to rise to $\left(1 - \frac{1}{e}\right) I_{DC} \simeq 0.63 I_{DC}$, and the subscript DC denotes that the parameter is a DC parameter. In this particular case equation (33) translates into

$$L_{stator} = L_\sigma + L_m = \tau_{RL} R_{DC} \tag{34}$$

Where L_σ is the leakage inductance and L_m is the magnetizing inductance. Another way of finding the parameters is to simply apply an AC voltage to the machine and measure the currents and the losses in the machine. This is the preferred method in this project. The reason for choosing this approach is that it also provides the opportunity to study the frequency dependence of these parameters. The chosen approach is to first apply a very low frequency voltage and to increase the frequency and voltage in logarithmic steps using the condition $\frac{V}{f} = constant$, thus keeping the flux and current approximately constant. The reason why we want to keep the flux and current constant, is that this will minimize the transient period for every step of the procedure. This to minimize simulation time and data storage requirements. The reason why it is necessary to test for so many frequencies, is that it is expected that the damper winding parameters will depend quite a lot on frequency.

To determine the parameters, one must measure the phase angle between voltage and current. The most straightforward way of finding this angle is by measuring the time by which the current lags the voltage, this approach, however, has proven difficult to accurately measure due to DC offset in the currents during transients. To find the phase angle the losses in the machine are measured. Since the machine is not doing any work, these losses must be equal to the real power flowing into the machine. We then find the RMS of these losses over a period of time and divide by 3 to get the per phase power. The RMS of the current and voltage in one phase is then measured over the same period of time. We then find the apparent power flowing into the machine per phase by using the well known relation

$$S^{ph} = V^{ph}_{RMS} I^{ph}_{RMS} \tag{35}$$

where superscript ph means phase. The phase angle is then found by using

$$\phi = arccos\left(\frac{P^{ph}}{S^{ph}}\right) \tag{36}$$

Since the machine is perfectly symmetrical, the per phase resistance and inductance must be exactly equal those of the two axis system. We can see this from the power invariant Park transform where the scaling factors end up cancelling each other out when inserted into equation (37). Therefore we can say

$$R_D = R_Q = R^{ph} = \frac{P^{ph}_{losses}}{\left(I^{ph}_{RMS}\right)^2} \tag{37}$$

$$X_D = X_Q = R_D tan(\phi) \tag{38}$$

$$L_D = L_Q = \frac{X_D}{2\pi f} \tag{39}$$

We then have all the stator resistance and the sum of the magnetizing and leakage inductance. It remains to separate the inductances.

C. Determining stator leakage inductance

One of the most difficult parameters to determine is the stator leakage inductance. For many machines it is simply determined by rule of thumb. This procedure also only needs to be carried out once, as it deals with stator parameters. This parameter represents the flux produced in a coil that does not link with other coils. This flux therefore does not contribute to useful torque production in the air-gap, hence the name leakage. This parameter will be determined by applying a unit current to one of the windings, the induced voltages in the all windings are then measured. If we apply the current to winding a, we can use the fact that induces voltages in the windings b and c are direct consequences of flux that links these windings with coil a. In equations (40) to (45), e_a refers to induced voltage in phase a, the subscript pu refers to per unit, $L_{\sigma,pu}$ denotes the per unit leakage inductance and superscript denotes phase. The per unit induced voltage in coil a can be described by

$$e_{a,pu} = -\omega_{e,pu} L_{\sigma,pu} - \omega_{e,pu} L_{m,pu} \tag{40}$$

which, when rearranged gives

$$\omega_{e,pu} L_{\sigma,pu} = e_{a,pu} - \omega_{e,pu} L_{m,pu} \tag{41}$$

where $\omega L_{m,pu}$ can be said to represent the induced voltages in coils b and c, hence $\omega L_{m,pu} \approx e_{b,pu} + e_{c,pu}$. Because of this we can say

$$\omega_{e,pu} L_{\sigma,pu} = e_{a,pu} - e_{b,pu} - e_{c,pu} \tag{42}$$

which upon rearrangement gives

$$L^a_{\sigma,pu} = \frac{e_{a,pu} - e_{b,pu} - e_{c,pu}}{\omega_{e,pu}} \tag{43}$$

Analogously when applying current to wingdings b and c we get respectively

$$L^b_{\sigma,pu} = \frac{e_{b,pu} - e_{a,pu} - e_{c,pu}}{\omega_{e,pu}} \tag{44}$$

and

$$L^c_{\sigma,pu} = \frac{e_{b,pu} - e_{a,pu} - e_{c,pu}}{\omega_{e,pu}} \tag{45}$$

Finally we take the average of $L^a_{\sigma,pu}$, $L^b_{\sigma,pu}$ and $L^c_{\sigma,pu}$ and arrive at our final per unit stator leakage inductance. As the machine being investigated is perfectly symmetrical, the direct and quadrant leakage inductances will be identical and equal in per unit to the inductance found in this procedure. This means $L_{\sigma d,pu} = L_{\sigma q,pu} = L_{\sigma,pu}$

D. Determining damper winding parameters

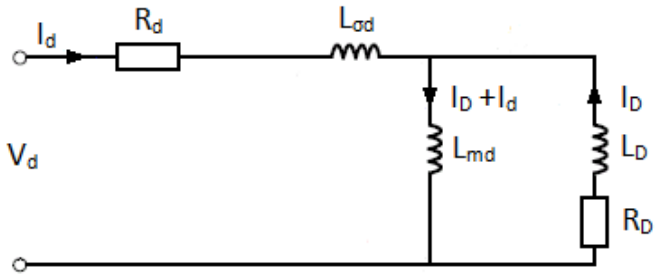

Figure 25. Equivalent circuit for the damper winding parameter test.

In order to determine the damper winding parameters, the same test as for the stator parameters must be performed, with the damper winding enabled. This test effectively simulates a slip frequency equal to the applied frequency.

The reason why it is chosen to test for so many of the lower frequencies is that it is expected that the machine will always be very close to synchronous speed, making the slip frequency very low. Therefore the region from 0.1 Hz to 5 Hz is the most interesting. As for stator parameters, the symmetrical geometry of the machine and the fact that we are using the power invariant Park transform, means that this power based approach will yield per phase parameters identical to the two axis parameters for the machine. We begin by finding the RMS value of the total losses in the machine per phase. The RMS of individual losses can be found directly from the software. Again, since no work is being done, the losses must equal the active power drawn by the machine. The currents and voltages are then measured, and the apparent power and power angle are calculated using equation (35) and equation (36) respectively.

Since the stator parameters have already been determined, the damper winding parameters can be calculated in a straightforward manner using basic circuit theory. It is expected that we will see a significant rise in damper winding resistance as frequency increases, this is due to the well known skin effect. [29]

E. Determining permanent magnet flux linkage ψ_{pm}

This parameter is found by disconnecting the stator, disabling the damper winding, and rotating the machine at a steady speed. The induced voltages are then measured and transformed into the dq reference frame. Now, the voltage equation for the direct axis becomes

$$V_d = -\omega\psi_q = 0 \tag{46}$$

since there is no source of flux in the quadrature axis $\psi_q = 0$. For the quadrature axis the voltage equation becomes

$$V_q = \omega\psi_d \tag{47}$$

Because of this we can say

$$V_s = \sqrt{V_d^2 + V_q^2} = V_q = \omega\psi_d = \omega\psi_{pm} \rightarrow \psi_{pm} = \frac{V_s}{\omega} \tag{48}$$

F. Determining permanent magnet current equivalent i_{pm}

When the other parameters are known, this parameter can be found by measuring voltages and currents at no load. The motivation for doing this at no load is to avoid flux in the machines quadrature axis. the $\omega\psi_q$ term can then be omitted. Simple circuit theory can then be used to find this current-equivalent.

Results will not be presented for i_{pm}, ψ_{pm}, $\omega\psi_q$ or $\omega\psi_d$ as they are not the parameters that are of interest in this thesis.

VI. Results

A. Results from stability testing

1) Case A: Only permanent magnets provide damping

As we can see from Fig. 26, the machine is able to remain in synchronism during the loss of load transient. It does, however, not manage to significantly reduce the speed

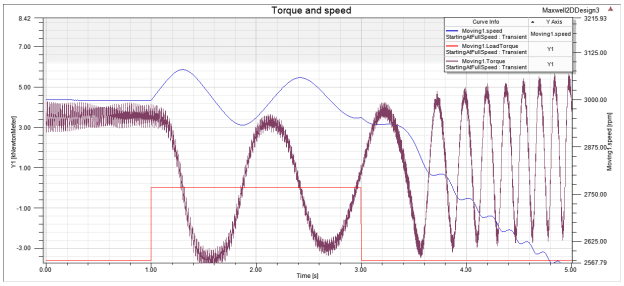

Figure 26. Case A: Rotational speed in blue, load torque in red and produced torque in purple. Loss of load gives oscillations that is not significantly dampened. Shortly after the load comes back on, the machine loses synchronism.

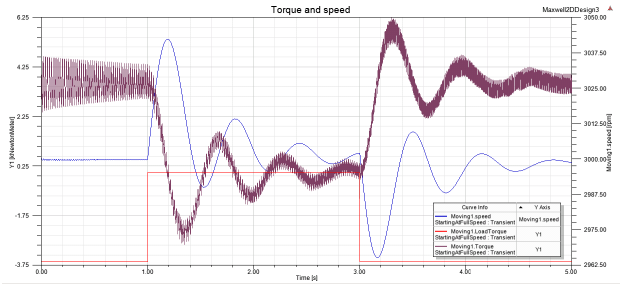

Figure 29. Case B: Rotational speed in blue, load torque in red and produced torque in purple. Loss of load gives oscillations that are dampened to a low amplitude by the time the load comes back on, at which point we get a new oscillation that is also effectively dampened.

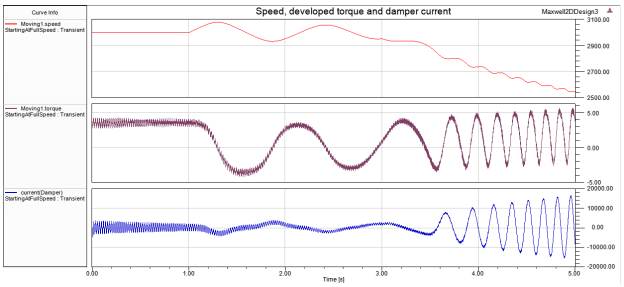

Figure 27. Case A: Rotational speed in red, developed torque in purple and the current in the damper winding in blue. We can see that there is a clear relation between the current in the damper winding, developed torque and the speed of the machine.

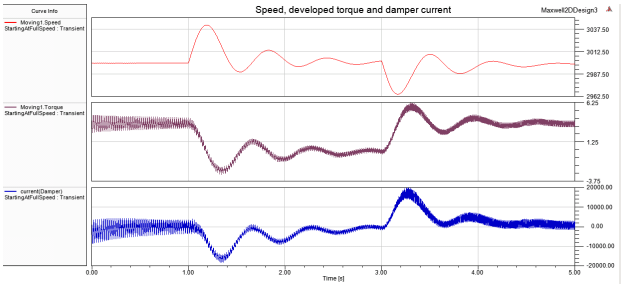

Figure 30. Case B: Rotational speed in red, developed torque in purple and the current in the damper winding in blue. Again there is a clear relation between the current in the damper winding, developed torque and the speed of the machine.

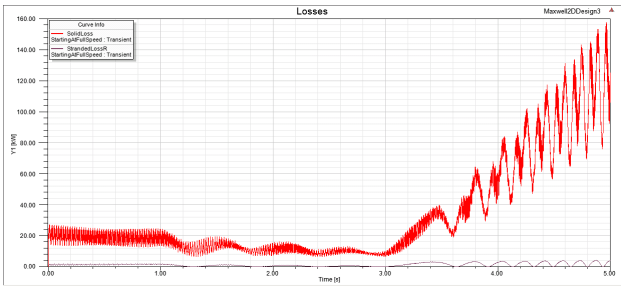

Figure 28. Case A: Losses in the machine. The red line shows the losses in the damper winding, the purple line shows the losses in the stator windings. As we can see, the wast majority of the losses take place in the damper winding.

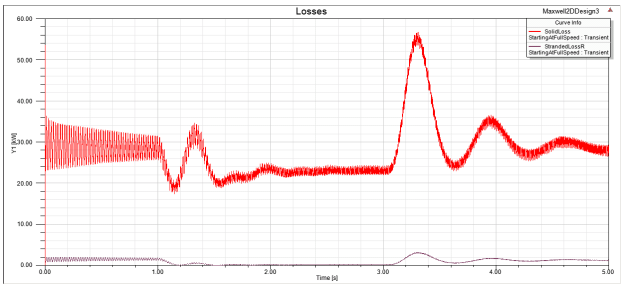

Figure 31. Case B: Losses in the machine. The red line shows the losses in the damper winding, the purple line shows the losses in the stator windings.

oscillations during the two second period after it. When the load torque is switched back on, the machine does not manage to produce the torque required to keep synchronous speed.

Shortly after the load torque is switched back on, the machine experiences a pole slip,. Consequently, the torque production, and therefore also the speed, immediately collapses. Note that all load torques are defined as negative. During the load drop transient, the rotors angle in relation to the stator field δ changes by $87.63°$. Fig. 27 shows developed torque, speed and current in the damper winding. We can see the relation between the speed of the machine, the current in the damper winding and the production of torque in the machine. When the machine loses synchronism, the slip, and consequently, the damper winding current increases. The reason why the average developed torque does not increase, is that the machine is not running at synchronous speed. Fig. 28 shows the losses in the machine. As we can see, as the slip of the machine increases, the losses also increase significantly.

2) Case B: Damper sleeve made of reduced copper

As we can see from Fig. 29, as the load is dropped, the speed of the machine starts oscillating with an initial amplitude of about 42 rpm, but oscillations are damped to roughly 2 rpm by the time the load is reintroduced. When the load is reintroduced, the machine has no trouble producing the necessary torque to remain in synchronism.

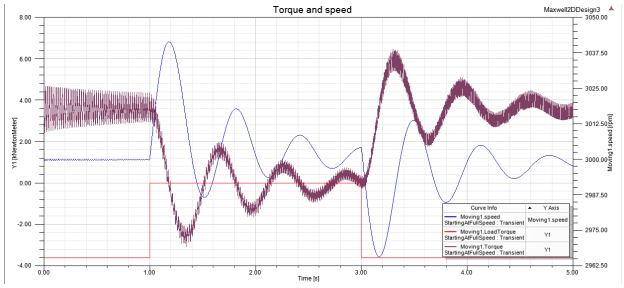

Figure 32. Case C: Rotational speed in blue, load torque in red and produced torque in purple. Loss of load gives an oscillation that is dampened to a low amplitude when load comes back. When the load comes back a new oscillation starts which is also dampened in due course.

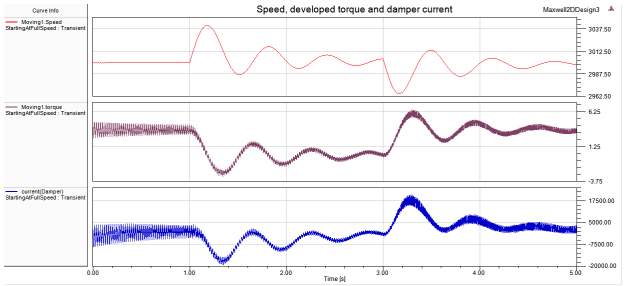

Figure 33. Case C: Rotational speed in red, developed torque in purple and the current in the damper winding in blue.

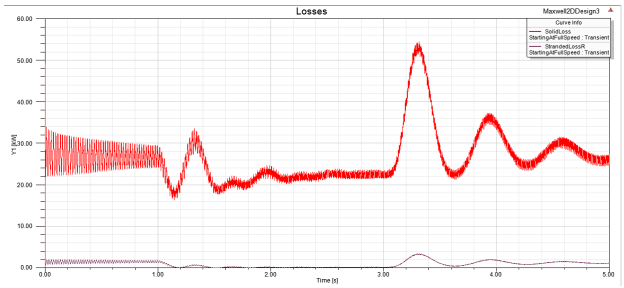

Figure 34. Case C: Losses in the machine. The red line shows the losses in the damper winding, the purple line shows the losses in the stator windings.

Initially the machine's oscillation has an amplitude of 35 rpm. At the end of the simulation oscillations have been reduced to about 1 rpm. So the damper winding is relatively effective in damping oscillations. During the transients, the rotors angle δ to the stator field changes by $79.74°$ and $-64.68°$ respectively. Fig. 30 shows developed torque, speed and damper current. We can clearly see the relation in oscillations between the three parameters. We can also see that, with the exception of overharmonic noise, when the oscillations in speed are low, there is little current flowing in the damper. Fig 31 shows the losses in the machine. Since there are large losses in the damper winding even at steady state, the majority of the losses in the damper winding can be attributed to the fact that no effort has been made to reduce overharmonic induced currents in the damper winding. Since the damper winding design is a continuous sheet of metal, rather than a squirrel-cage made up of discrete

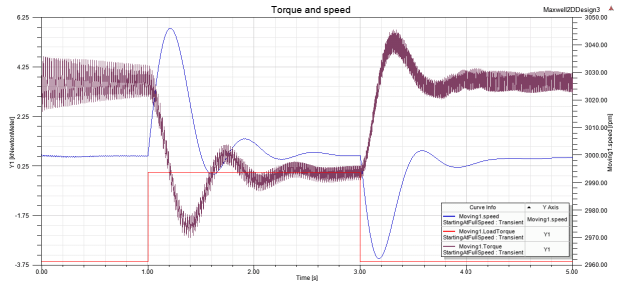

Figure 35. Case D: Rotational speed in blue, load torque in red and produced torque in purple. Loss of load gives an oscillation that dies out as the load comes back. When the load comes back, a new oscillation starts which is also very well dampened.

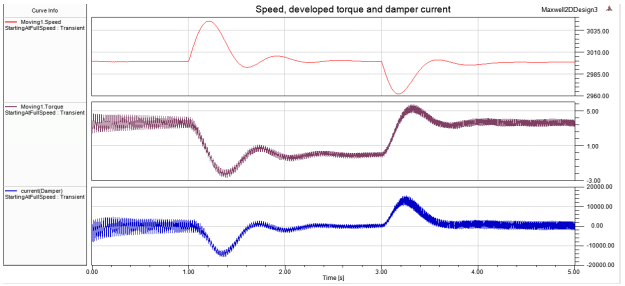

Figure 36. Case D: Rotational speed in red, developed torque in purple and the current in the damper winding in blue.

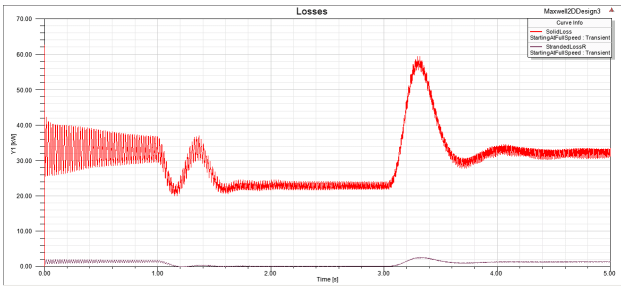

Figure 37. Case D: Losses in the machine. The red line shows the losses in the damper winding, the purple line shows the losses in the stator windings.

bars, it is impossible to completely avoid these overharmonic components. The losses due to this seem to be proportional to the machines load, and therefore to the currents in the stator and the flux in the air-gap.. If we look beyond the apparent load-proportional component of the losses, it is, however, evident that the during the transients, the losses in the damper winding are increasing. And more so when the load is reintroduced than when it is removed. This is expected since in that period the machine must accelerate a large load and therefore must produce a high torque. The losses in this damper winding peak at 57 kW during the second transient.

3) Case C: Damper sleeve made of aluminium

Fig. 32 shows the speed, load torque and developed torque for the machine for the case of aluminium damper

winding. As the load is dropped, the speed of the machine starts oscillating with an initial amplitude of about 41 rpm but oscillations are damped to roughly 4 rpm by the time the load is reintroduced. In the second transient, initial amplitude is 35 rpm, and the amplitude at the end of the simulations is 3 rpm. During the transients, the rotors angle δ to the stator field changes by $76.31°$ and $-56.85°$ respectively. In fig. 33 we can see the developed torque, speed and current in the damper winding. We can clearly see the correlation between the current in the damper winding, slip and the developed torque. Fig 34 shows the losses in the machine. The same situation as in the last case can be observed, where the damper winding produces extensive losses at steady state, but a transient is clearly visible during speed oscillations. Losses in the damper winding peak at 55 kW during the second transient.

4) Case D: Damper sleeve made of brass

Fig. 35 shows the speed, load torque and developed torque. When the load is dropped, the machines initial oscillations reach an amplitude of about 46 rpm. The oscillations are quickly dampened, and two seconds after the load drop, the oscillations have reached zero amplitude. This damper winding is clearly the most effective at damping oscillations.

During the transients, the rotors angle δ to the stator field changes by $83.21°$ and $-77.79°$ respectively. This is the closest the machine has been to ending up at the same angle δ before and after the transients. Fig. 36 shows developed torque, speed and damper current. In fig. 36 we can again see the same correlations between the measured quantities. Fig. 37 shows losses in the machine, which again shows that losses increase during the transients, and more so when the load increases. Table V and table VI sum up the stability tests.

Table V
Summary; Load drop

Case	Initial a.mp	End amp.	$\Delta\delta$
Case A	80 rpm	40 rpm	$87.63°$
Case B	42 rpm	2 rpm	$79.74°$
Case C	41 rpm	4 rpm	$76.31°$
Case D	46 rpm	0 rpm	$83,21°$

Table VI
Summary; Load rise

Case	Initial amp.	End amp.	$\Delta\delta$
Case A	N.A.	N.A.	N.A.
Case B	35 rpm	1 rpm	$-64.68°$
Case C	35 rpm	3 rpm	$-56.85°$
Case D	38 rpm	0 rpm	$-77.79°$

B. Machine Parameters

Using the procedure presented in this thesis the parameters in table VII are found. As mentioned earlier, since the machine is perfectly symmetrical , the machines direct and quadrature axis parameters will be equal. As expected, the parameters are fairly constant, and therefore not dependent on frequency. If eddy currents had been included in the stator windings, the resistance would increase somewhat with frequency. The per unit leakage inductance $L_{s\sigma,pu}$ was found to be 0.1938, and the magnetizing inductance L_m was found to be 0.8062. This was used to separate the two stator inductance parameters.

Table VII
Stator parameters

$f[Hz]$	$R_s[m\Omega]$	$L_{\sigma s}[mH]$	$L_m[mH]$
0.1	10.00	9.37	38.98
0.2	10.16	9.24	38.45
0.5	10.35	9.72	40.42
1	10.08	9.23	38.38
2	10.21	9.11	37.91
5	10.04	9.10	37.85
10	10.12	8.94	37.20
20	10.05	8.88	36.94
50	10.03	8.86	36.86
100	10.18	9.00	37.42

In the following, the damper parameters for the different damper windings are presented.

1) Case A: Only permanent magnets provide damping

The parameters found for the case of only permanent magnets acting as damper winding are shown in table VIII. The reason why the results for frequencies lower than 2 Hz have been omitted is that the calculated values for the lower frequencies made very little sense and even resulted in negative inductances. Calculated parameters for the higher frequencies yield results that are somewhat more convincing.

Table VIII
PM damper parameters

$f_s[Hz]$	$R_D, R_Q[m\Omega]$	$L_D, L_Q[mH]$
0.1	N.A.	N.A.
0.2	N.A.	N.A.
0.5	N.A.	N.A.
1	N.A.	N.A.
2	1397.47	11.63
5	1227.49	12.00
10	1102.79	7.19
20	1079.02	4.01
50	1237.60	2.83
100	1406.62	2.56

2) Damper sleeve made from reduced copper

Ther parameters for the reduced copper damper winding are shown in table IX.

Table IX
Cu damper parameters

$f_s[Hz]$	$R_D, R_Q[m\Omega]$	$L_D, L_Q[mH]$
0.1	47.87	7.11
0.2	47.67	5.68
0.5	45.53	3.45
1	47.08	2.99
2	47.86	2.69
5	47.92	2.42
10	51.67	2.57
20	56.12	2.55
50	75.10	2.56
100	104.89	2.32

3) Damper sleeve made from aluminium

The results for the aluminium damper winding are shown in table X.

Table X
Al damper parameters

$f_s[Hz]$	$R_D, R_Q[m\Omega]$	$L_D, L_Q[mH]$
0.1	37.43	7.54
0.2	36.15	5.14
0.5	34.9	3.00
1	35.74	2.81
2	36.76	2.62
5	38.08	2.47
10	40.21	2.53
20	45.38	2.57
50	65.60	2.52
100	90.86	2.29

4) Damper sleeve made from reduced brass

The results for the aluminium damper winding are shown in table XI.

Table XI
Brass damper parameters

$f_s[Hz]$	$R_D, R_Q[m\Omega]$	$L_D, L_Q[mH]$
0.1	90.57	14.37
0.2	91.94	8.55
0.5	87.55	5.47
1	87.96	3.52
2	88.14	3.51
5	97.82	2.07
10	96.24	2.65
20	96.19	2.59
50	115.17	2.59
100	153.59	2.37

Figures 38 anf 39 summarize the damper winding parameters for cases B, C and D.

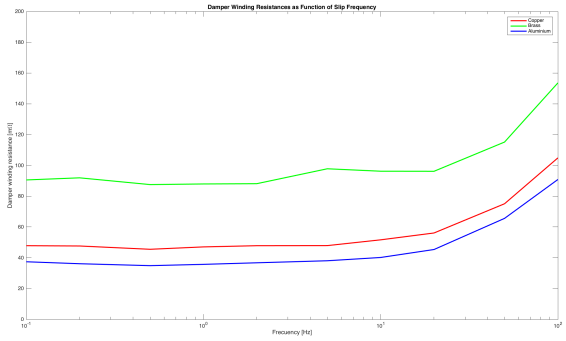

Figure 38. Damper winding resistances as function of slip frequency. Green line shows the parameter for brass, red shows reduced copper and blue shows aluminium. Note that the x-axis is logarithmic.

As expected, the resistances increase by quite a lot as the frequency rises. In cases B and C the resistance at 100 Hz is actually more than double the DC resistance, while in case D it increases by a factor of 1.7.

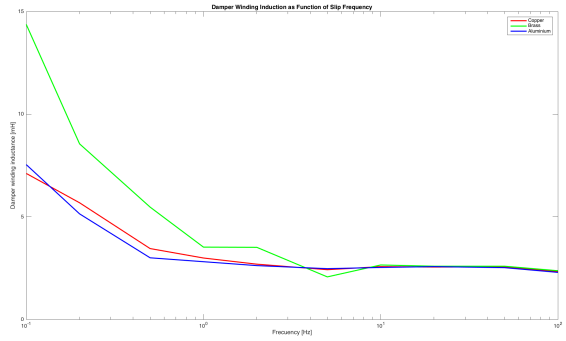

Figure 39. Damper winding inductances as function of slip frequency. Green line shows the parameter for brass, red shows reduced copper and blue shows aluminium. Note that the x-axis is logarithmic.

The fact that the damper winding inductances change with frequency is slightly more surprising. However there exists research that predicts exactly what is seen here. [30] The reason why this happens, is that in a geometry such as this damper winding is that there will be nonuniform current profiles across the damper winding.

VII. Discussion

A. Challenges and process

The most significant challenges during this work has been finding a way of determining the damper winding parameters. The most fundamental challenge around this has been finding a way of separating the stator leakage inductance from the magnetizing inductance. In machine textbooks and literature this is done by use of empirical knowledge and experience. A more rigorous way of

separating these parameters was found and successfully implemented.

Another time consuming challenge arose from the fact that the parameters were to be found for many different frequencies. It was decided that in order to test the machine for different frequencies, a simulation procedure where the machines rotor was locked, and the simple control principle of $\frac{V}{f} = constant$ was implemented for a range of frequencies from 0.1 Hz to 100 Hz in 10 logarithmic steps. This was done in order to reduce the transient period for every step. These transients proved to be so long, it became very difficult to, with any kind of acceptable accuracy, measure the power angle ϕ between voltage and current. In retrospect, far too much time and effort was spent trying to make this method work, even attempts in trying to account for the transient DC offsets in the currents were made, without yielding satisfactory results.

In the end, a method using a power approach was attempted. In this method, the same simulation results could be used to calculate RMS consumption of apparent power and RMS losses in the machine, this method made it very easy to accurately calculate the power angle, which has been vital in this project.

When the method for finding the parameters was found, the decision to test the method for several different materials was made.

B. Stability test results

The results from the stability analysis of case A were largely as expected. The initial amplitude of oscillations was very big, at 80 rpm, for the loss of load, and these oscillations are only dampened to an amplitude of 40 rpm as the load is switched back on. Shortly after the load torque comes back, the machine experiences a pole slip, loses synchronism, and torque production collapses. This is no great surprise, as the machine suddenly needs to produce a lot of torque with no damper winding present.

In case B, the initial oscillation has an amplitude of 42 rpm, and is dampened to only 2 rpm before the load torque comes back two seconds later. During the second transient, the initial amplitude of the oscillation is 35 rpm, and is reduced to 1 rpm after two seconds. This means that with this damper winding, the machine can ride through extremely rough conditions without coming close to losing synchronism. Losses in the damper winding reach a peak of about 57 kW during the second transient. The torque angle δ between rotor and stator field changes by 79.74° during the first transient, and -64.68° during the second transient, the sum of these angles should ideally be zero, the torque angles should be the same for an equal load The most likely reason why they are not equal is that the transients are given enough time to die out, and a complete steady state is therefore never reached.

For case C, the first oscillation reaches an initial amplitude of 41 rpm which is reduced to 4 rpm after two seconds. During the second transient, the initial amplitude of the oscillation is 35 rpm and it is dampened to 3 rpm after two seconds. In this case, the machine is slightly less dampened than it is in case B. Damper winding losses reach a maximum of about 55 kW, which is slightly lower than in case B. The torque angle between rotor and stator field changes by 76.31° during the first transient, and -56.85° during the second transient. Again, these angles should be far more similar.

In case D, The initial oscillation during the first transient has an initial amplitude of 46 rpm and is dampened to zero after two seconds. During the second transient has an initial amplitude of 38 rpm and is reduced to zero after less than two seconds. Losses in the damper winding reach a peak of about 60 kW during the second transient, higher than both cases B and C. The torque angle between rotor and stator field changes by 83.21° during the first transient, and -77.79° during the second transient. Even though these angles are the most similar of the studied cases, these angles should ideally be equal. The fact that the machine that has the best damping gets the most equal torque angles supports the claim that the mismatch is related to lack of steady state. This damper winding performs, by far, the best at damping oscillations.

These tests are really asking a lot from the machine, yet all the realistic damper winding alternatives provide sufficient damping for the machine not only to ride through extreme conditions without experiencing pole slipping or loss of synchronism, but also to reduce oscillations very quickly. This proves that these damper windings are able to produce large amounts of torque, and to do so very quickly after a disturbance. We can see a correlation between the losses produced in the damper winding and how quickly oscillations are reduced. A general worry throughout these tests is the amount of losses in the damper winding even during steady state operation.

From a dynamics point of view, a weakness in this model is that it only includes the inertia of the rotor, in reality the mechanical device being driven by the machine would also have a rotational inertia, which would reduce the amplitude of the oscillations. On a basis of this we can say that this model provides a worst case scenario.

C. Parameter test results

As expected, the damper winding resistances increase as the frequency increases, this is a result of the well known skin effect. The frequency dependency of the damper

winding inductances is perhaps more counterintuitive, however this phenomenon is also well described in literature for geometries such as this damper winding. An interesting note is that, at the lower frequencies, the ratios of damper winding resistances are within a few percent of the inverse ratio of the conductivities defined in the simulation models. This is a clear sign that this model is on to something.

D. Correlation between damper parameters and damping qualities

Although the dataset is quite sparse, with only three realistic materials being investigated, these tests suggest that the higher the resistance of the damper winding material, the more energy is converted into heat losses in the damper winding, and the better its damping abilities.

VIII. Conclusion

In this thesis, a numerical simulation model for a permanent magnet motor with an experimental damper winding design has been developed. The model has been solved using finite element method software. The damper winding has been modelled as a cylinder that forms the outer circumference of the rotor assembly. The machine has been tested using damper windings made of a modified copper material, aluminium and brass. The machine has also been tested using only the permanent magnets to provide damping. This was done to provide reference. The results from the test procedures have been used to find the individual two axis parameters for the machine, the procedure for finding these parameters is limited to symmetrical machines.

In the test procedure, the machine was tested when going from full load to no load in one step, and vice versa. These are extreme circumstances for the machine to be tested under. The results from these tests show that all the realistic damper materials provide sufficient torque for the machine to remain in synchronous operation both when going from full load to no load and when going from no load to full load. Even the case where only permanent magnets provide damping does, although poorly damped, remain in synchronism during the loss of load transient. It does, however, experience pole slipping and a collapse in torque production for the sudden increase in load.

The machine parameters have been identified using the presented method, which mainly consists of an array of locked rotor tests at various frequencies. The results suggest that the brass damper winding has the greatest resistance, followed by the modified copper material and aluminium. The ratios between the various damper winding resistances are as expected from the conductivities of the materials. At low frequencies, the inductances of the modified copper, and aluminium windings are very similar, while that of the brass winding is significantly larger. At higher frequencies the inductances of all winding are very found to be similar. These phenomena of frequency dependent parameters are well documented in literature.

Tests show that the brass damper winding provides the best damping, followed by the copper and the aluminium. This suggests there is a positive relation between damping abilities and damper winding resistance.

IX. Further work

An interesting aspect of the damper winding design that might need revisiting is the fact that even at steady state, the damper winding produce significant losses. It would be interesting to look into redesigning the geometry of the damper winding to minimize induced currents due to slot-harmonics and harmonic contents in the MMF wave. This would significantly reduce the steady state losses in the damper winding. Thus far, no effort has been made to study the effect the damper winding has on the thermal performance of the machine, the damper winding obviously creates a lot of heat and this needs to be studied in detail before a physical model can re realized. It is vital that the damper winding is studied from a mechanical point of view, since it must withstand great forces during steady state as well as during transients. Both thermal and mechanical assessments could have significant impacts on both damper winding geometry and choice of material.

An integral part of the further work must be to provide more rigorous empirical data to test the validity of the described method for parameter determination. It would also be useful if the model could be expanded in order to account for asymmetrical rotor geometries.

X. Acknowledgements

The author would like to express his gratitude towards his thesis supervisor Professor Robert Nilssen, from the Department of Electric Power Engineering at NTNU, for his invaluable guidance and inspiration throughout this project process. Thanks to Professor Roy Nilsen from the Department of Electric Power Engineering at NTNU for input on parameter estimation. Thanks also to co-supervisors Kristen Jomås and Alexey Matveev from Rolls-Royce Marine AS for their advise and guidance. Lastly, a special thanks to Dr. Mostafa Valavi from the Department of Electric Power Engineering at NTNU for his all his help on simulation related issues.

XI. Appendices

Please find the following appendices

A Validation of conclusion from earlier project work
B Larger copes of all figures used in this thesis
C A brief study of the currents drawn by the machine
D A brief study of the currents in damper winding

REFERENCES

[1] Ole Bjørn Silset Warvik, "Using finite element method simulations to determine the transient behaviour of a permanent magnet motor with a damper winding sleeve," NTNU, Tech. Rep., 2015.

[2] *Petromarks Consortium Workshop*. SmartMotor AS, 2010.

[3] Sergey Klyapovskyi, "Subsea motor drived with long subsea cable," Master's thesis, NTNU, June 2014.

[4] Integrated Magnetics, "Rare earth pricing bulletin," http://bit.ly/1Rj151W, accessed: 13.12.2015.

[5] K. Kamiev, J. Nerg, and J. Pyrhonen, "Design of damper windings for direct-on-line permanent magnet synchronous generators," in *EUROCON 2009, EUROCON '09. IEEE*, May 2009, pp. 783–790.

[6] J. Kinnunen, J. Pyrhonen, O. Liukkonen, and P. Kurronen, "Analysis of directly network connected non-salient pole permanent magnet synchronous machines," in *Industrial Electronics, 2006 IEEE International Symposium on*, vol. 3, July 2006, pp. 2217–2222.

[7] Ansys Electromagnetics, *Maxwell Online Help*, 16th ed., Ansys, 2012.

[8] Ansoft Maxwell Field Simulator, *Study of a Permanent Magnet Motor with MAXWELL 2D: Example of the 2004 Prius IPM Motor*.

[9] P. Pillay and R. Krishnan, "Modeling, simulation, and analysis of permanent-magnet motor drives. i. the permanent-magnet synchronous motor drive," *Industry Applications, IEEE Transactions on*, vol. 25, no. 2, pp. 265–273, Mar 1989.

[10] Fridtjov Irgens, *Dynamikk*, 5th ed. Tapir forlag, 1999.

[11] J. G. Balchen, T. Andresen, and B. A. Foss, *Reguleringsteknikk*. Institutt for teknisk kybernetikk, Norges teknisk-naturvitenskapelige universitet, 2004.

[12] "Damping in damped oscillators," http://bit.ly/1OtYyfv, accessed: 15.11.2015.

[13] "Damped oscillator," http://bit.ly/21ZZp1p, accessed: 20.11.2015.

[14] Stephen J. Chapman, *Electric Machinery Fundamentals*, 5th ed. McGraw-Hill Education, 2012.

[15] Electrical Engineering Blog, "How damper winding provides smooth starting to synchronous machine," http://bit.ly/1NXMoej, accessed: 05.11.2015.

[16] Johannes Skaar, "Tfe4120 elektromagnetisme," Kompendium, 2012.

[17] Duane C. Hanselman, *Brushless Permanent-Magnet Motor Design*. McGraw-Hill Education, 1994.

[18] Leander W. Matsch, "Inductance in terms of magnetic reluctance and magnetic permeance," http://bit.ly/1Z6zMtm, accessed: 09.12.2015.

[19] Slobodan N. Vukosavic, *Electrical Machines*, 1st ed. Springer, 2013.

[20] J. Pyrhonen, T. Jokinen, and V. Hrabovcova, *Design of Rotating Electrical Machinery*, 1st ed. John Wiley and Sons, Ltd., 2008.

[21] Prabha Kundur, *Power System Stability and Control*, 1st ed. McGraw-Hill, Inc., 1994.

[22] E. H. Westgaard, "To-akseteorien for løsning av transiente tilstander i elektriske maskiner," Forelesning i elektromaskinbygg, 1961.

[23] Electrical Engineering Design and Tutorial Resources, "Poles and frequency of alternating current generators basic and tutorials," http://bit.ly/1NjjjMW, accessed: 09.11.2015.

[24] Vacuumschmelze GmbH & Co. KG , "Reduction in the cogging torque of motors," http://bit.ly/221Yw8j, accessed: 14.12.2015.

[25] C. Studer, A. Keyhani, T. Sebastian, and S. Murthy, "Study of cogging torque in permanent magnet machines," October 1997.

[26] Paresh C. Sen, *Principles of Electric Machines and Power Electronics*, 3rd ed. John Wiley and Sons, Inc., 2014.

[27] E. Kreyzig, *Advanced Engineering Mathematics*, 8th ed. John Wiley and Sons, Inc., 1999.

[28] Robert Nilssen, "Winding programme," matlab application.

[29] H. A. Wheeler, "Formulas for the skin effect," *Proceedings of the IRE*, vol. 30, no. 9, pp. 412–424, Sept 1942.

[30] P. N. Murgatroyd and N. J. Walker, "Frequency-dependent inductance and resistance of foil conductor loops," *Electrical Engineers, Proceedings of the Institution of*, vol. 124, no. 5, pp. 493–496, May 1977.

Appendix A; Validation of conclusion from earlier project work

In the specialization project that preceded this thesis, it was found that as the damper winding was introduced, the damping qualities of the machine deteriorated. However, damping improved when the conductivity of the damper sleeve material was reduced. The explanation of this phenomenon was that in that somewhat simplified model, the rotor material was not laminated and that the magnets hadn't been modelled as segmented.This meant that even without a damper winding present, there was already quite a large volume where eddy currents could be induced. These materials have relatively low conductivities compared to copper, this means that currents in the rotor and magnets create quite a lot of heat losses. When, upon introduction of the damper winding, a layer of high conductivity copper is covering the surface between air gap and magnets, the eddy currents in the damper are very efficient at counteracting flux variations due to the transient. This means that the magnets and rotor material are no longer effected by the flux variations in the air gap. Now all eddy currents flow in the damper winding, the high conductivity of which means the flux variations in the air gap can no longer be decayed by heat losses in the rotor assembly, and hence the oscillations are less damped. This conclusion was not, however, tested in the project phase, but have now been conclusively tested and shown to be correct. This was tested by applying a laminated material to the rotor core, and breaking the permanent magnets in to segments to reduce the volume in which eddy currents could flow. In this thesis, a model with laminated rotor core and unsegmented magnets have been used. The reason why this has been chosen is that the main focus of this thesis has been on identifying the various equivalent circuit parameters of the machine. In this sense, eddy currents in the magnets can simply be viewed as an extension of the damper winding.

Figures 1 and 2 show the speed of the two respective machine during the test scenario. From figure 1 and 2 we can clearly see that the machine is far more efficiently damped in the modified machine. Figures 3 and 4 show the currents in the damper windings of the two machines. Unfortunately, as the damper winding was not defined as a winding in the preceding work, the damper current could only be attained for the saved field solutions. Quite few field solutions were saved as the take up a lot of space. As the latter damper winding was defined as a winding, data was automatically saved for every time step. Since the data is so sparse, it is not possible to draw conclusions on the basis of this. Figures 7 and 8 show more detailed images of the airgaps and rotor assemblies. Figures 5 and 6 show overviews of the two machines. Figures 9 and 10 show the total losses in the rotor assemblies for the respective machines. It is clear to see from 9 and 10 that the with the new design, there are no losses in the rotor core, so the laminations are working effectively. However, the segmentation of the magnets is not having as big an effect as believed. We can see that there are still significant losses in the new segmented magnets.

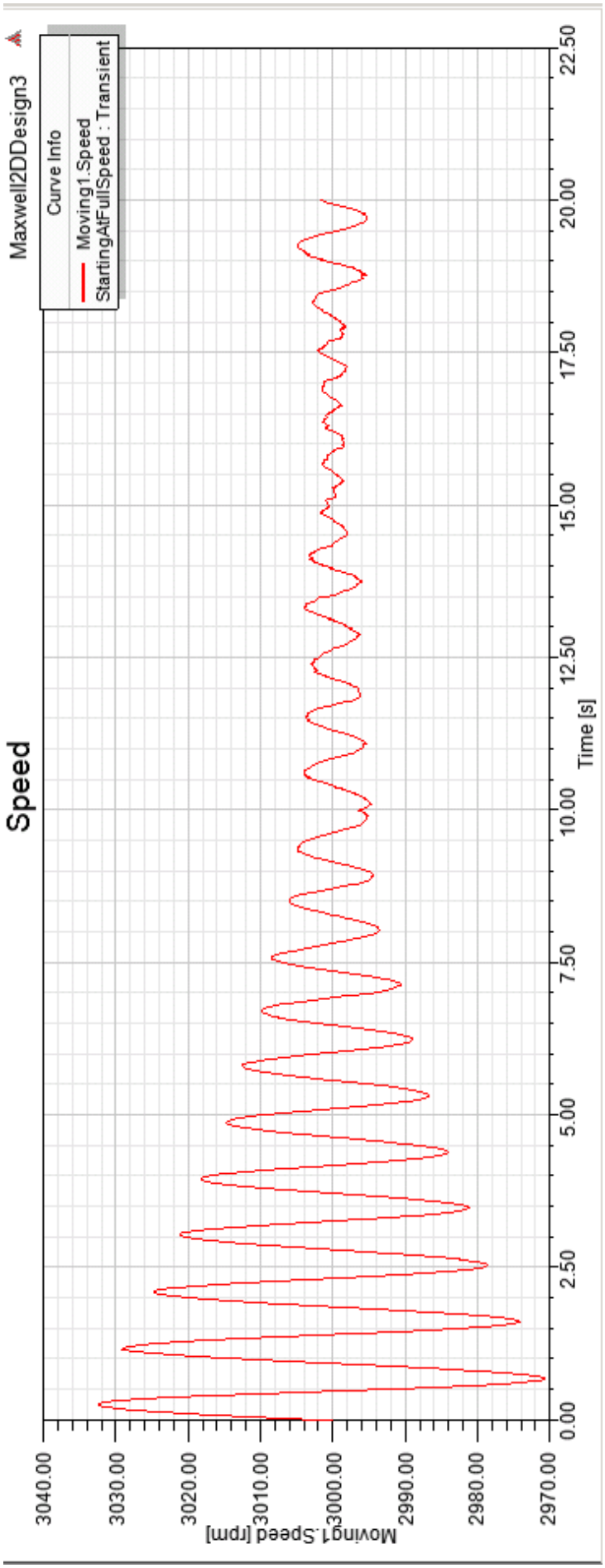

Figure 1: Speed of the original machine with the full damper winding

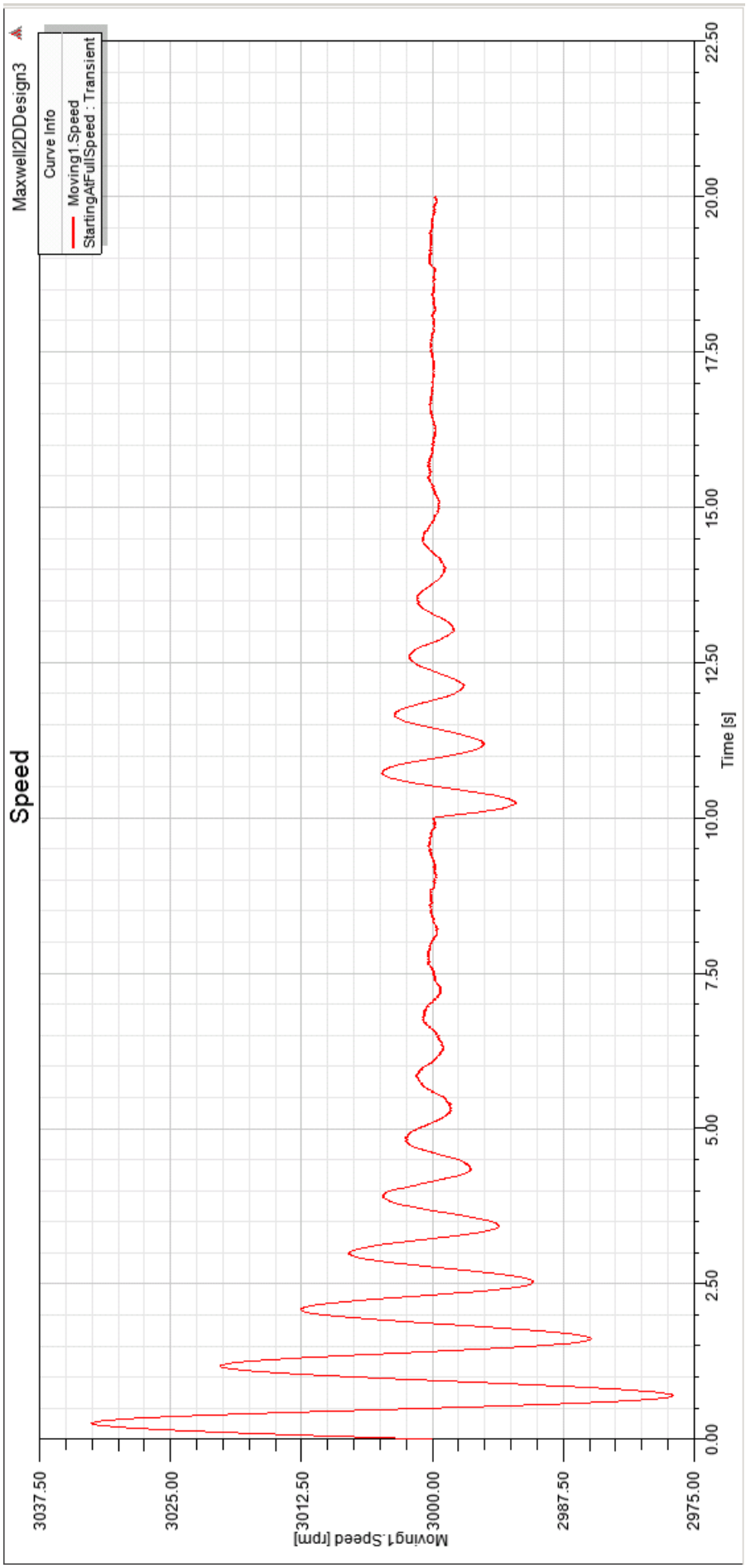

Figure 2: Speed of the modified machine with the reduced damper winding

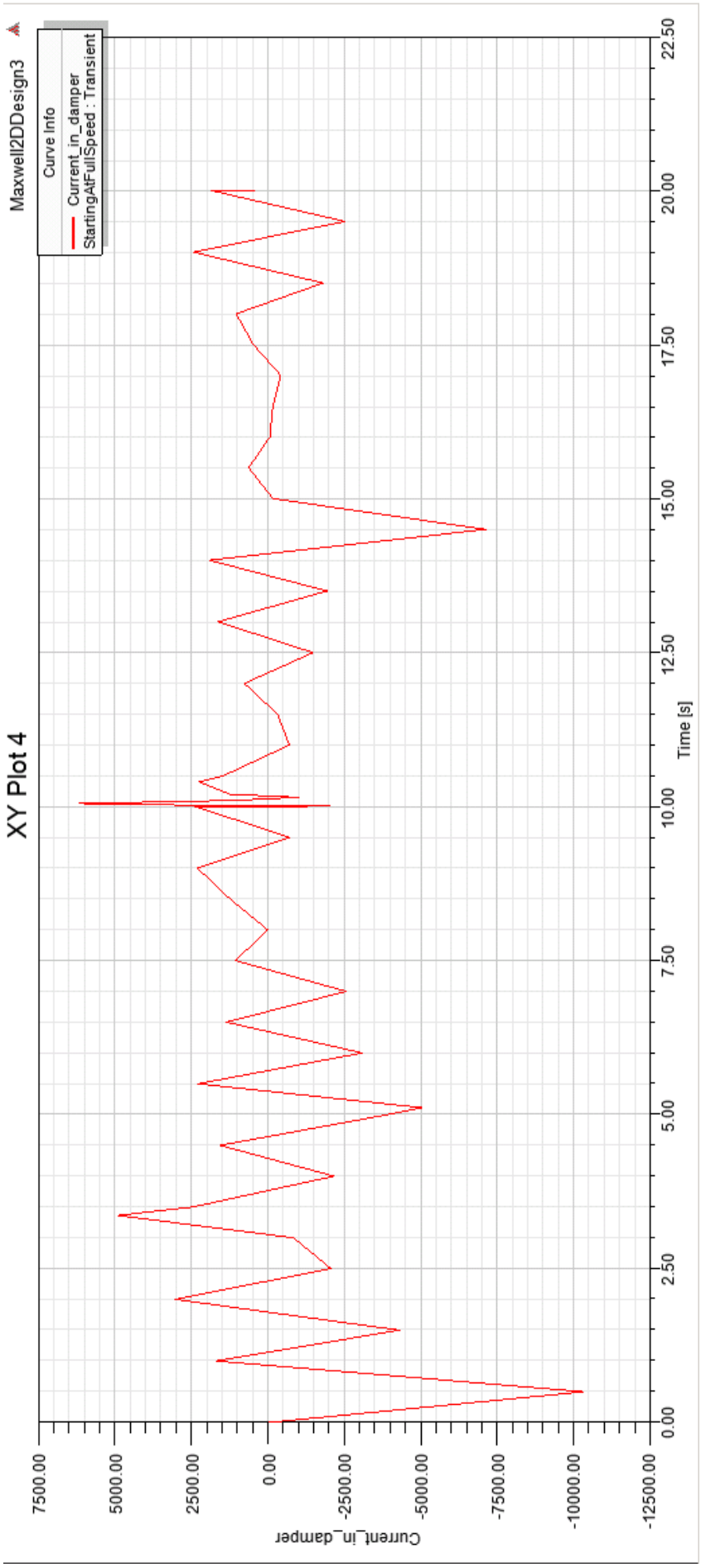

Figure 3: Current in the damper winding of the original machine with the full damper winding

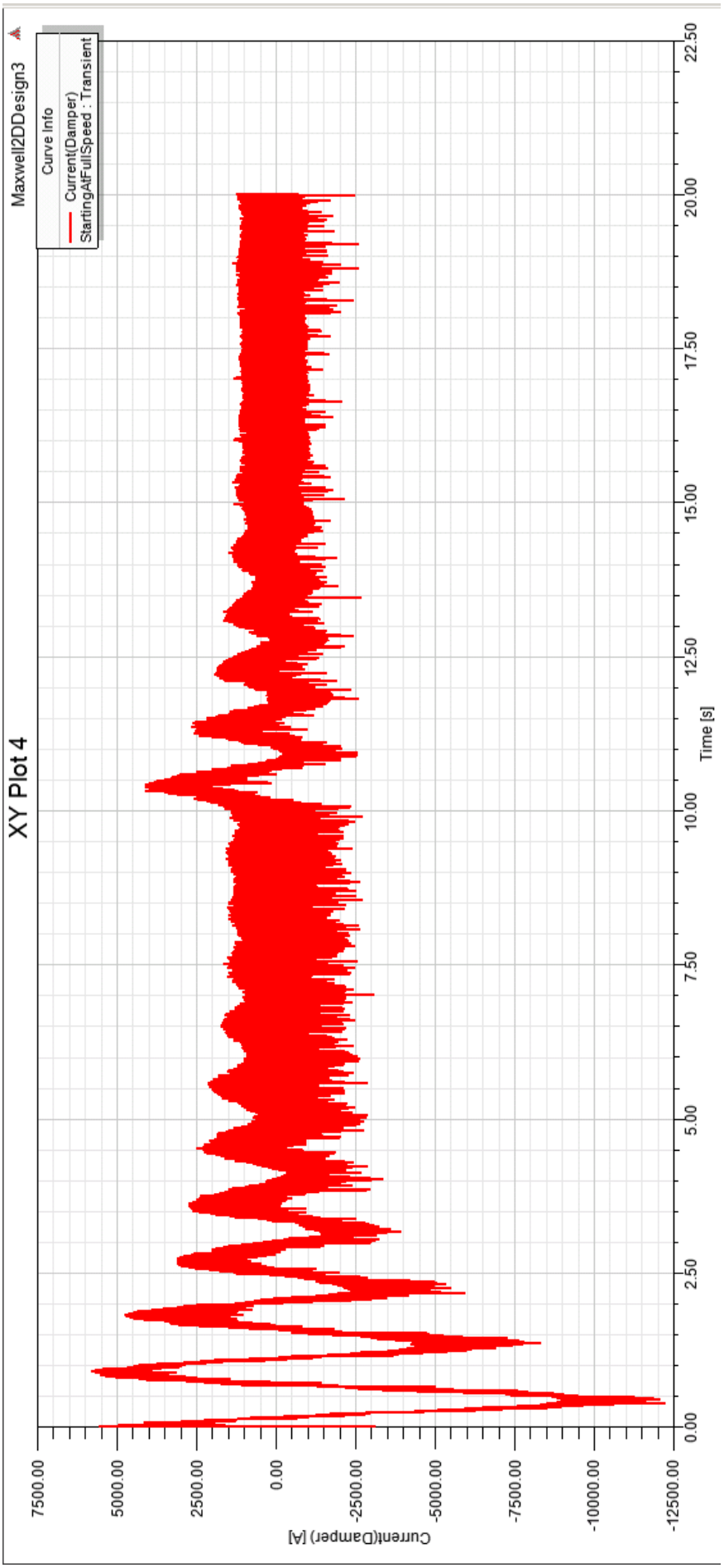

Figure 4: Current in the damper winding of the modified machine with the reduced full damper winding

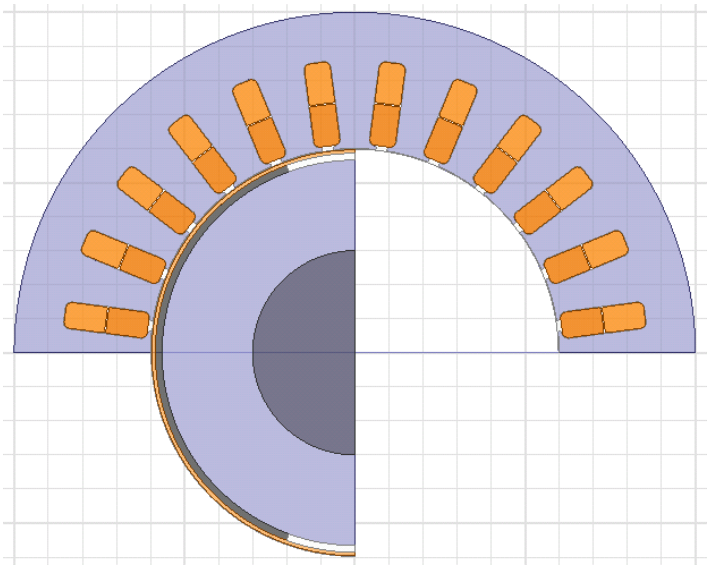

Figure 5: Overview of the original machine with the full damper winding

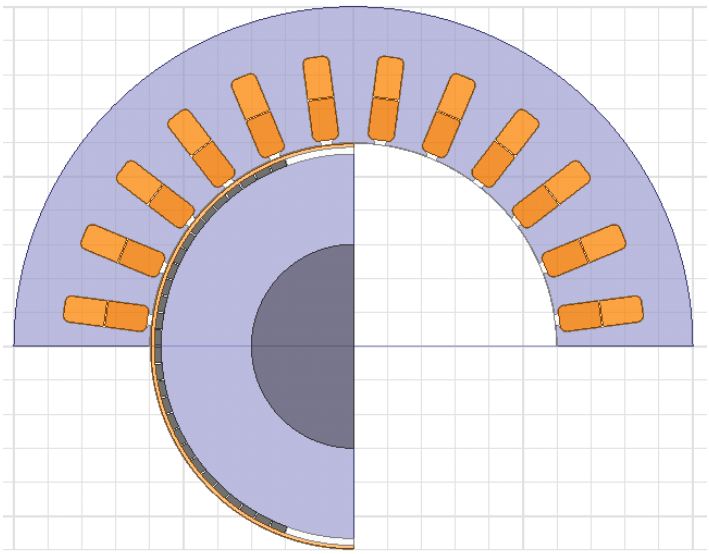

Figure 6: Overview of the modified machine with the full reduced winding

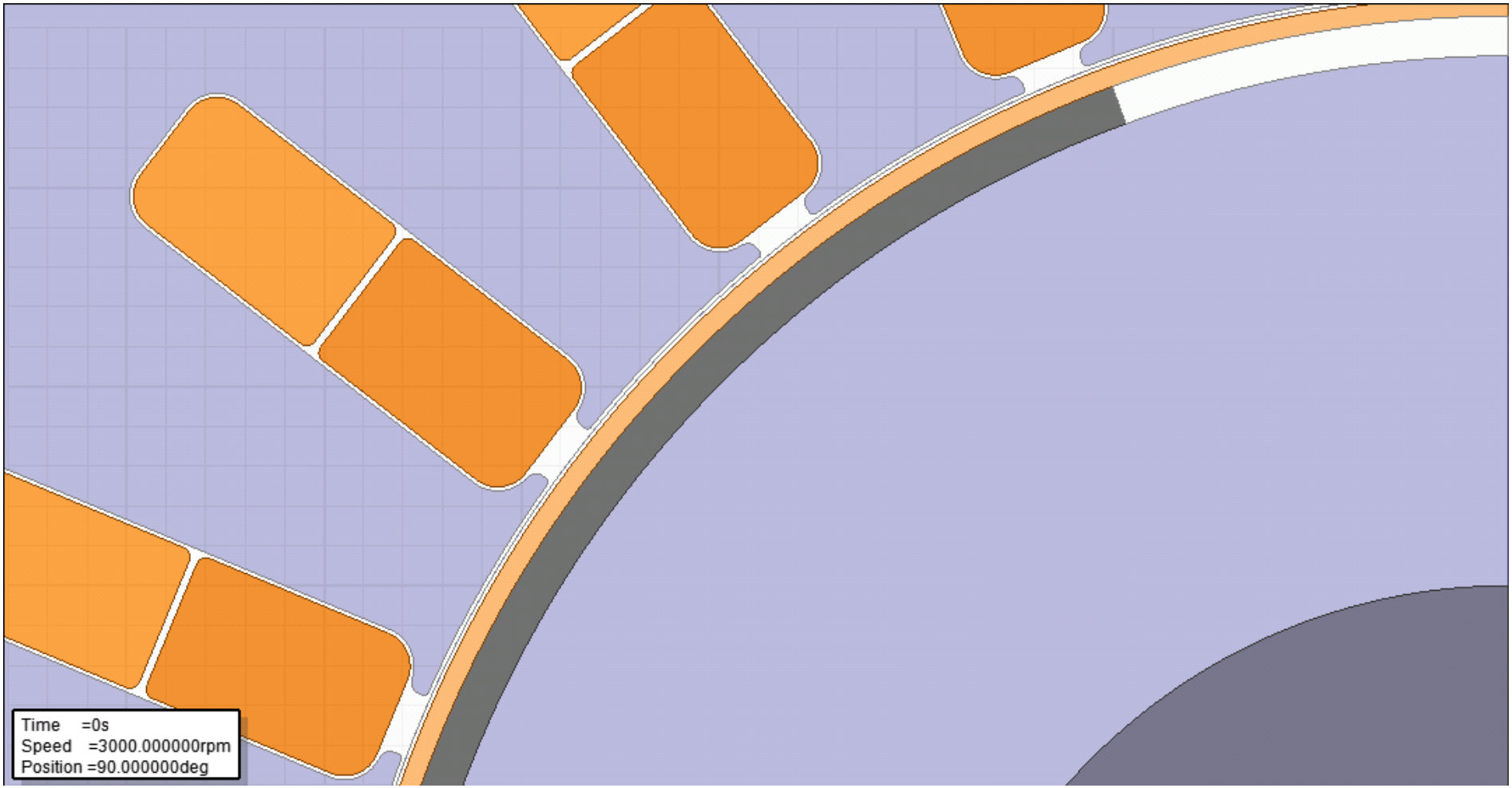

Figure 7: Closeup of the airgap in original machine with the full damper winding

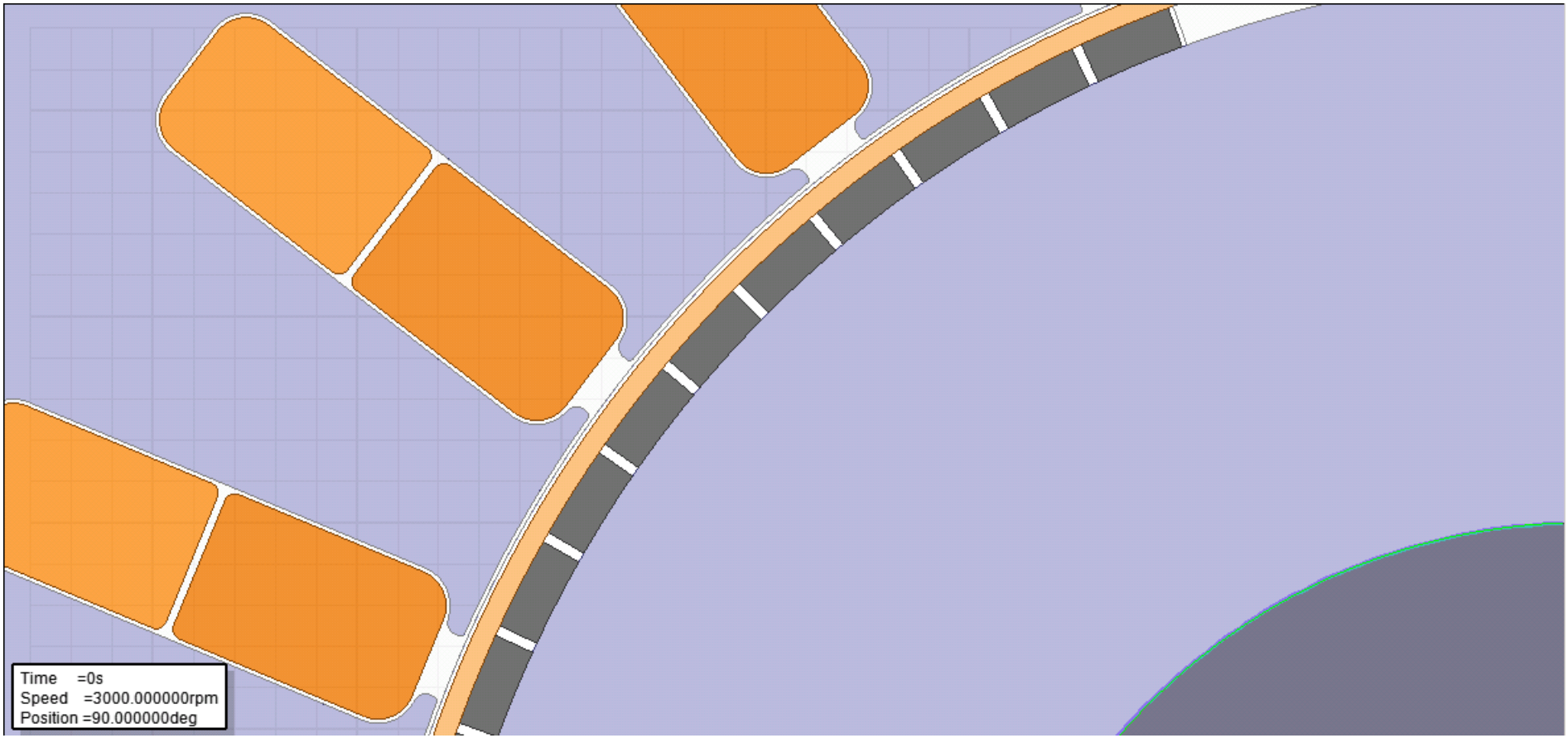

Figure 8: Closeup of the airgap in modified machine with the reduced damper winding

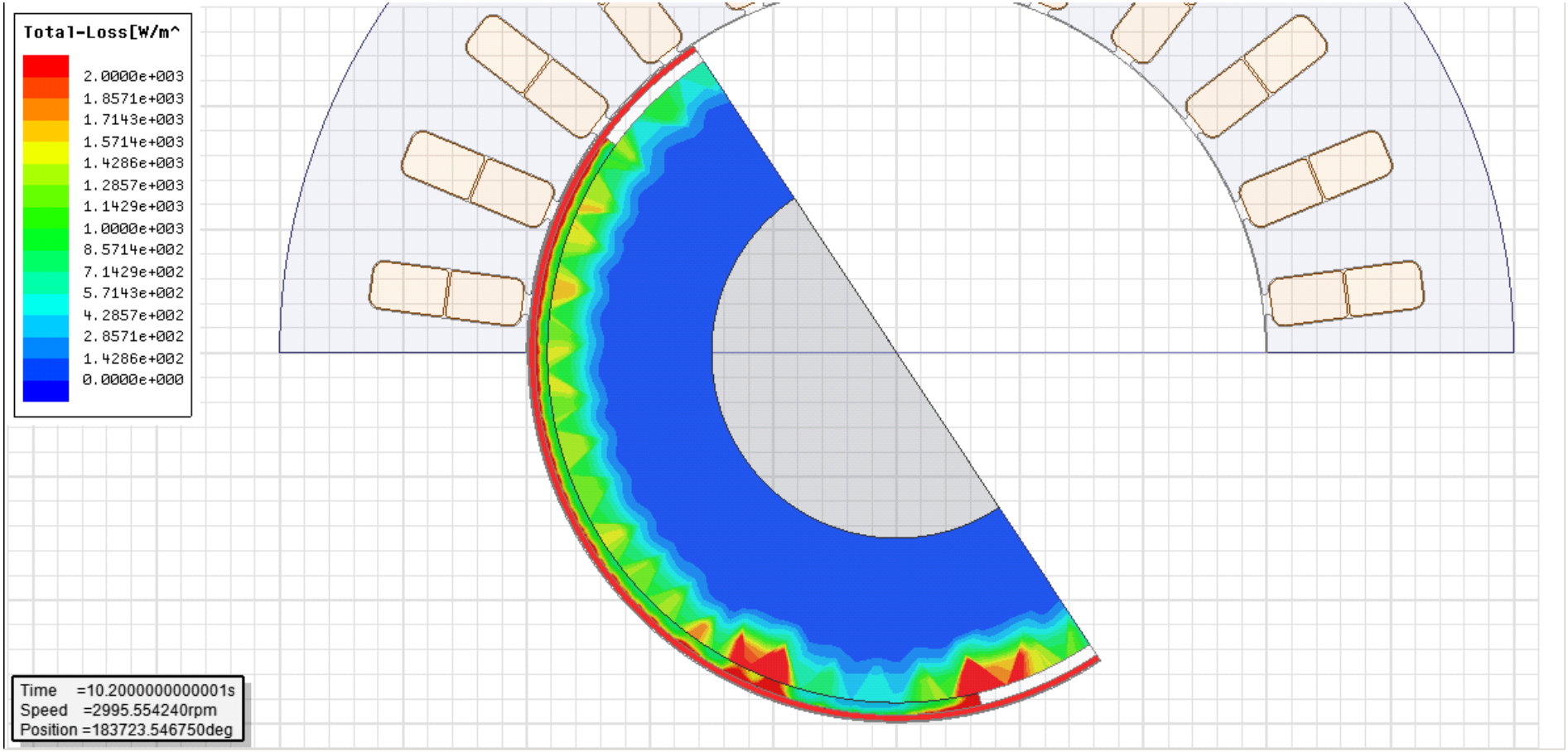

Figure 9: Total losses in the rotor assembly in original machine with the full damper winding

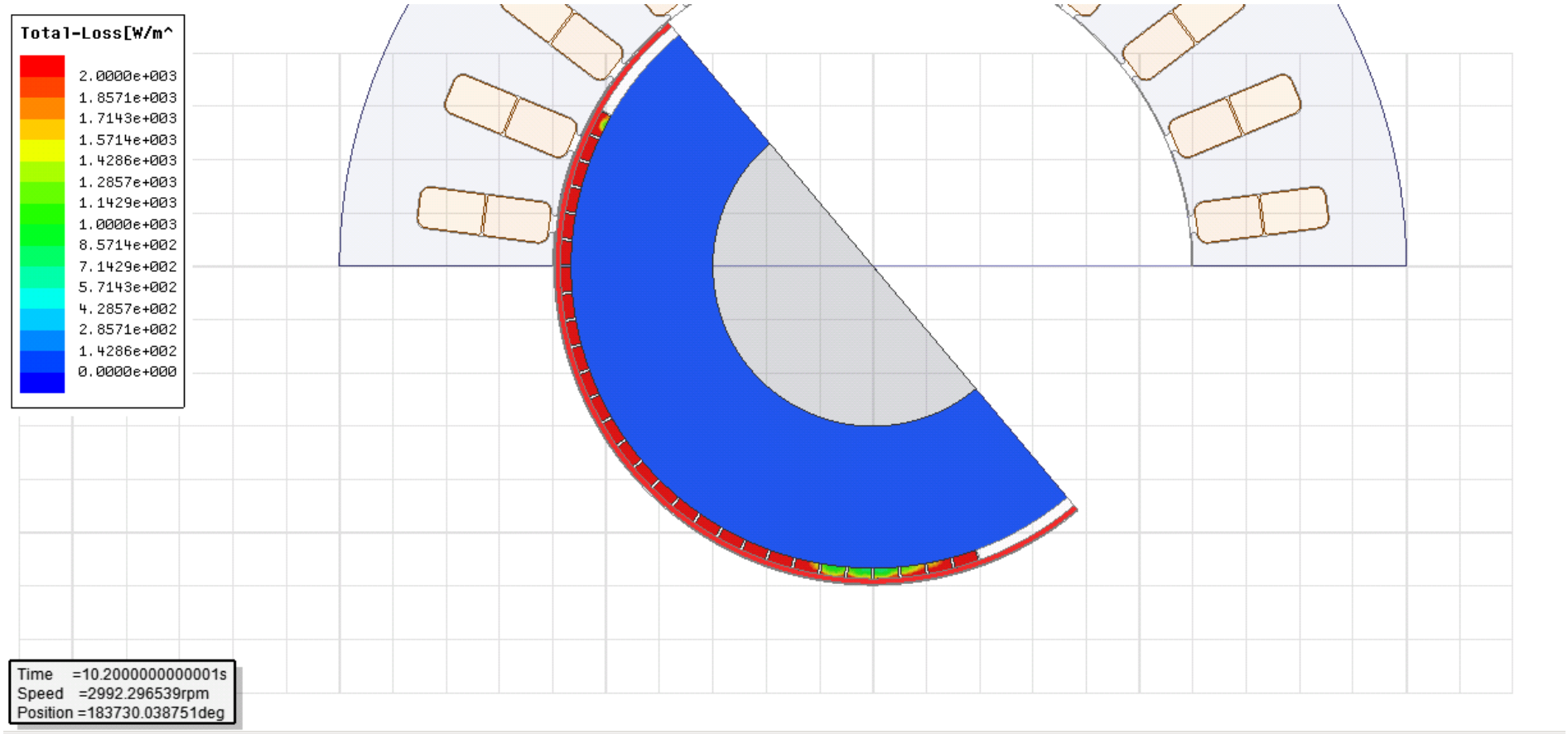

Figure 10: Total losses in the rotor assembly in modified machine with the reduced damper winding

Appendix B; Larger copies of all figures used in this thesis

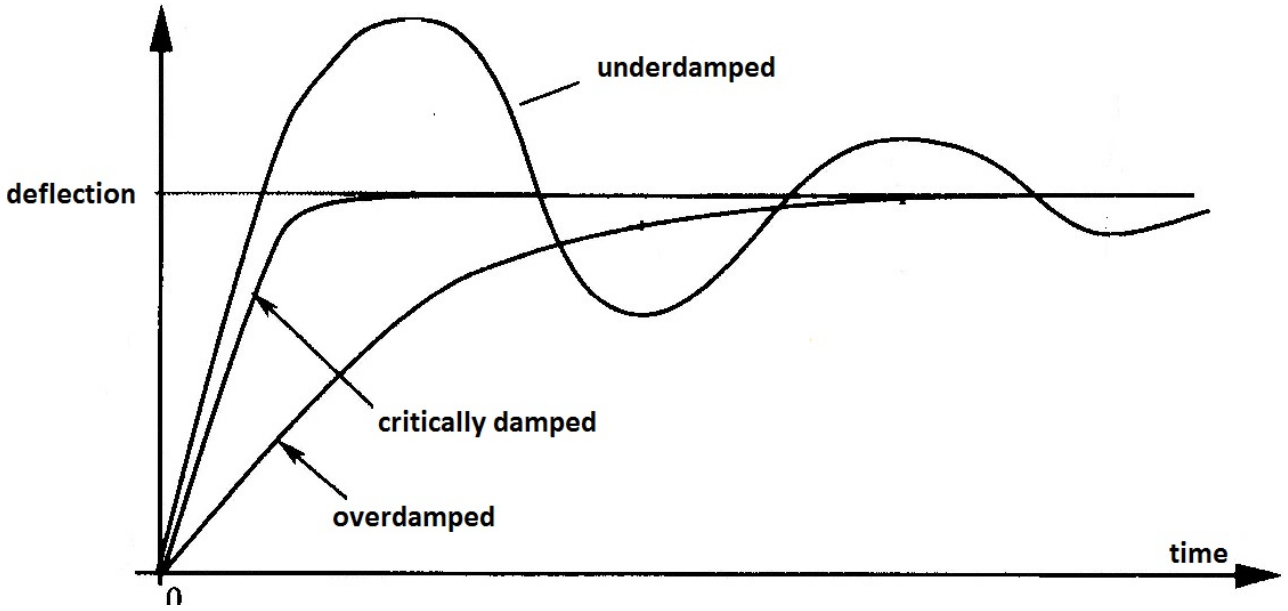

Figure 1: An example of the different cases of damping in a *damped oscillator*. *A critically damped oscillation, an overdamped oscillation* and an *underdamped* oscillation [12].

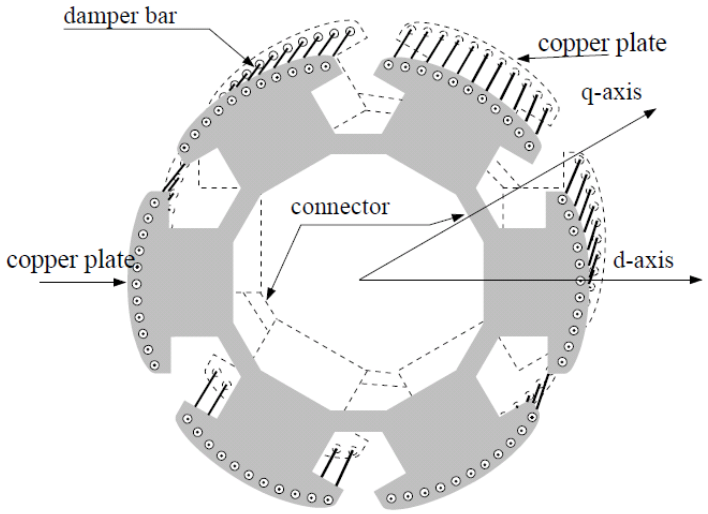

Figure 2: Example of a classical damper winding for a 6 pole salient pole machine [15].

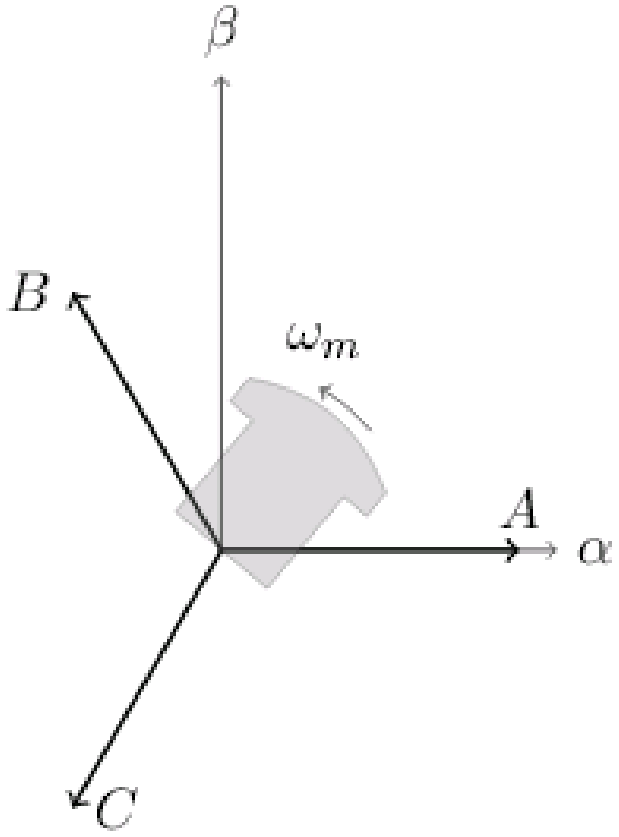

Figure 3: Visualization of the transformation from three phase abc reference frame to two phase $\alpha\beta$ reference frame [23].

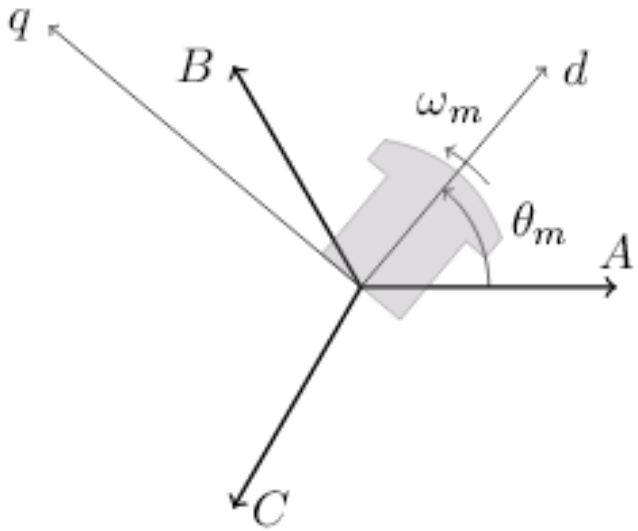

Figure 4: Visualization of the transformation from dq reference frame to two phase $\alpha\beta$ reference frame [23].

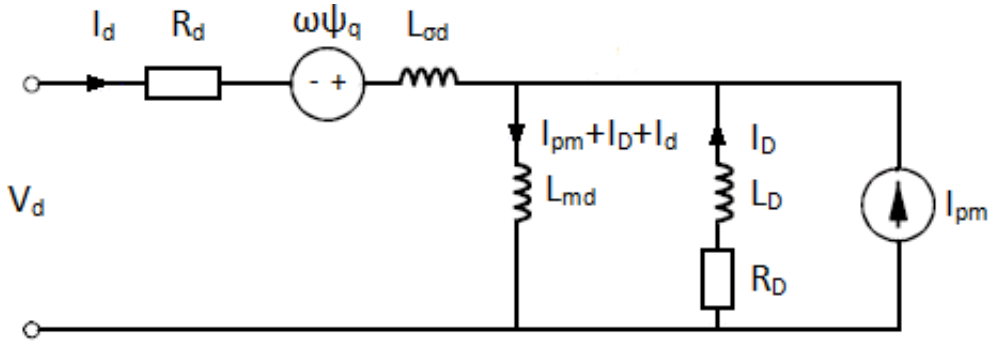

Figure 5: Direct axis equivalent circuit.

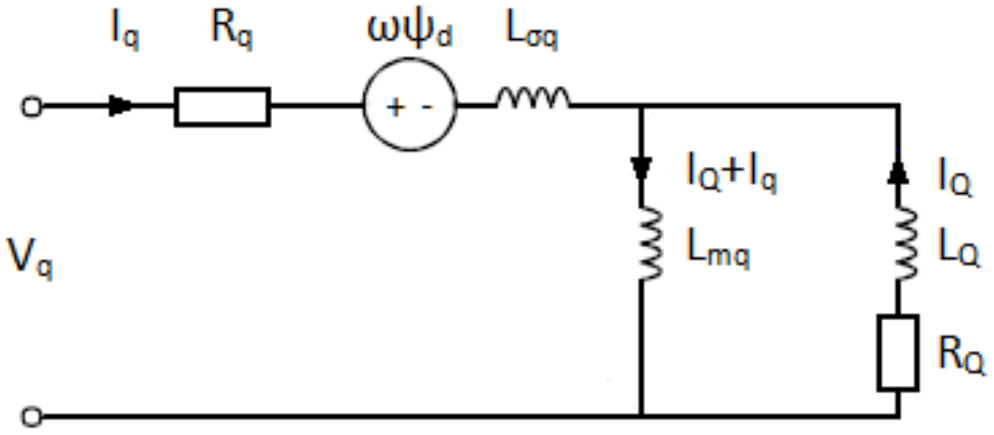

Figure 6: Quadrature axis equivalent circuit.

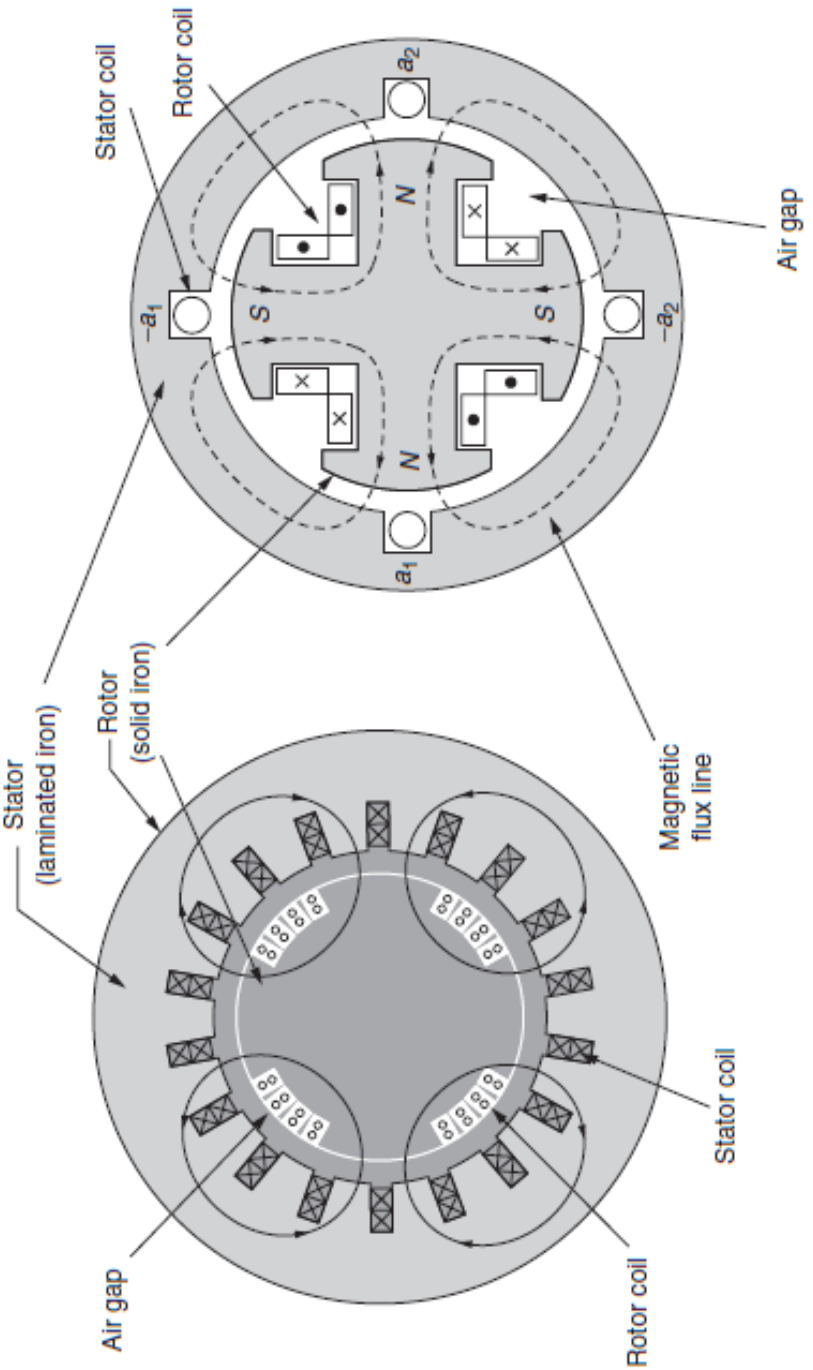

Figure 7: A non-salient pole machine and a salient pole machine [22].

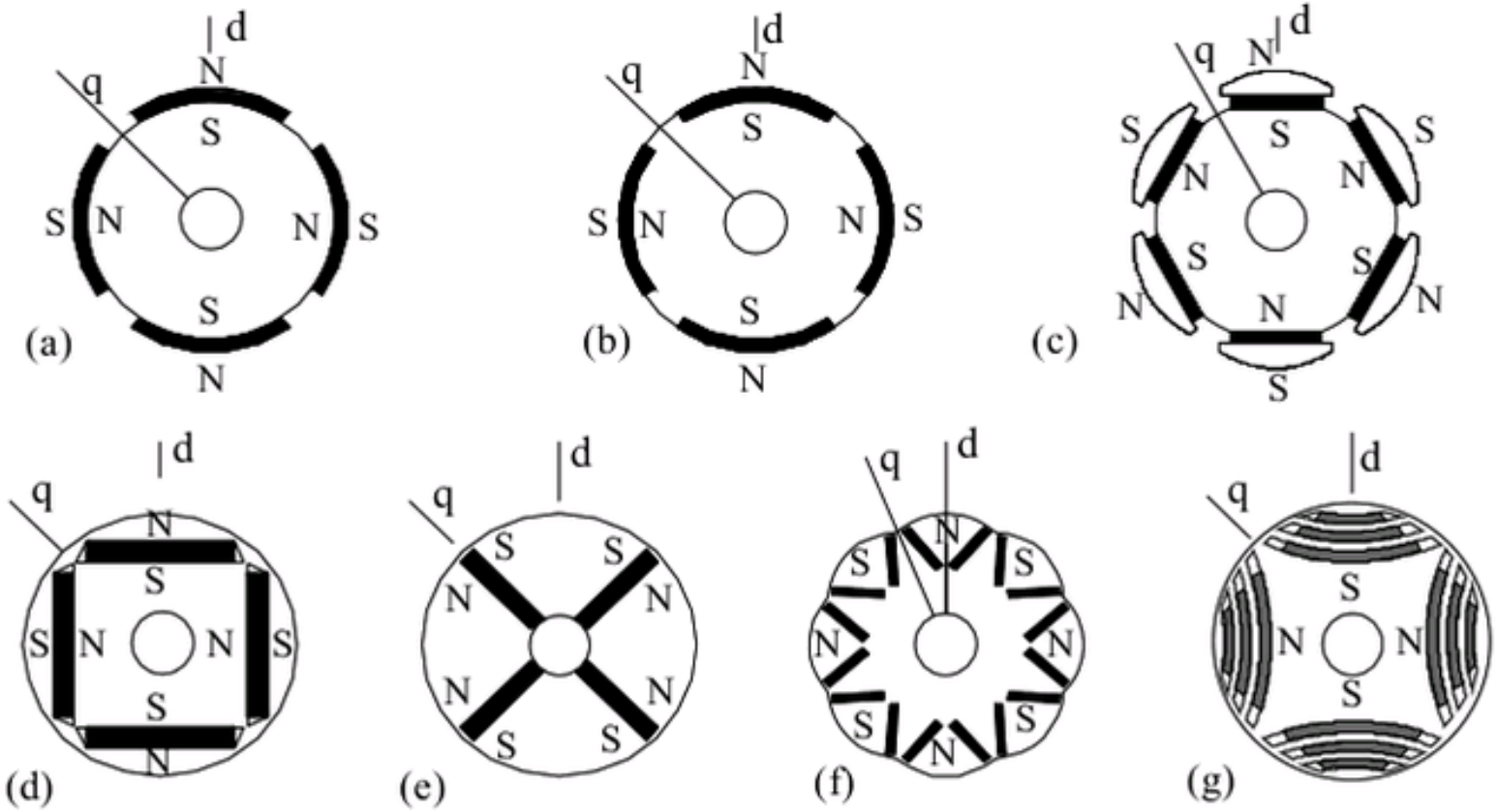

Figure 8: Examples of different rotor configurations in permanent magnet machines. a) shows an example surface mounted pm b) shows an example of inserted pm, c) d) e) f) and g) show various examples of interior pm [23].

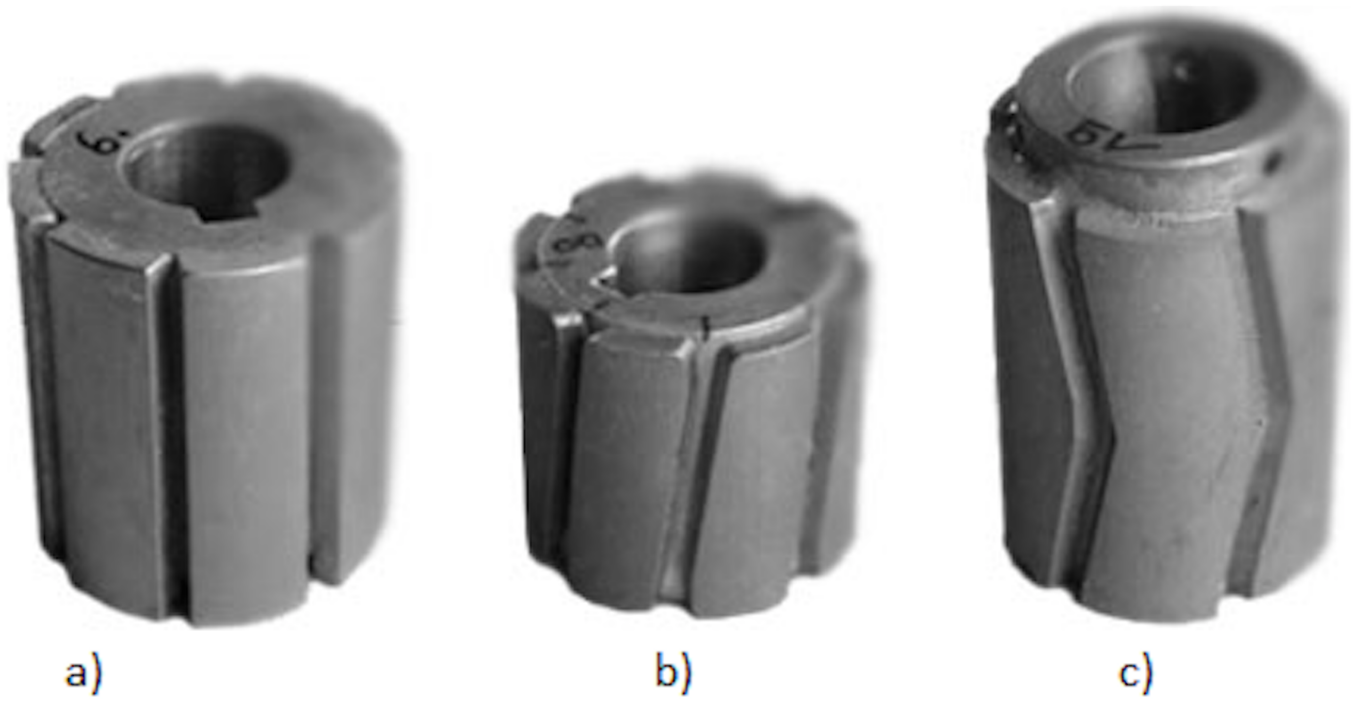

Figure 9: Different types of skewing. a) No skewing b) Unidirectional skew c) V skew [24].

Slot #	1	2	3	4	5	6	7	8	9	10	11	12	13	14	15	16	17	18	19	20	21	22	23	24
Phase R	R	R	R	R									-R	-R	-R	-R								
Phase S									S	S	S	S									-S	-S	-S	-S
Phase T					-T	-T	-T	-T									T	T	T	T				
RST	R	R	R	R	-T	-T	-T	-T	S	S	S	S	-R	-R	-R	-R	T	T	T	T	-S	-S	-S	-S
Bottom	R	R	R	R	-T	-T	-T	-T	S	S	S	S	-R	-R	-R	-R	T	T	T	T	-S	-S	-S	-S
SingleP																								

Figure 10: Layout of the windings in the machine [28].

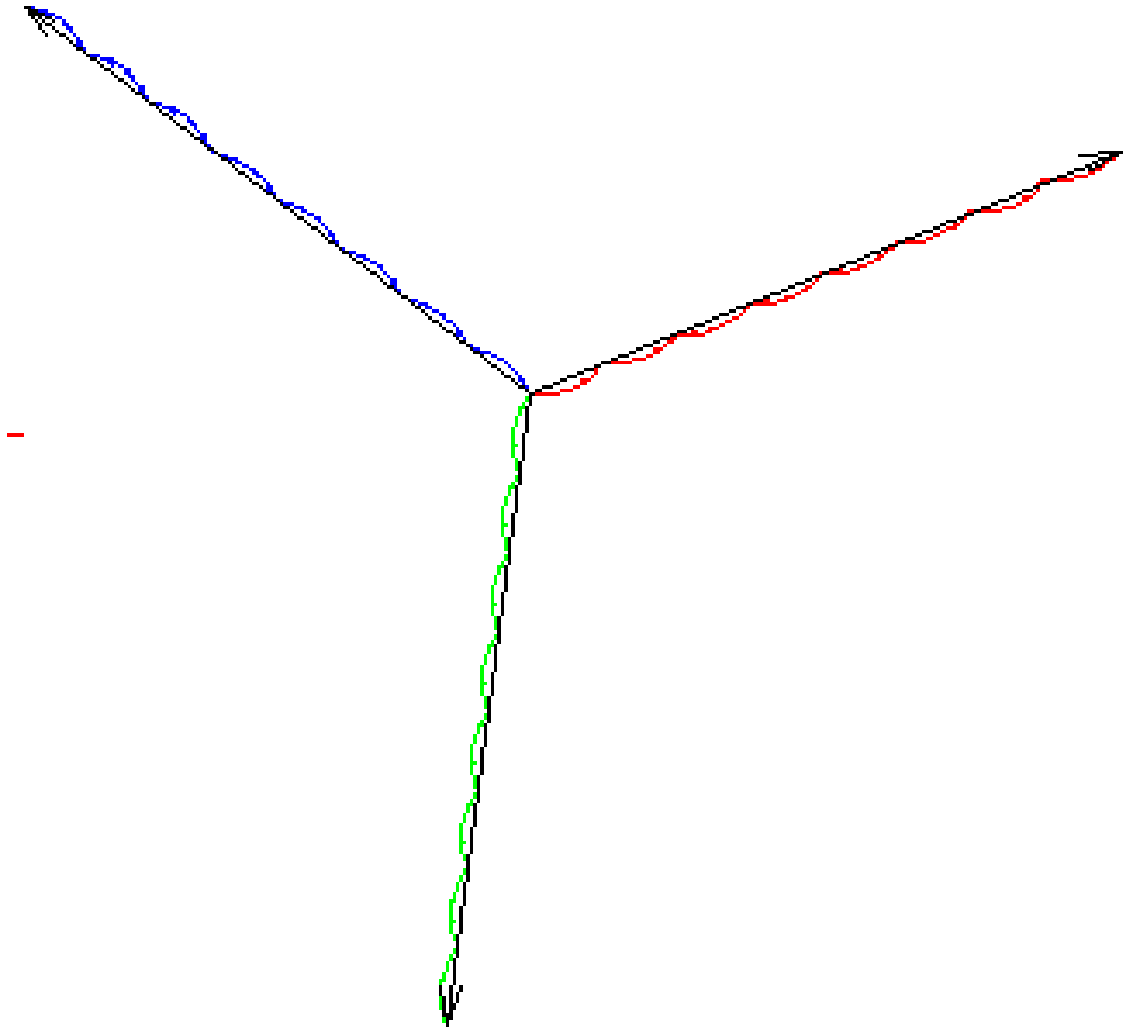

Figure 11: Resultant phase voltages in the stator [28].

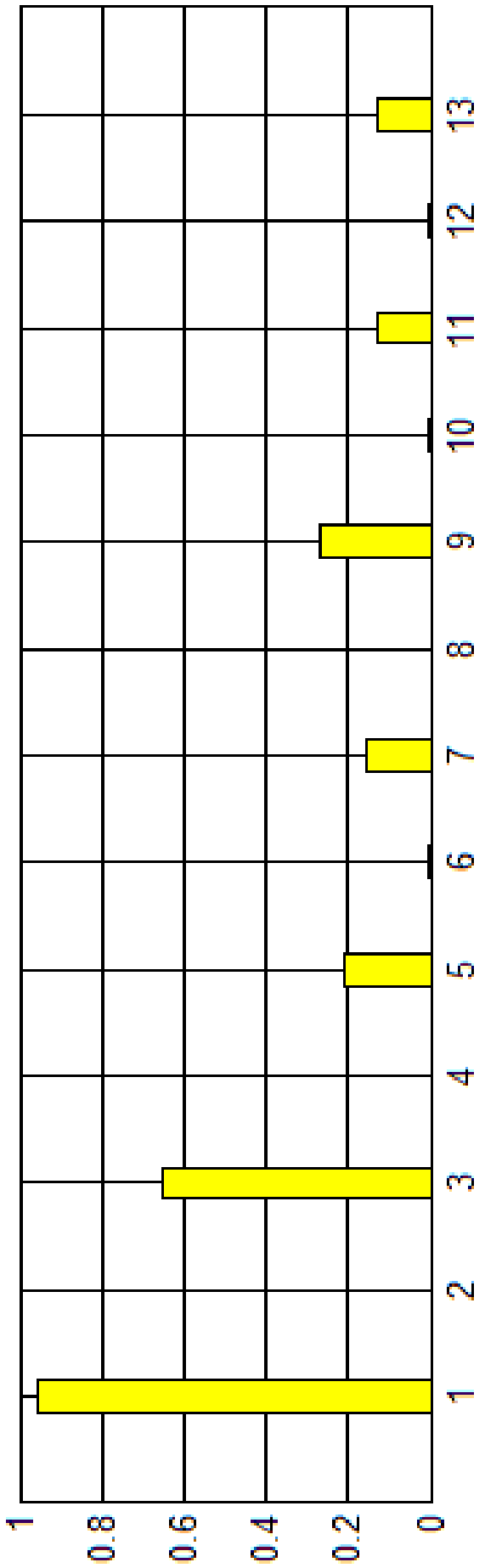

Figure 12: The harmonic content in the air-gap of the investigated machine [28].

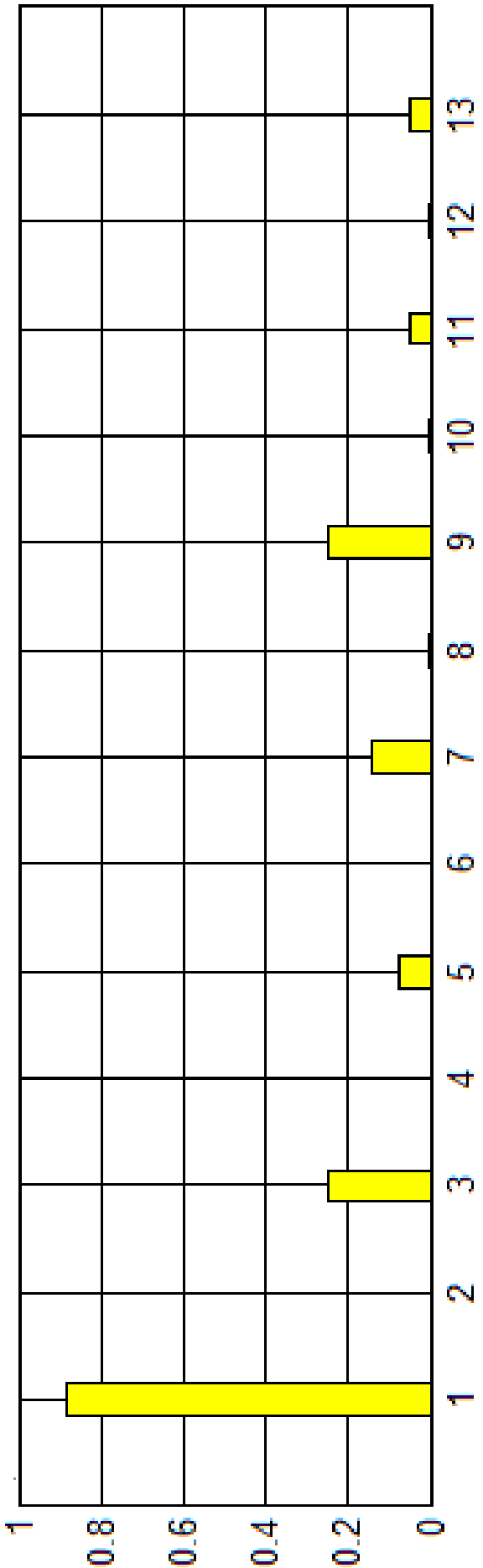

Figure 13: The harmonic content if the windings were short-pitched by 45° [28].

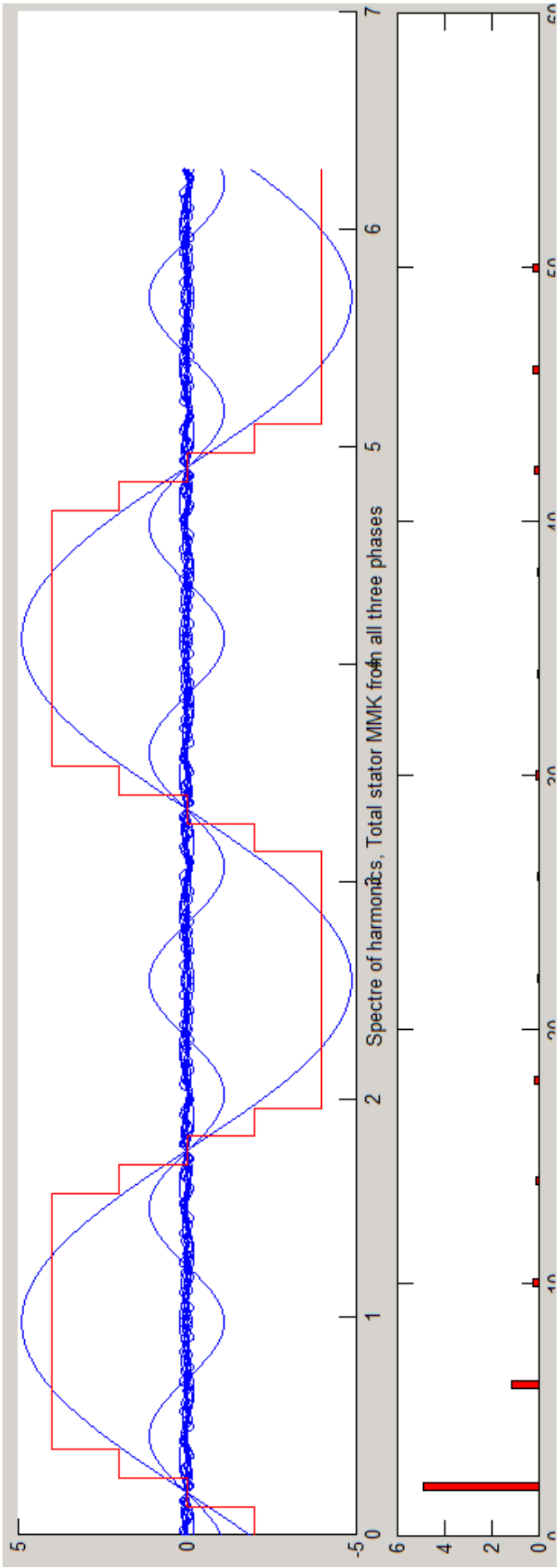

Figure 14: The harmonic MMF content in a phase in the machine [28].

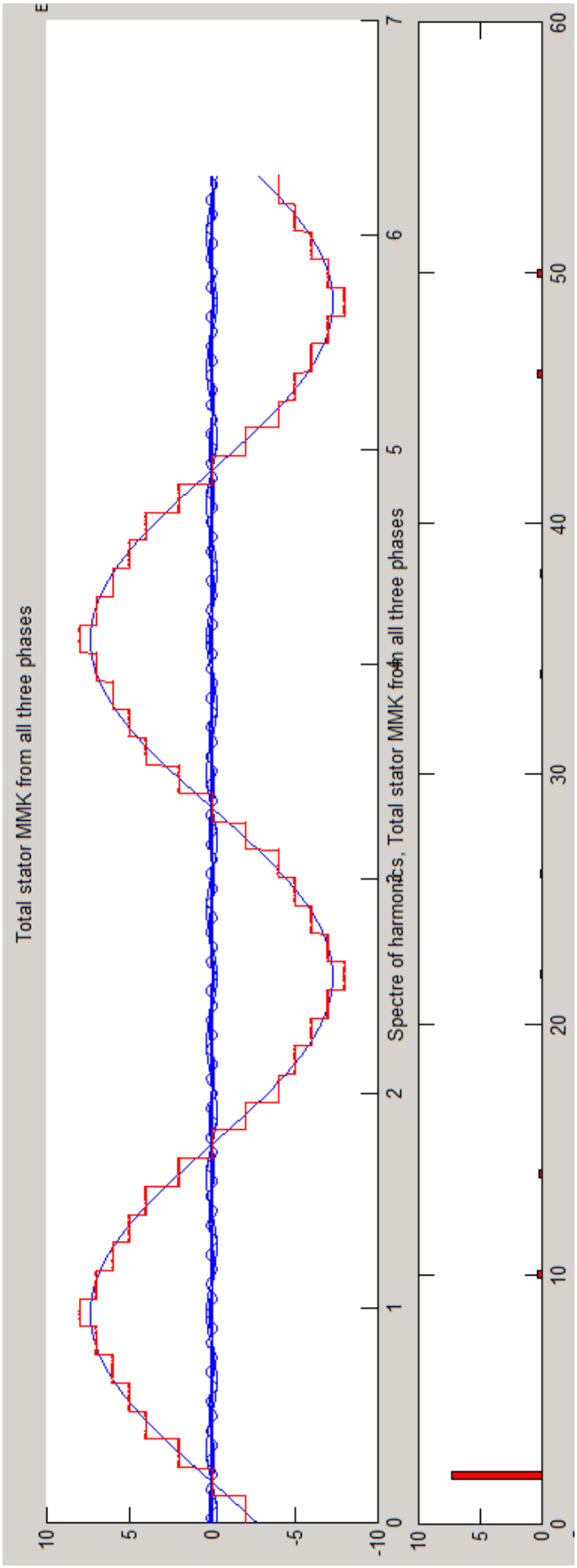

Figure 15: The harmonic MMF content in a line in the machine [28].

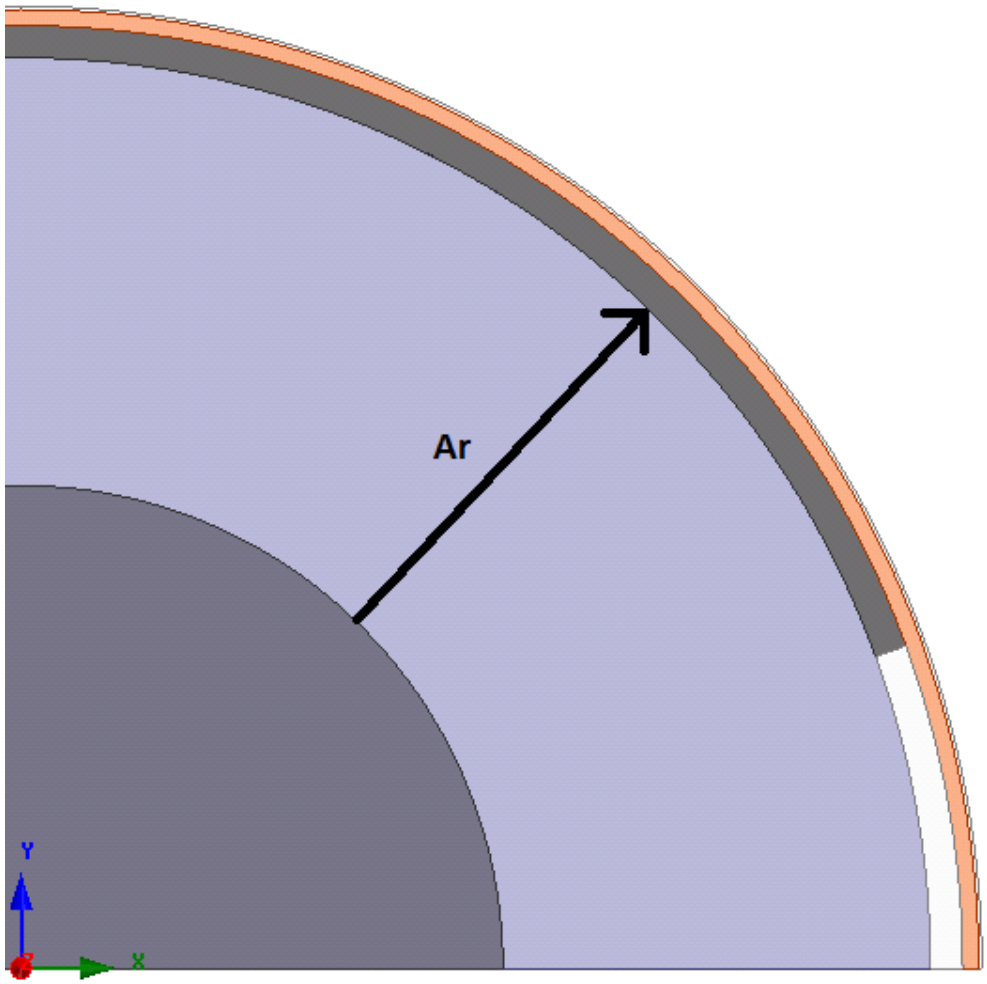

Figure 16: A quarter of the rotor design.

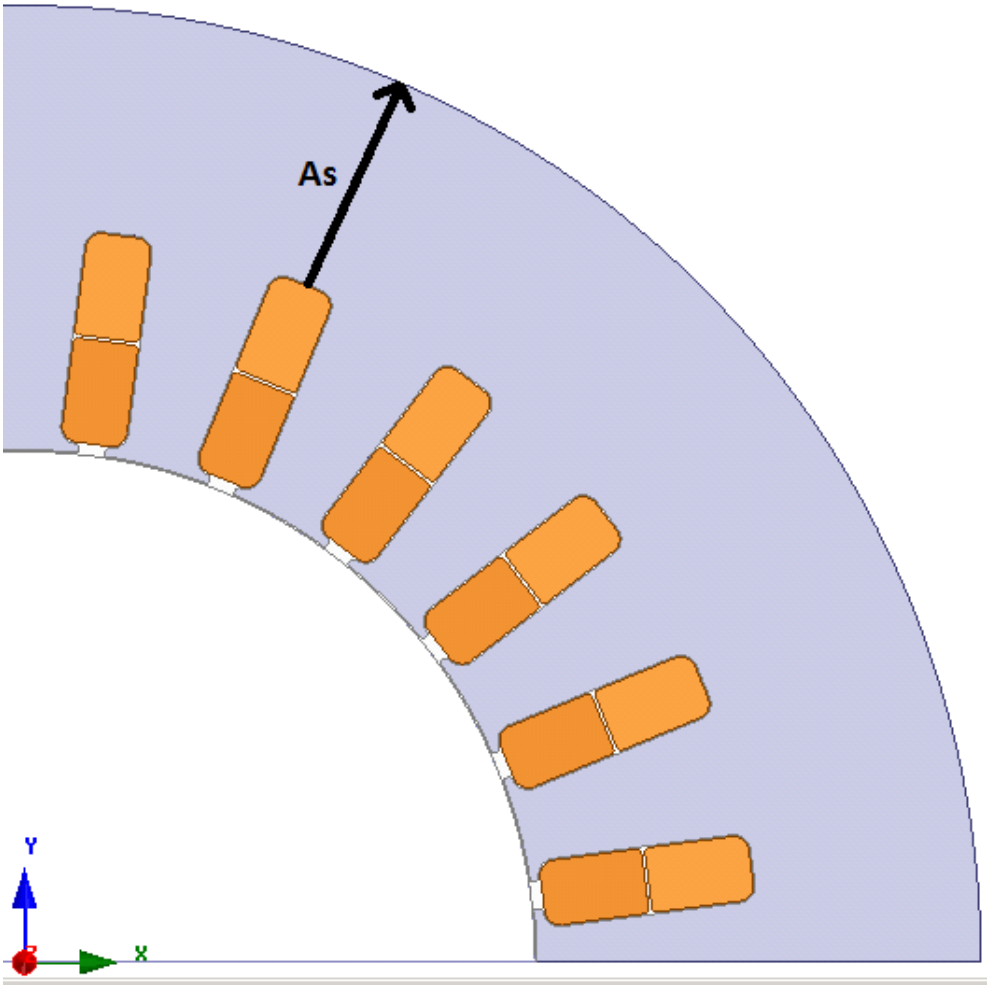

Figure 17: A quarter of the stator design.

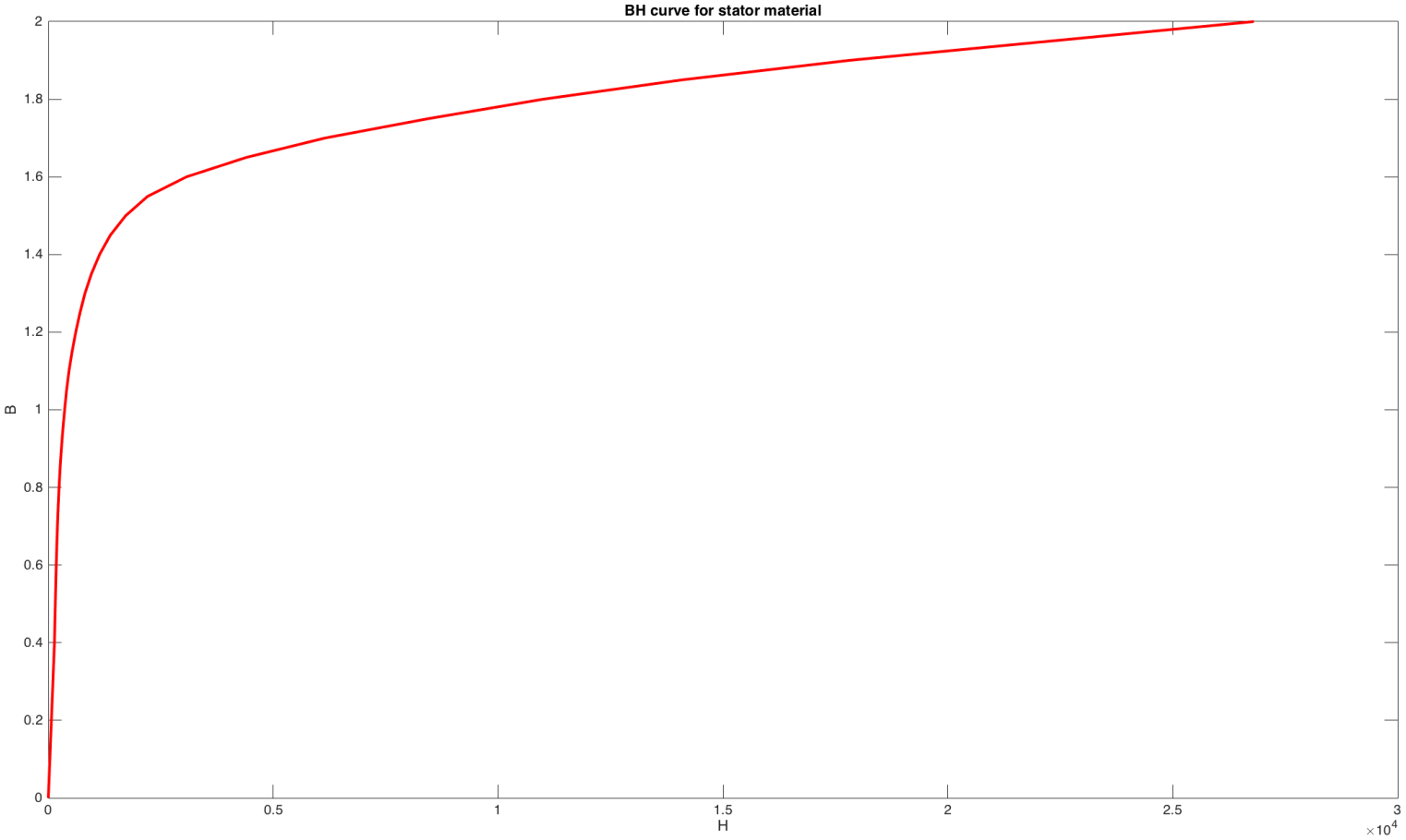

Figure 18: BH curve for the stator and rotor material.

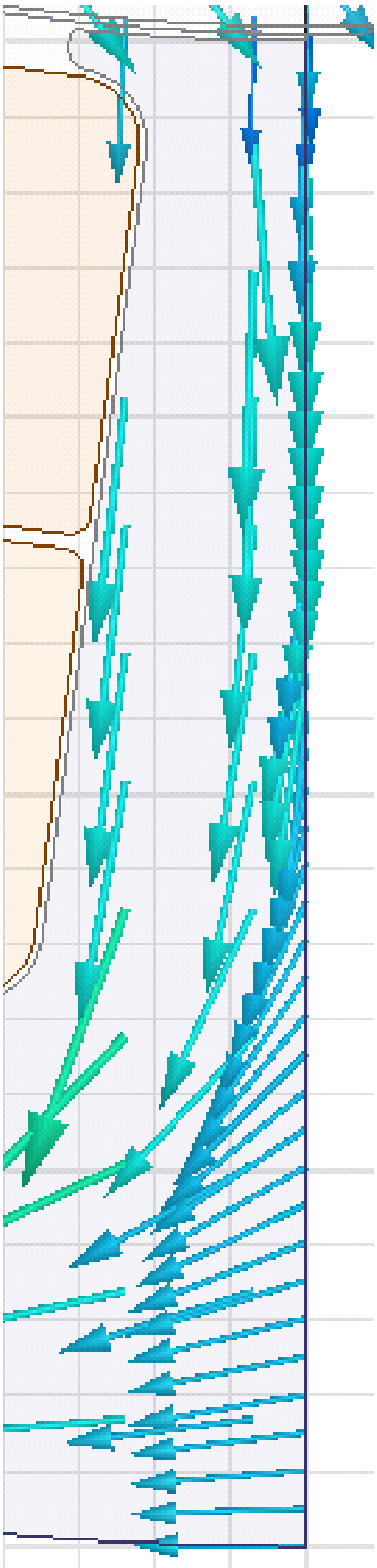

Figure 19: Flux density on master boundary.

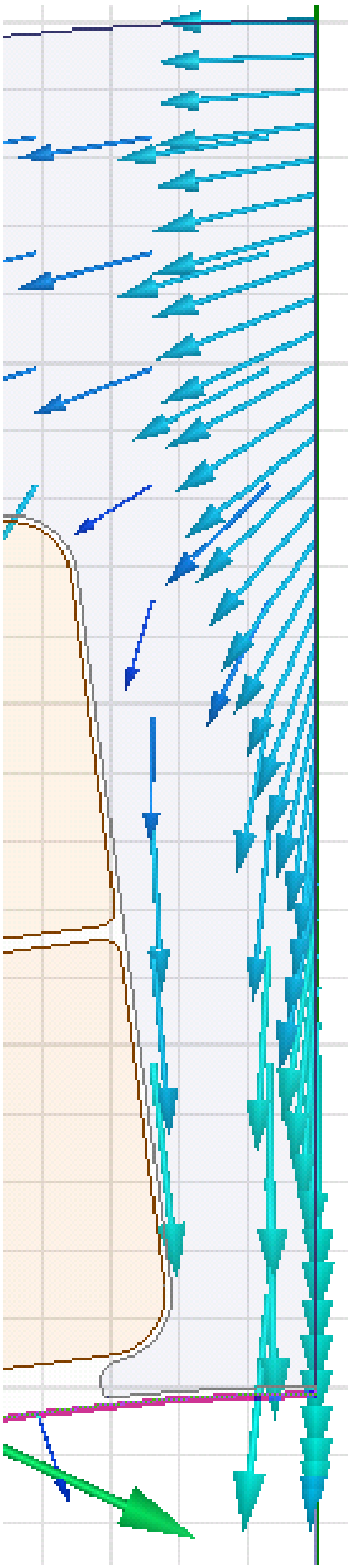

Figure 20: Flux density on the slave boundary.

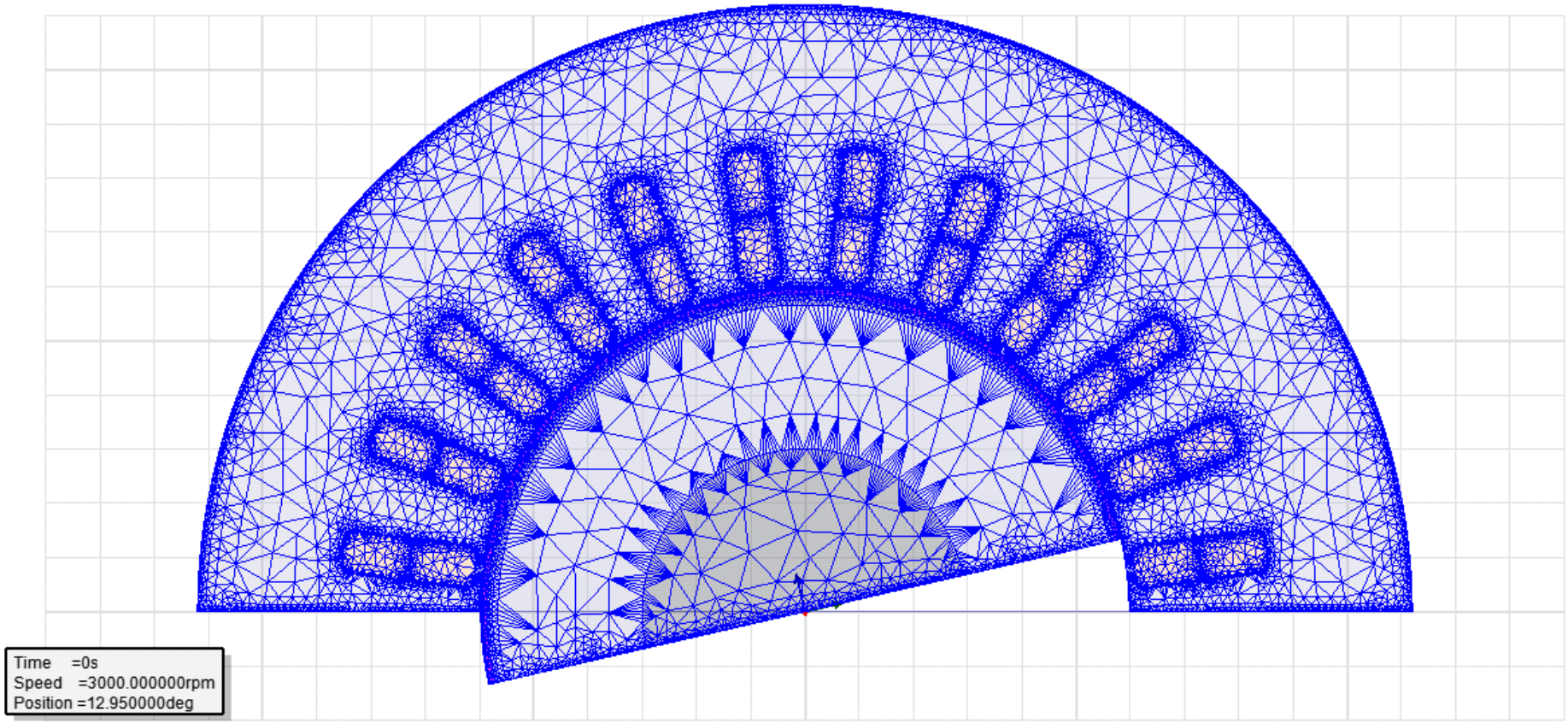

Figure 21: An overview of the mesh in the machine.

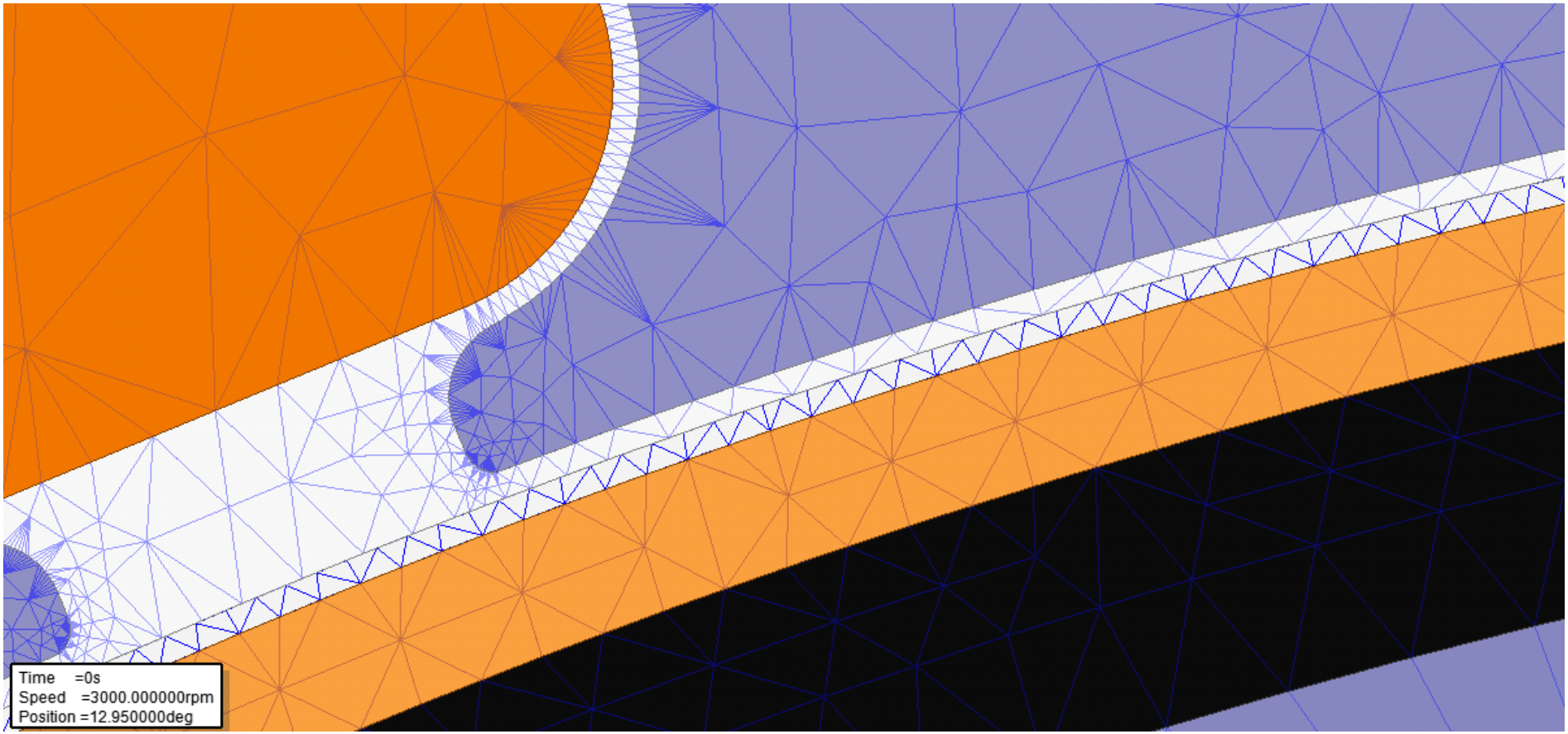

Figure 22: Closeup of the mesh in the air-gap and damper winding of the machine.

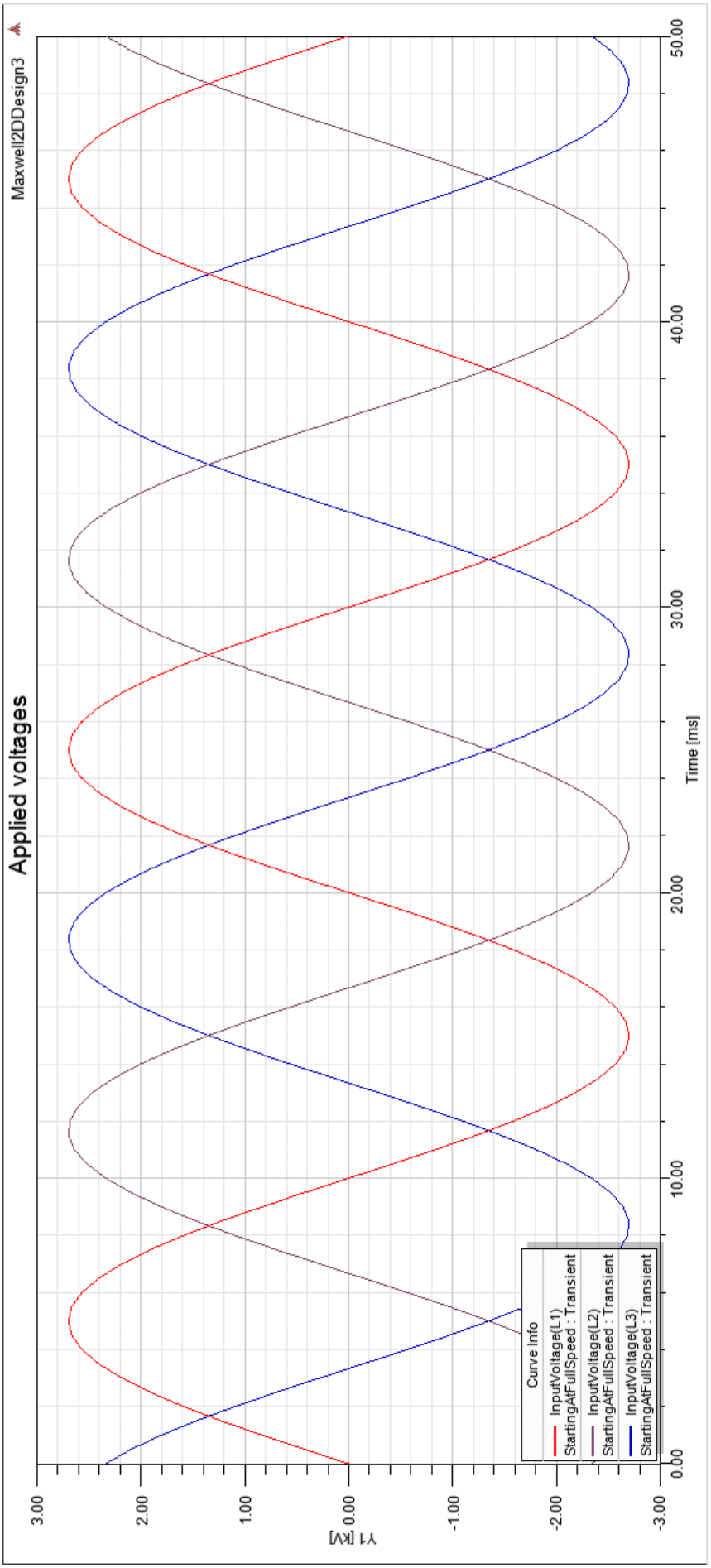

Figure 23: The phase voltages applied in all stability test cases.

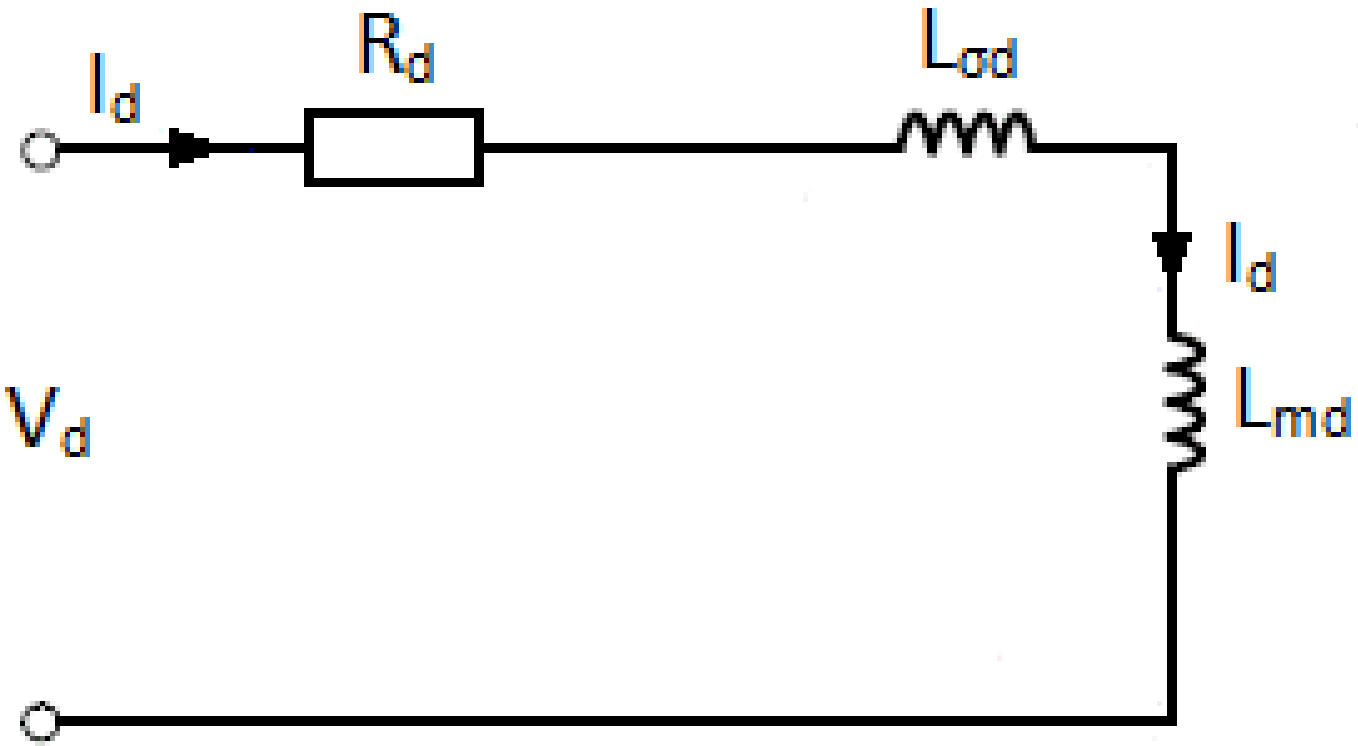

Figure 24: Equivalent circuit for the stator parameter test.

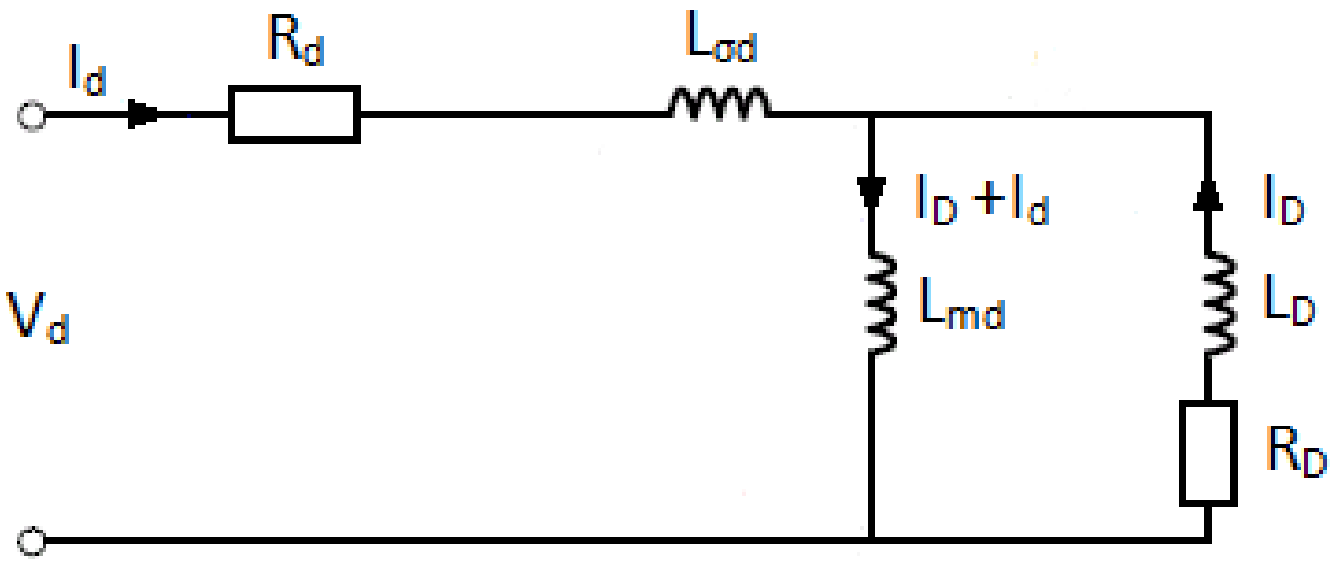

Figure 25: Equivalent circuit for the damper winding parameter test.

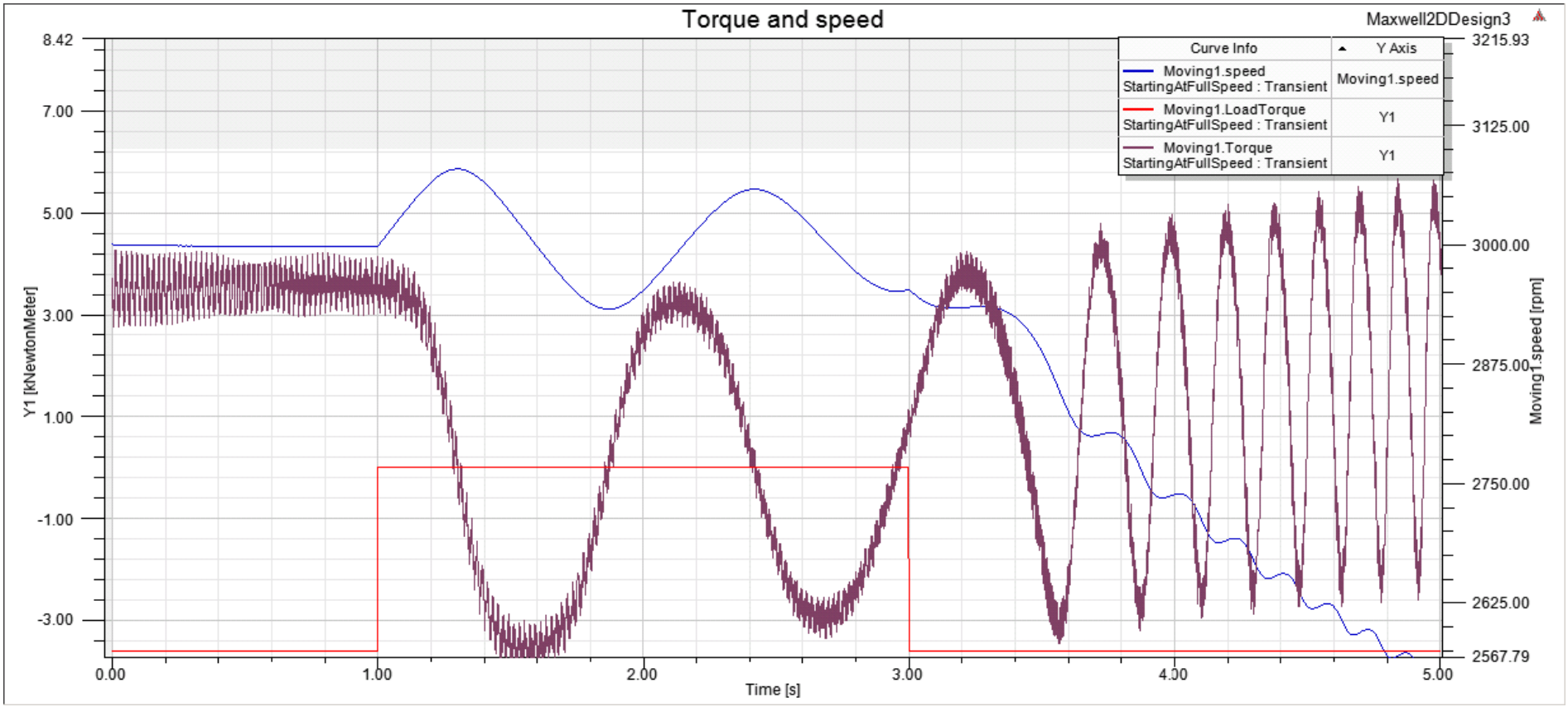

Figure 26: Case A: Rotational speed in blue, load torque in red and produced torque in purple. Loss of load gives oscillations that is not significantly dampened. Shortly after the load comes back on, the machine loses synchronism.

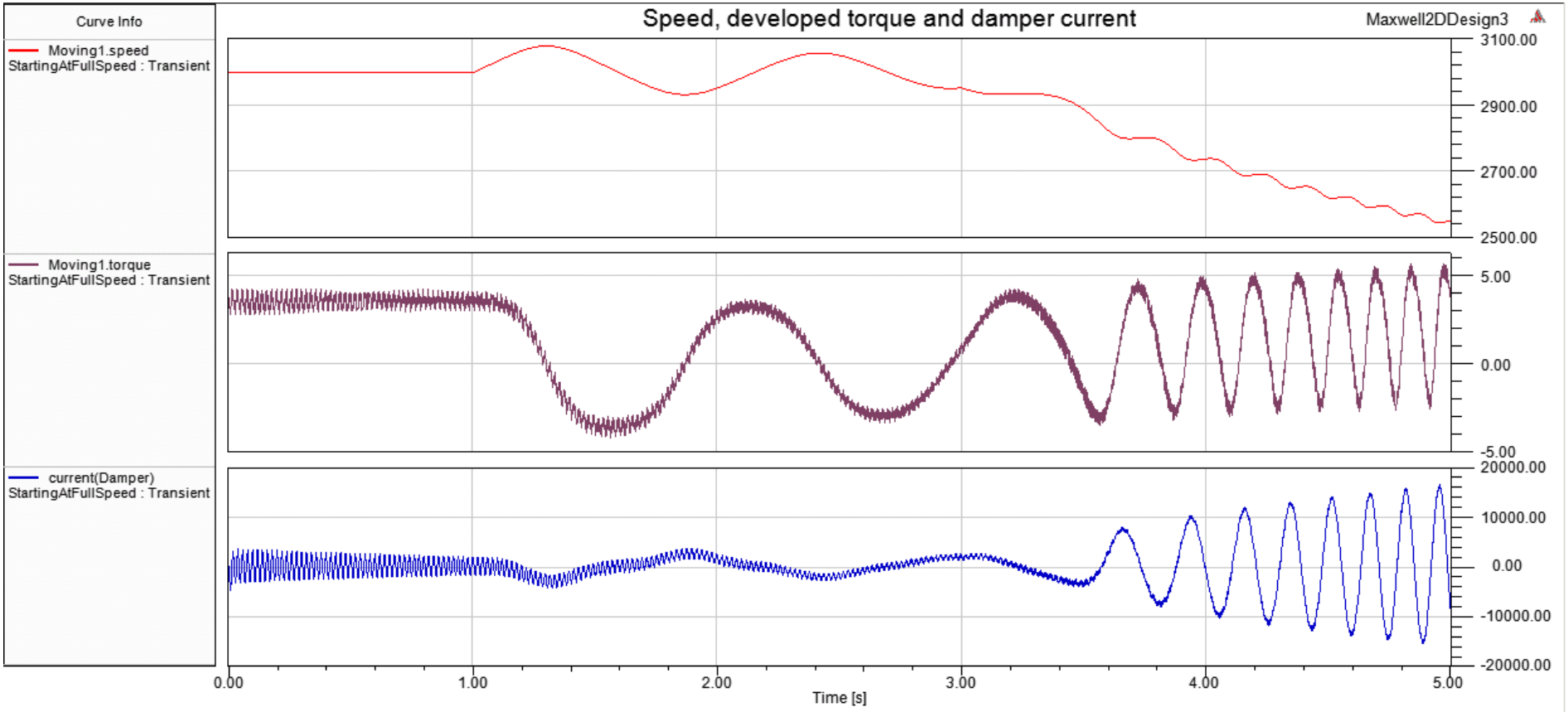

Figure 27: Case A: Rotational speed in red, developed torque in purple and the current in the damper winding in blue. We can see that there is a clear relation between the current in the damper winding, developed torque and the speed of the machine.

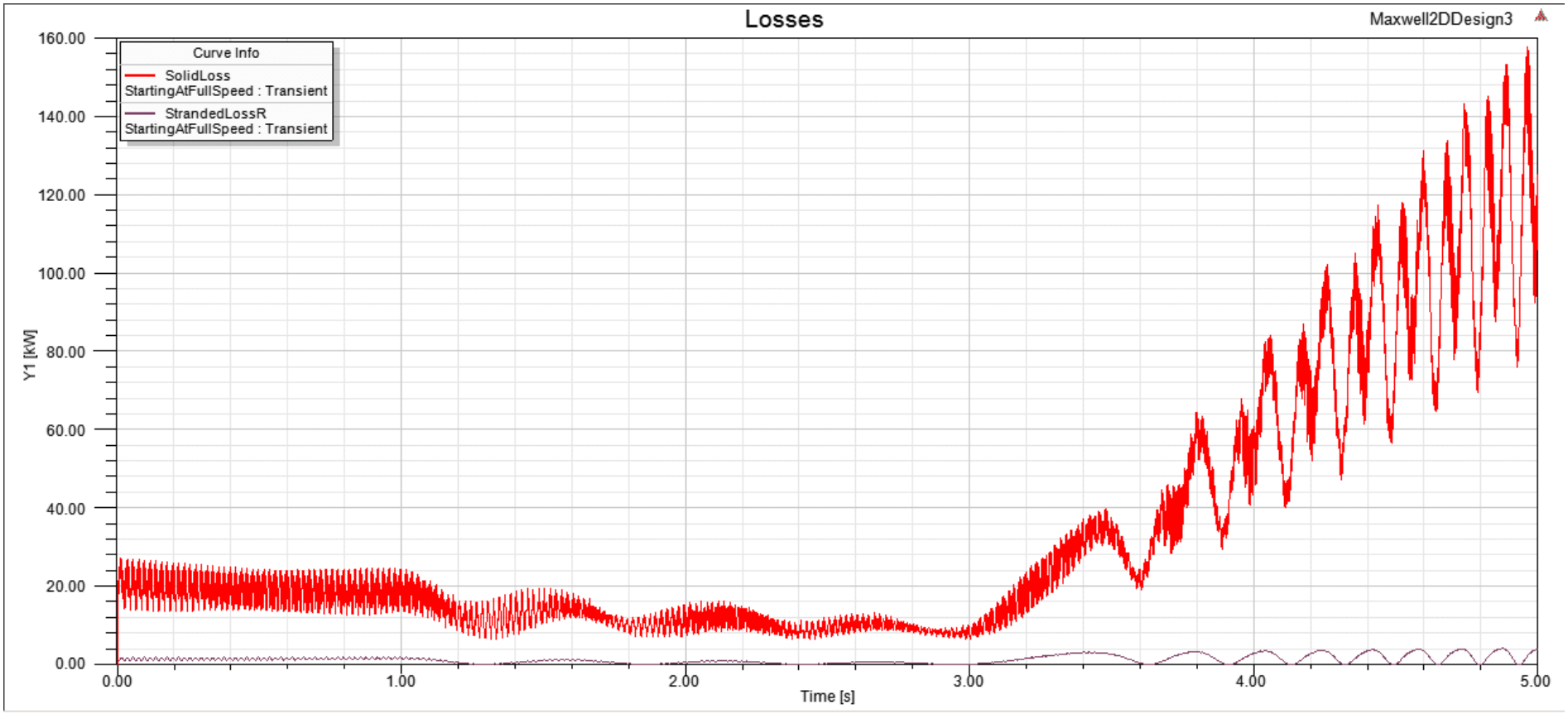

Figure 28: Case A: Losses in the machine. The red line shows the losses in the damper winding, the purple line shows the losses in the stator windings. As we can see, the wast majority of the losses take place in the damper winding.

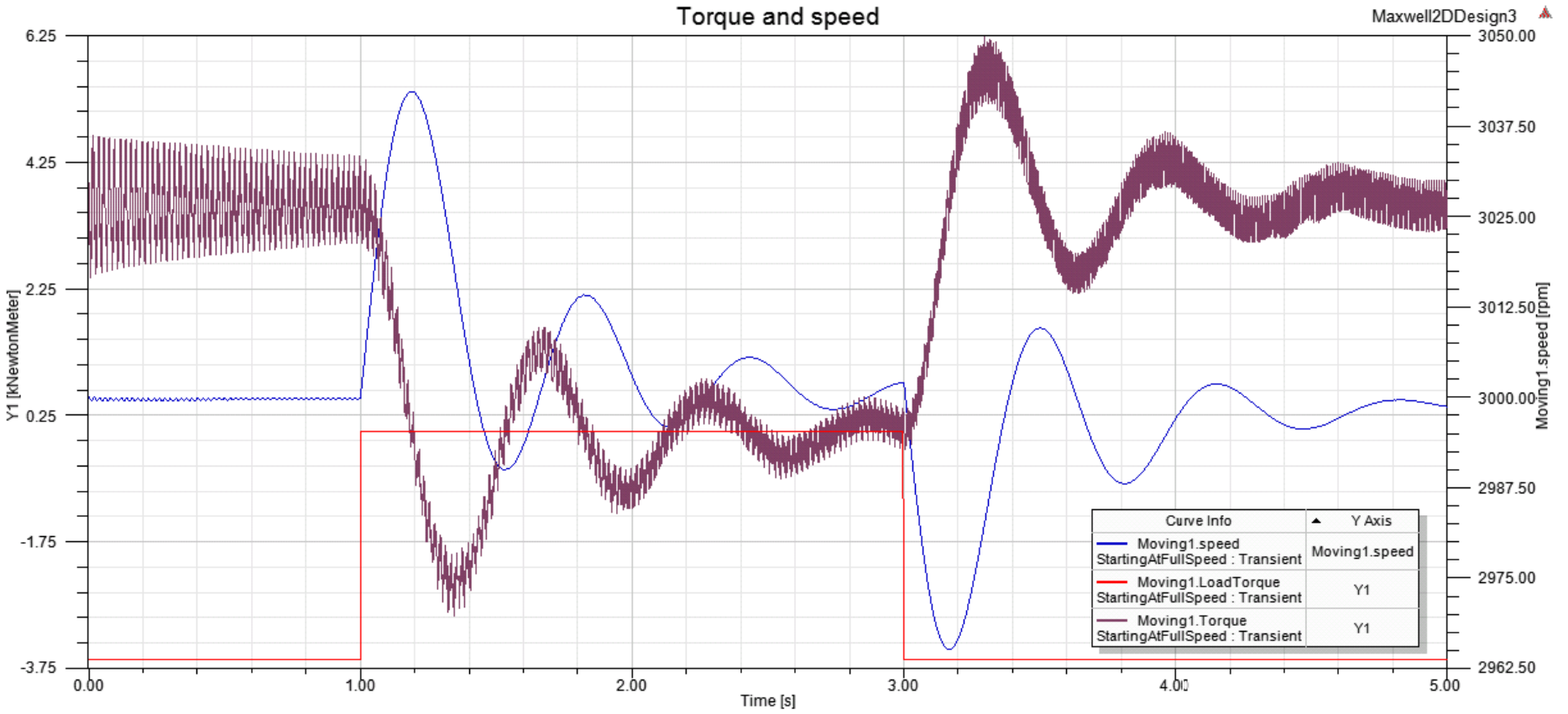

Figure 29: Case B: Rotational speed in blue, load torque in red and produced torque in purple. Loss of load gives oscillations that are dampened to a low amplitude by the time the load comes back on, at which point we get a new oscillation that is also effectively dampened.

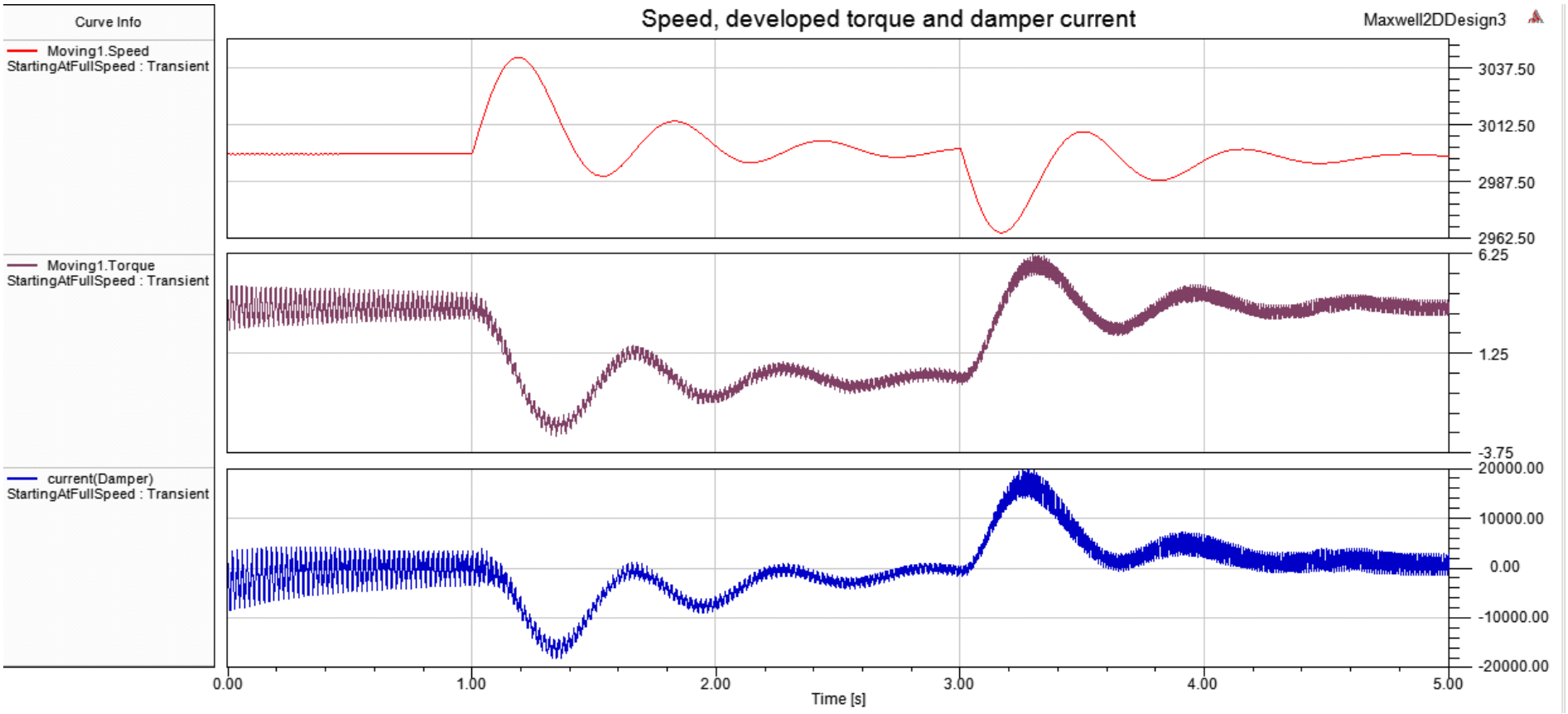

Figure 30: Case B: Rotational speed in red, developed torque in purple and the current in the damper winding in blue. Again there is a clear relation between the current in the damper winding, developed torque and the speed of the machine.

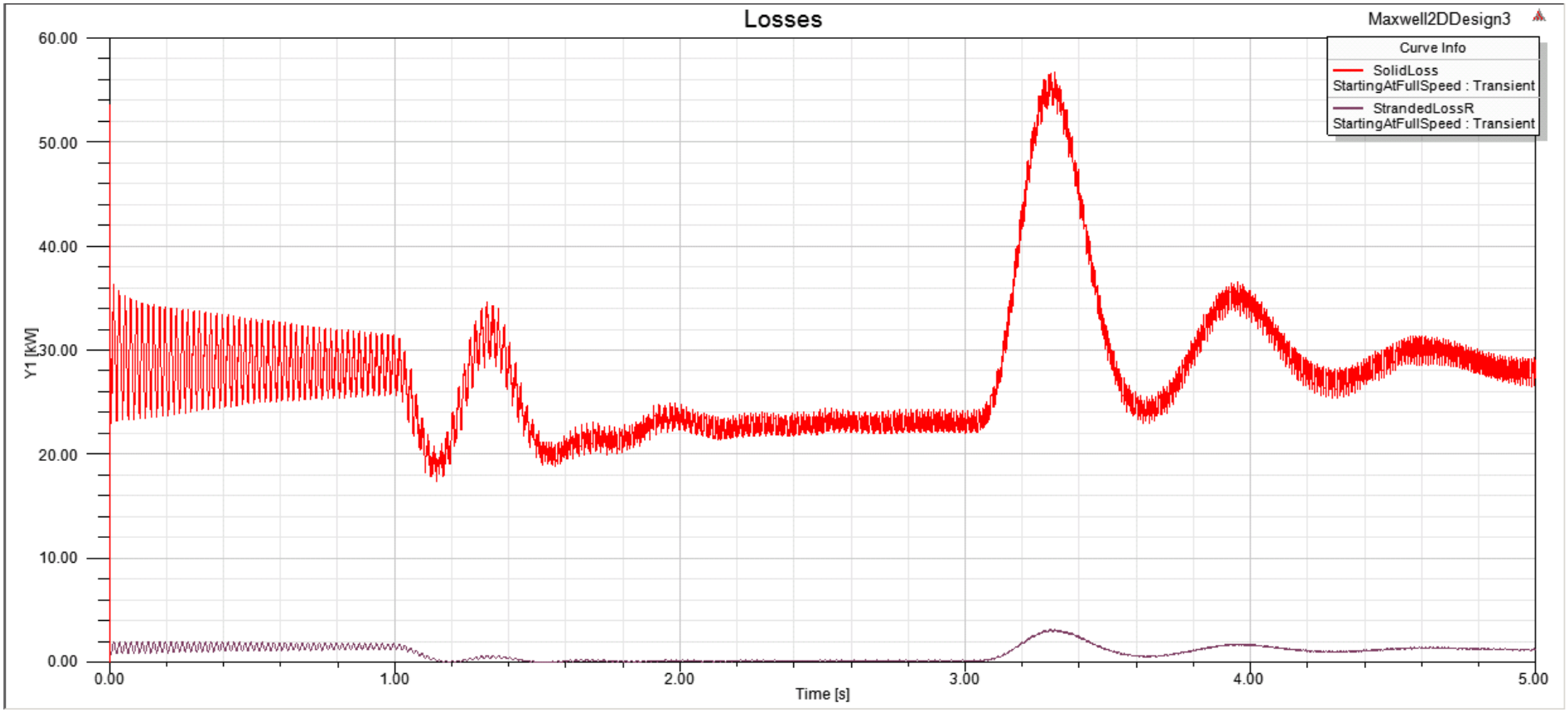

Figure 31: Case B: Losses in the machine. The red line shows the losses in the damper winding, the purple line shows the losses in the stator windings.

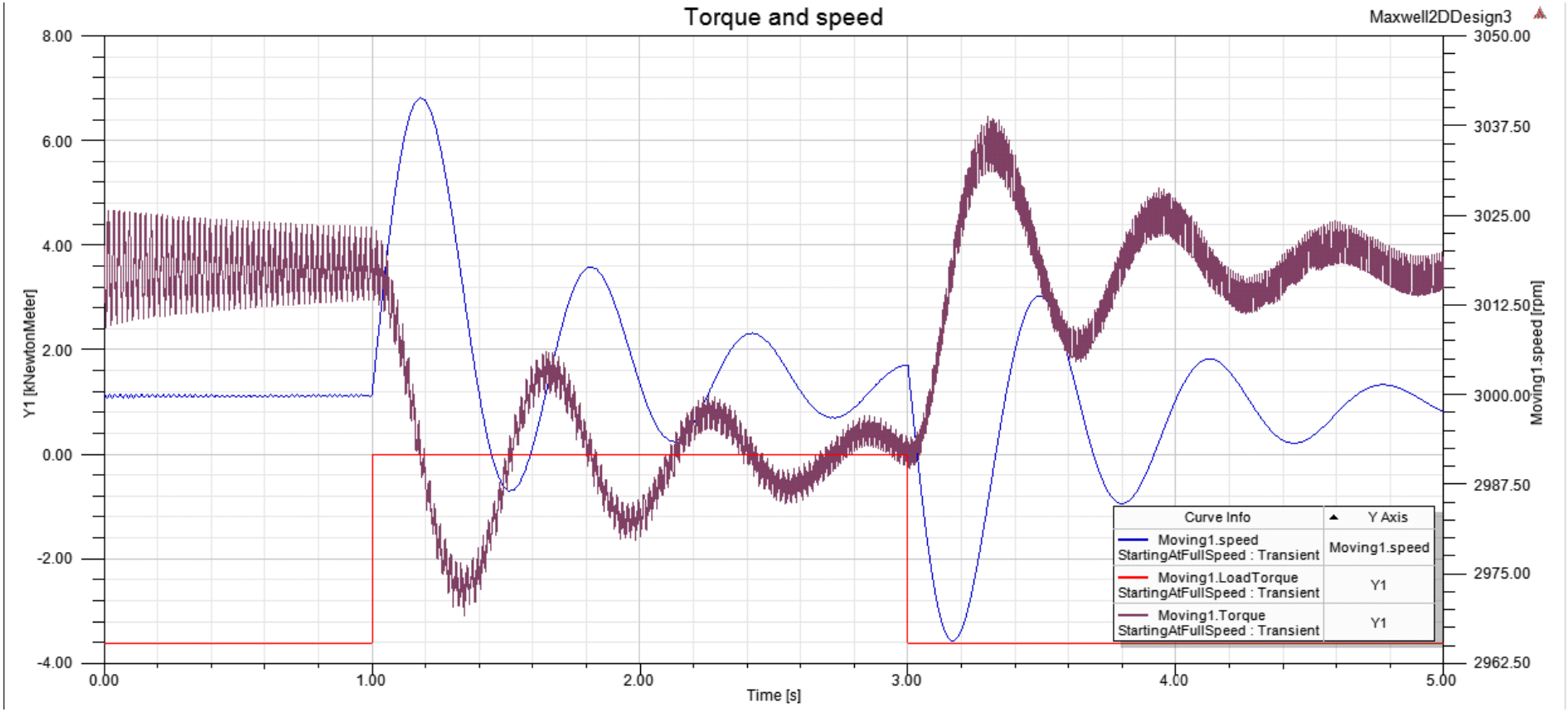

Figure 32: Case C: Rotational speed in blue, load torque in red and produced torque in purple. Loss of load gives an oscillation that is dampened to a low amplitude when load comes back. When the load comes back a new oscillation starts which is also dampened in due course.

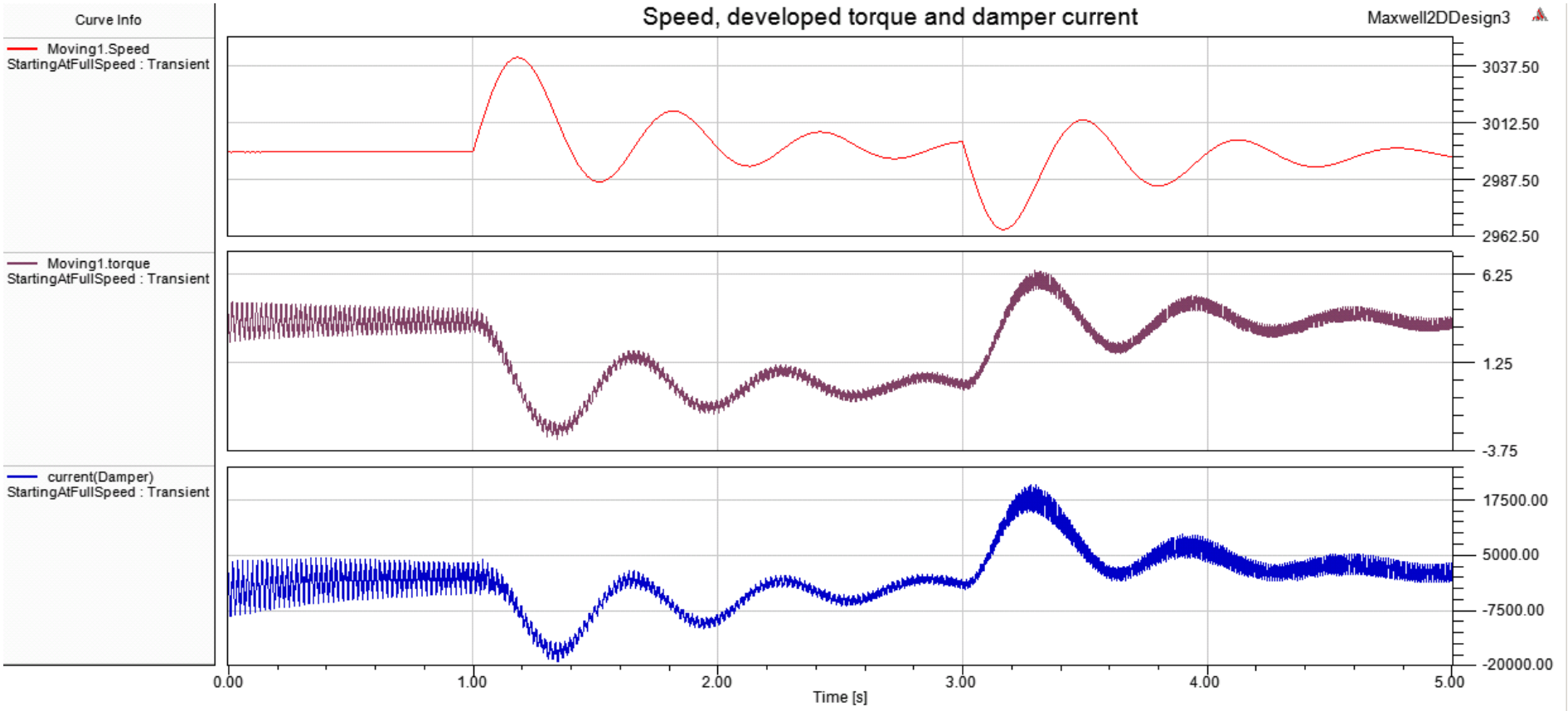

Figure 33: Case C: Rotational speed in red, developed torque in purple and the current in the damper winding in blue.

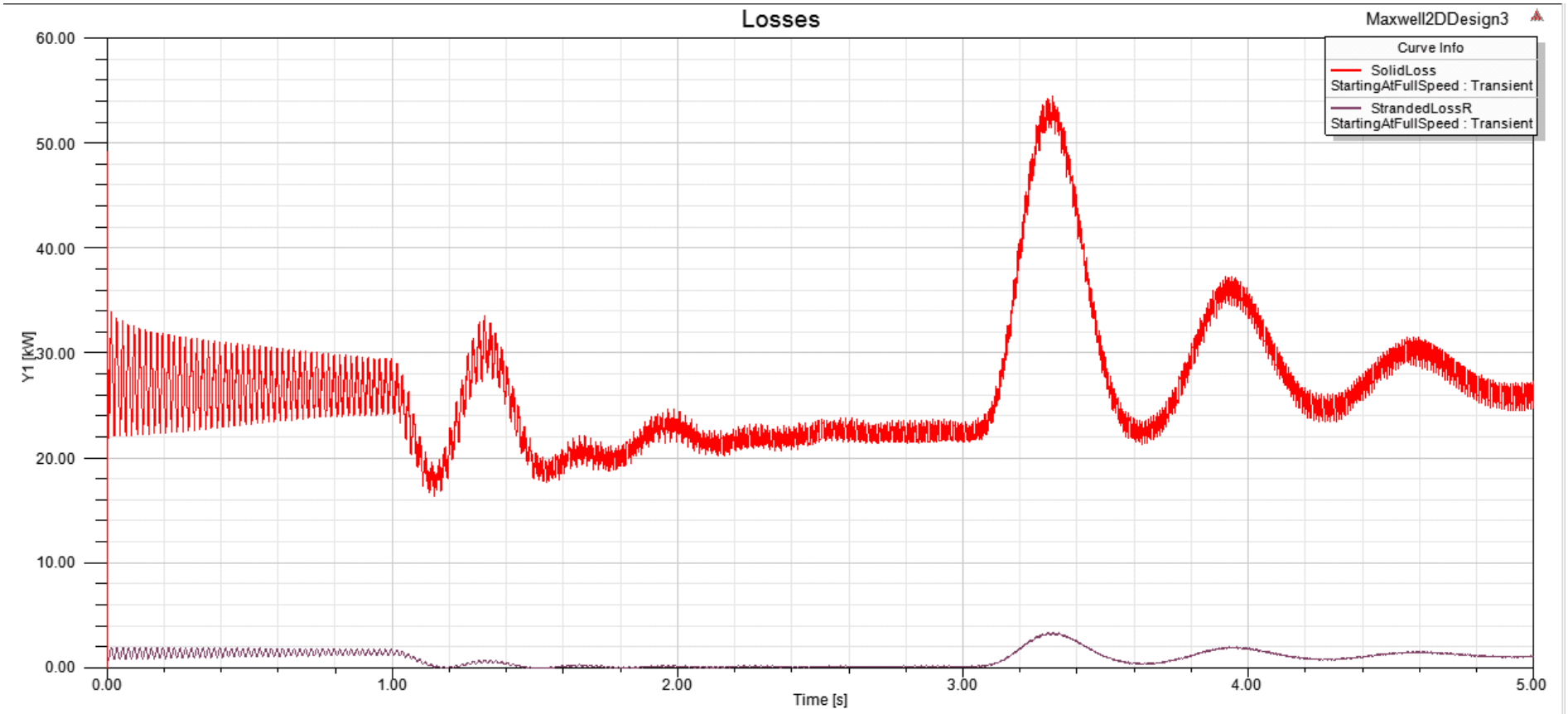

Figure 34: Case C: Losses in the machine. The red line shows the losses in the damper winding, the purple line shows the losses in the stator windings.

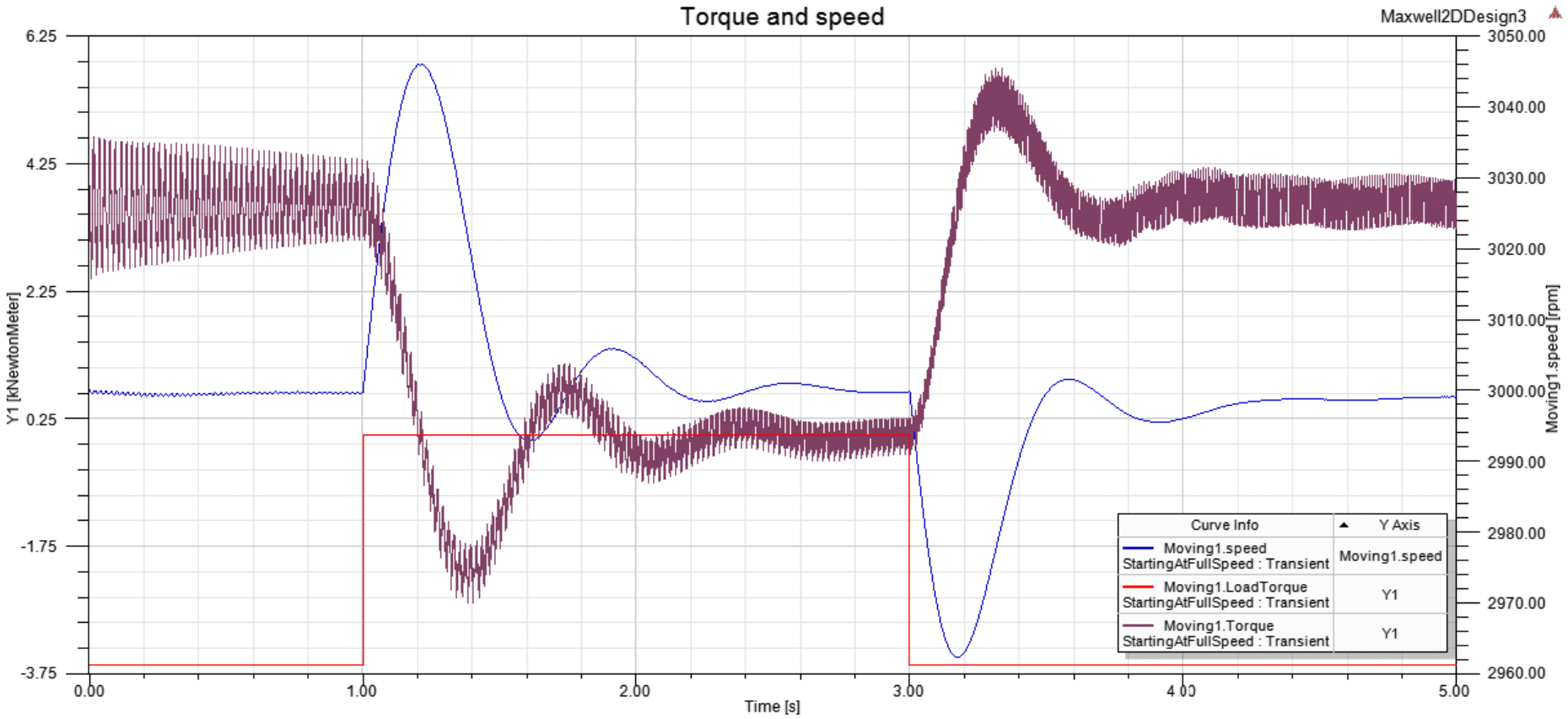

Figure 35: Case D: Rotational speed in blue, load torque in red and produced torque in purple. Loss of load gives an oscillation that dies out as the load comes back. When the load comes back, a new oscillation starts which is also very well dampened.

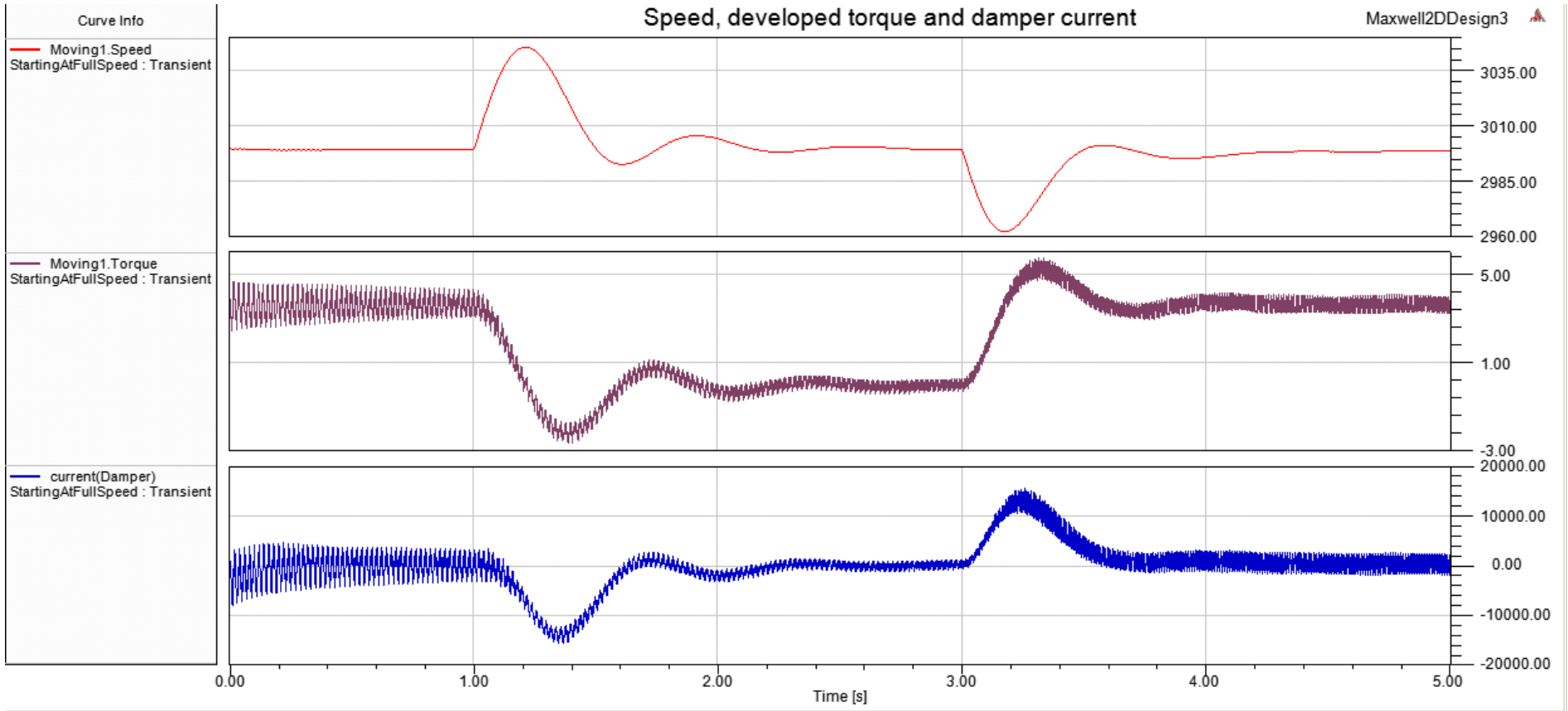

Figure 36: Case D: Rotational speed in red, developed torque in purple and the current in the damper winding in blue.

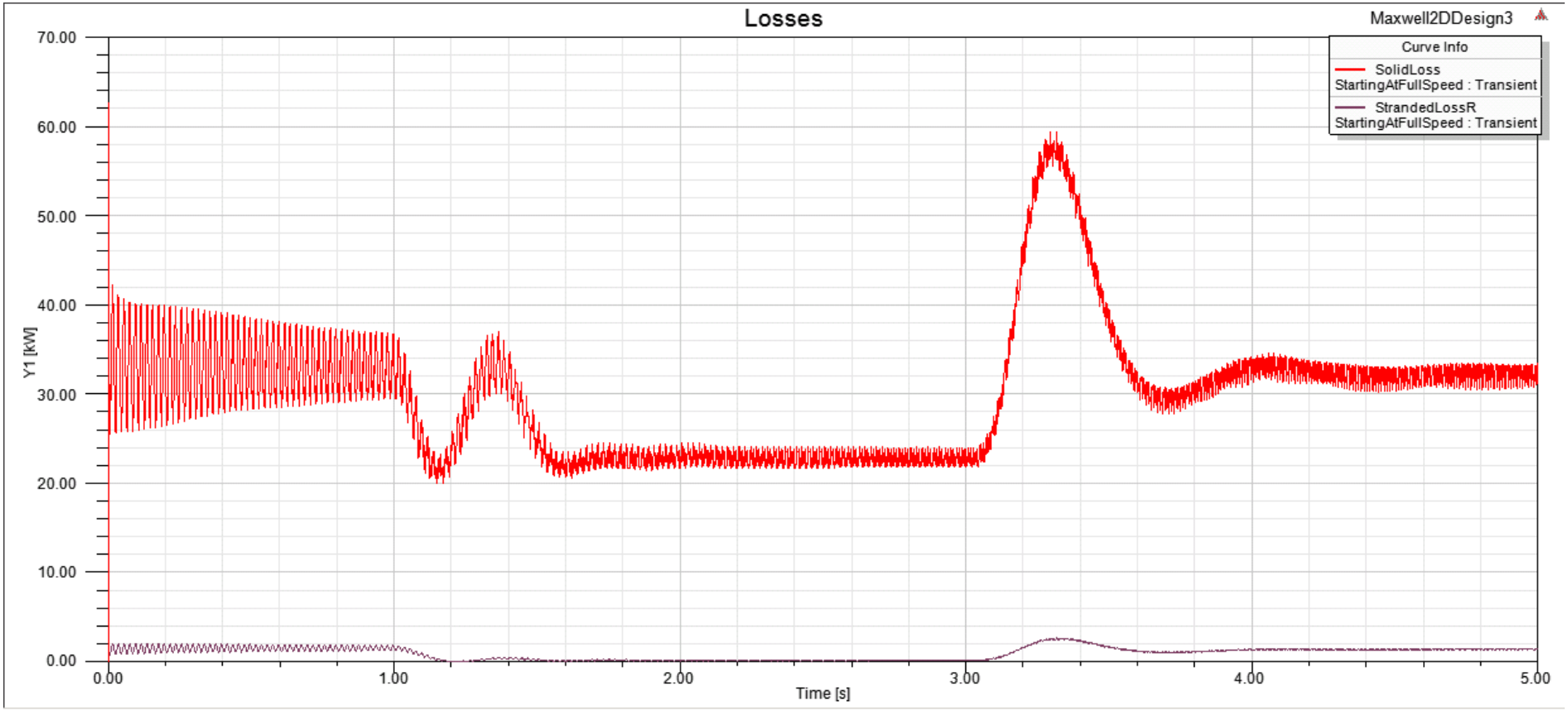

Figure 37: Case D: Losses in the machine. The red line shows the losses in the damper winding, the purple line shows the losses in the stator windings.

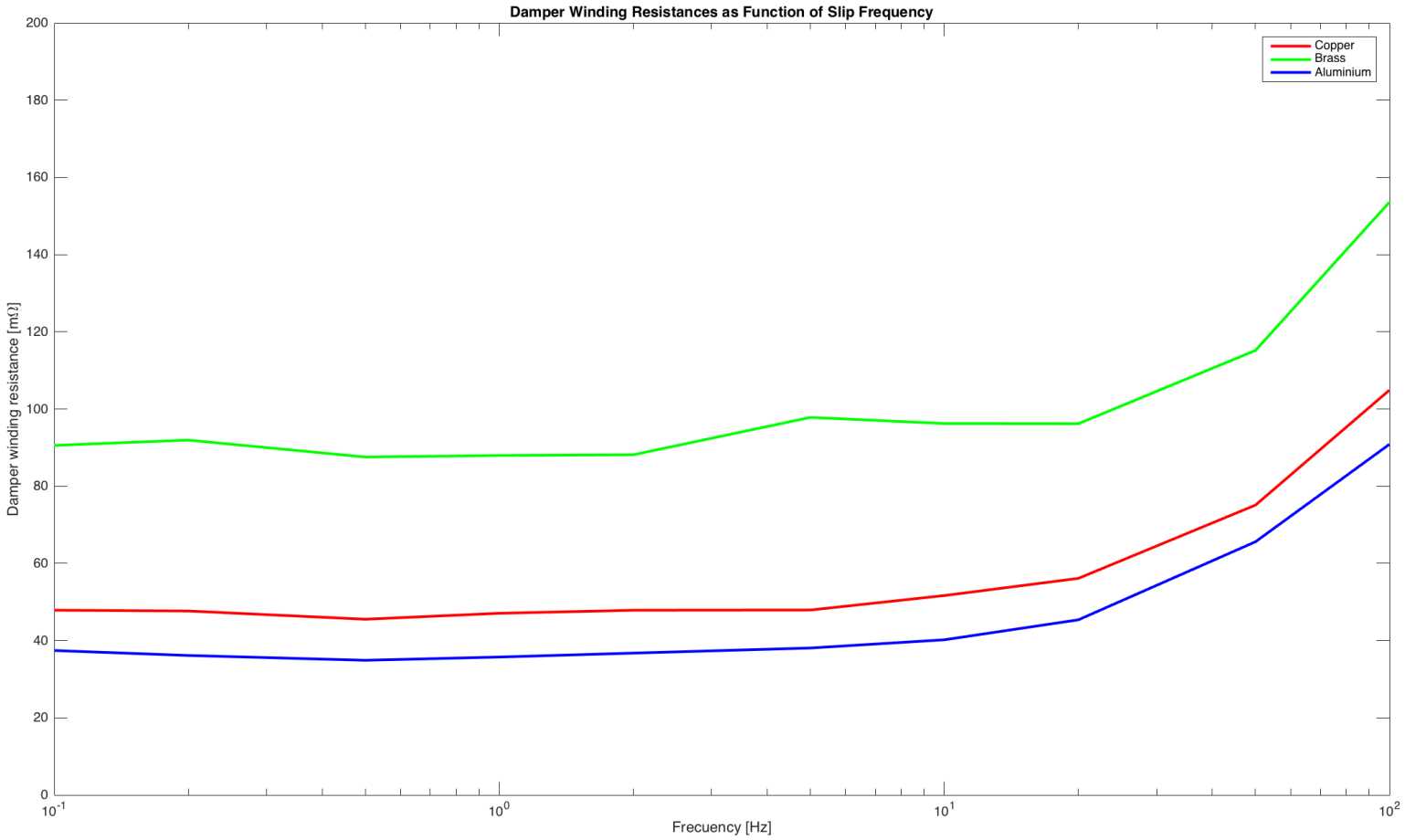

Figure 38: Damper winding resistances as function of slip frequency. Green line shows the parameter for brass, red shows reduced copper and blue shows aluminium. Note that the x-axis is logarithmic.

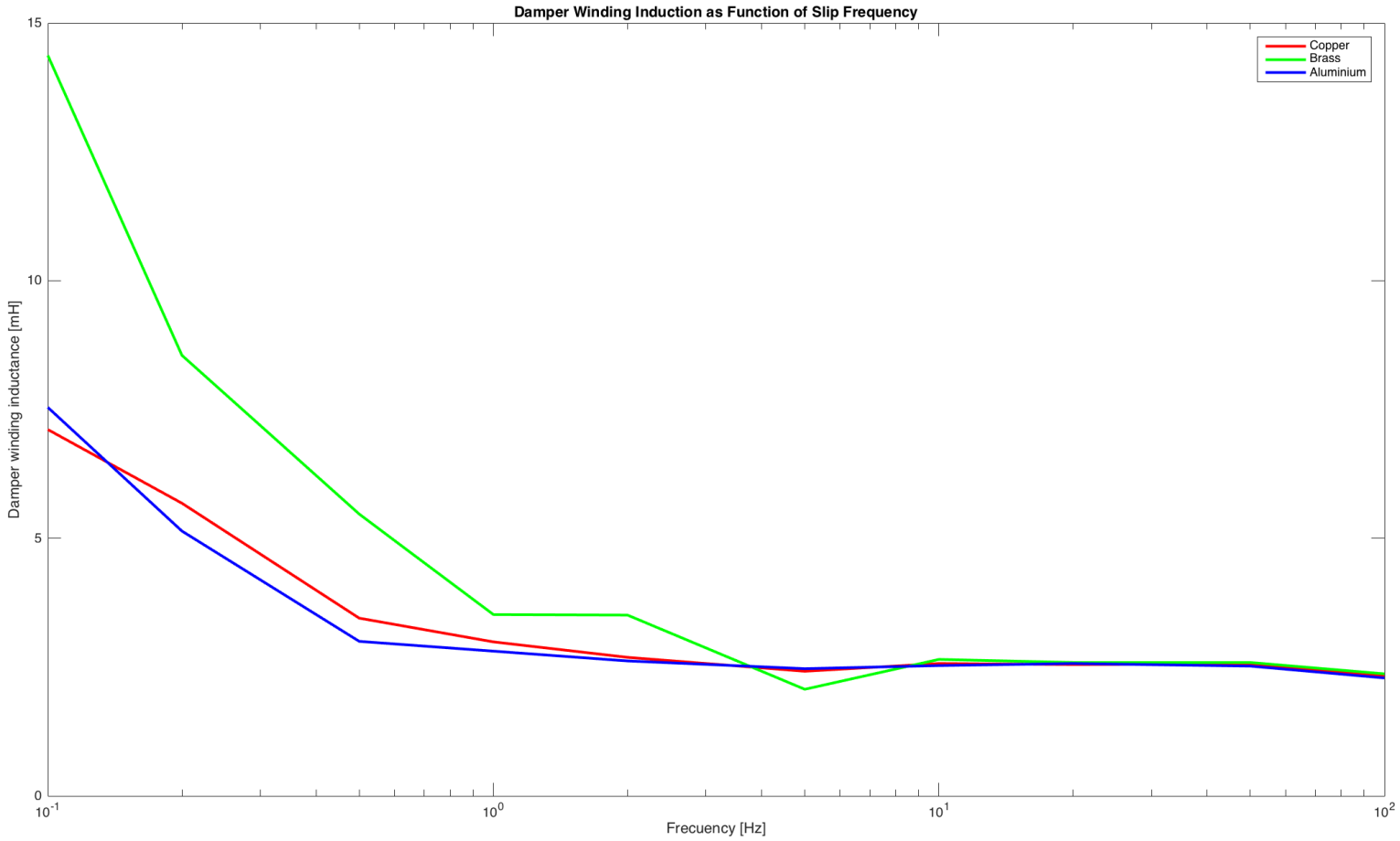

Figure 39: Damper winding inductances as function of slip frequency. Green line shows the parameter for brass, red shows reduced copper and blue shows aluminium. Note that the x-axis is logarithmic.

Appendix C; A brief study of the currents drawn by the machine

Fig. 1 and 2 show the phase current at full load, and its Fourier frequency spectrum respectively. We can see that the current, has some harmonic content,as it is not shaped as a perfect sinusoid. The FFT shows that the fundamental harmonic, at 50 Hz, has an amplitude of 287 A, while the third harmonic, at 150 Hz, has an amplitude of 44 A. The remaining harmonic components have very low amplitudes and can therefore be neglected.

Fig. 3 and 4 show the phase current at full load, and its Fourier frequency spectrum respectively. We can see that the current, has a significant harmonic content, is far from being shaped as a perfect sinusoid. The FFT shows that the fundamental harmonic, at 50 Hz, has an amplitude of 157 A, while the third harmonic, at 150 Hz, has an amplitude of 42 A. The remaining harmonic components have very low amplitudes and can therefore be neglected.

Fig. 5 and 6 show the phase current at full load, and its Fourier frequency spectrum respectively. We can see that the current, has a significant harmonic content, is very far from being shaped as a perfect sinusoid. The FFT shows that the fundamental harmonic, at 50 Hz, has an amplitude of 102 A, while the third harmonic, at 150 Hz, has an amplitude of 42 A. The remaining harmonic components have very low amplitudes and can therefore be neglected.

The fact that the third harmonic seems to be relatively constant as the load changes is an interesting observation. Sometimes harmonic contents can be attributed to magnetic saturation in the machine. Figures 7, 8 and 9 show flux density in the machine at the discussed loads. note the colourscale is from 0 to 1.2 T The machine is not saturated at full-load, but there is evidence to suggest that the machine is slightly saturated at half-load and no-load. The reason could be that, at no-load, the stator and rotor fields both contribute in the direct axis. At full-load, on the other hand, the stator field should only contribute in the quadrature axis. Superposition could therefore yield saturation in the case of half-load and no-load.

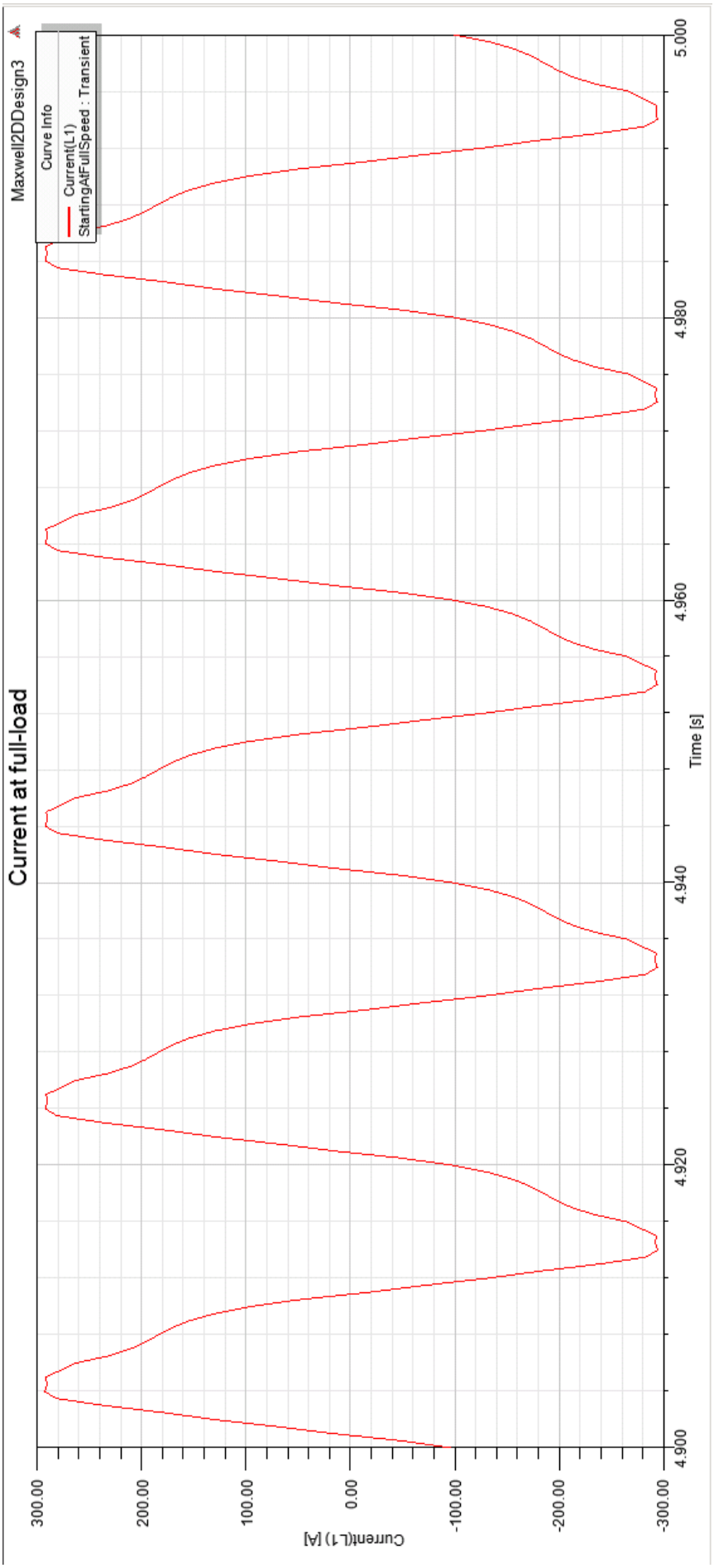

Figure 1: Phase current at full-load

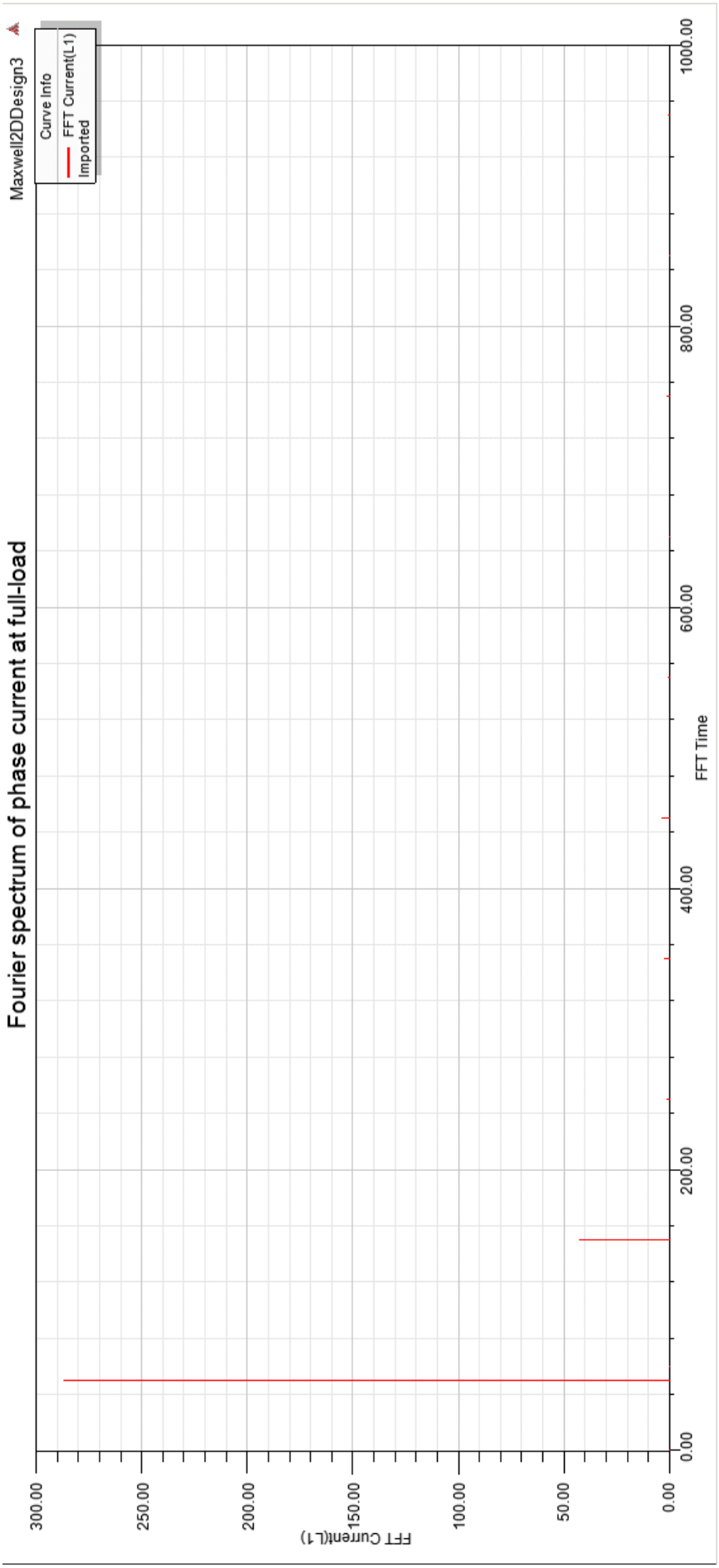

Figure 2: FFT of phase current at full-load

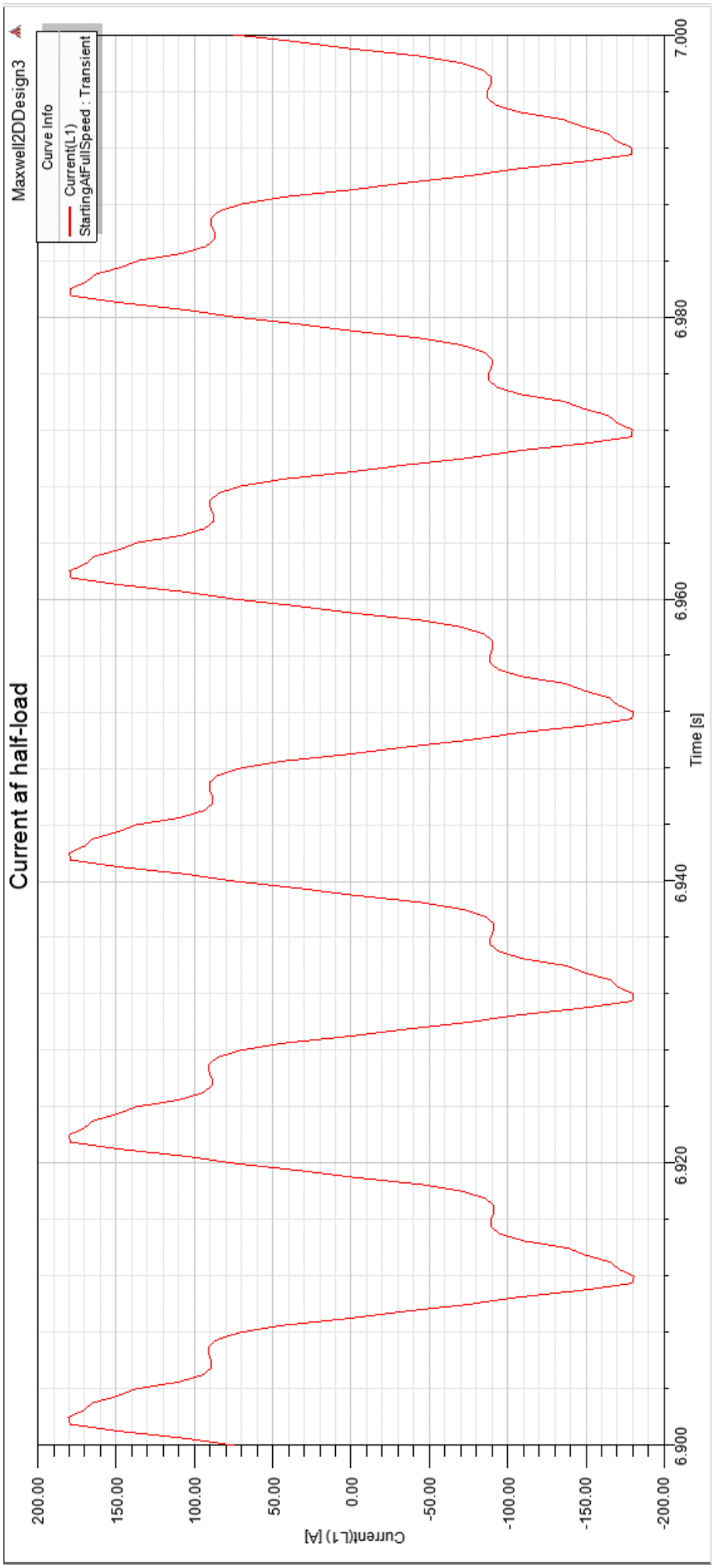

Figure 3: Phase current at half-load

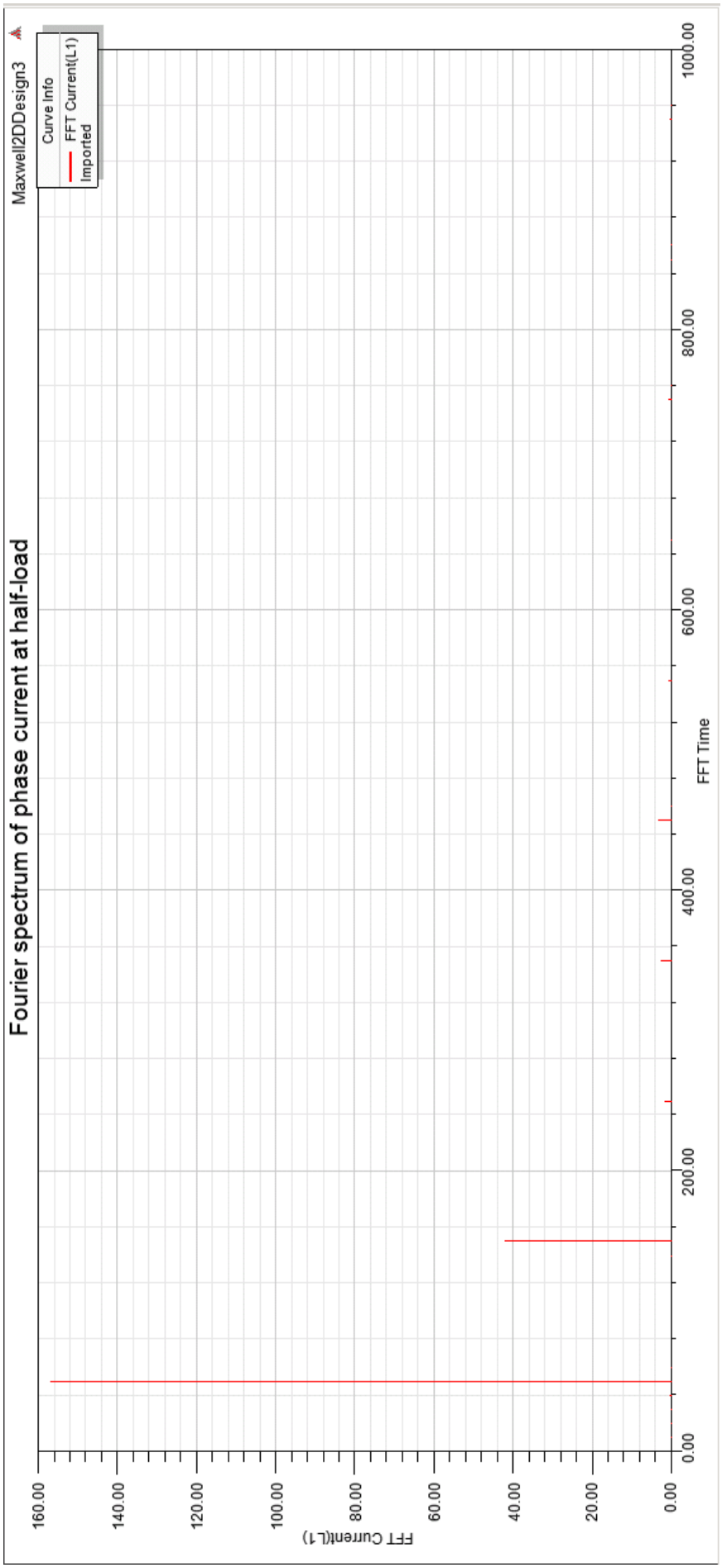

Figure 4: FFT of phase current at half-load

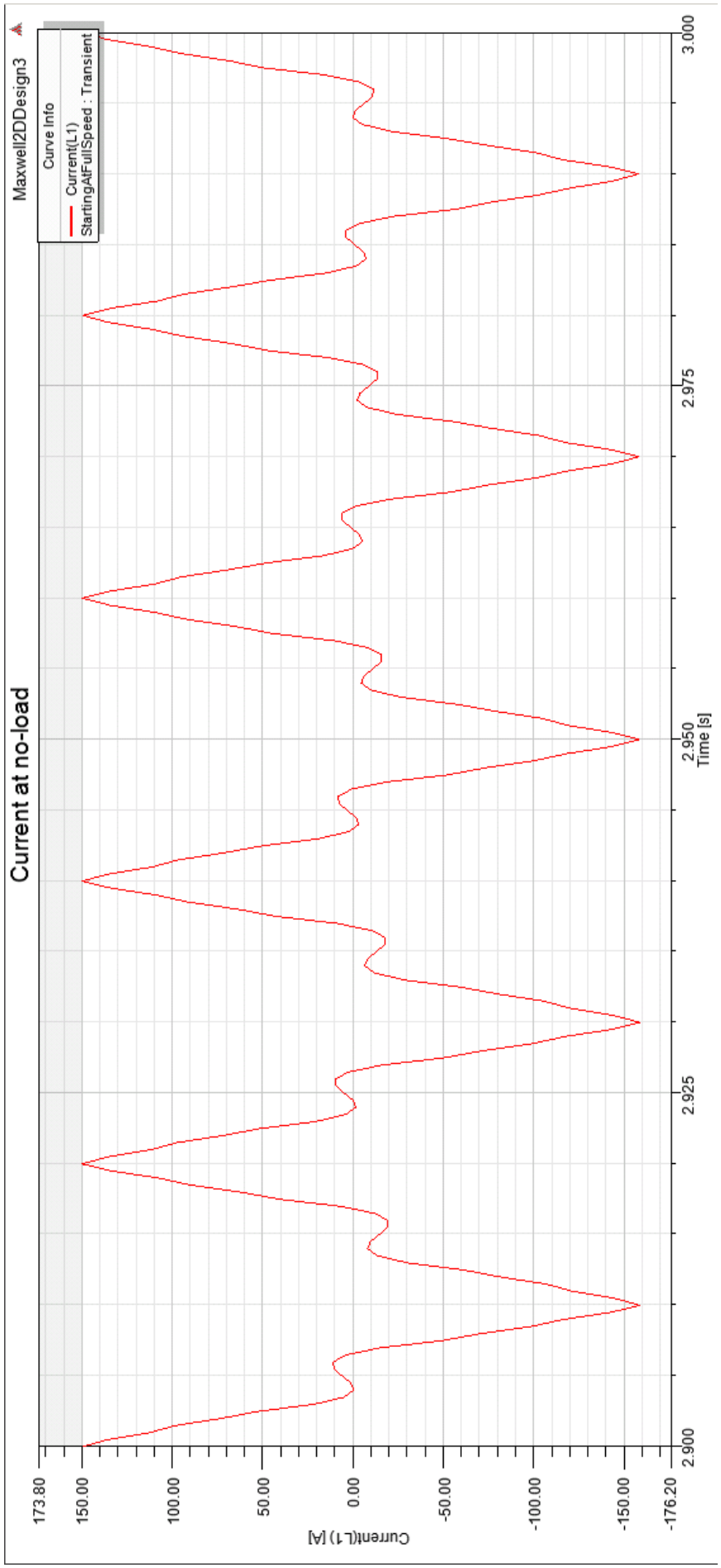

Figure 5: Phase current at no-load

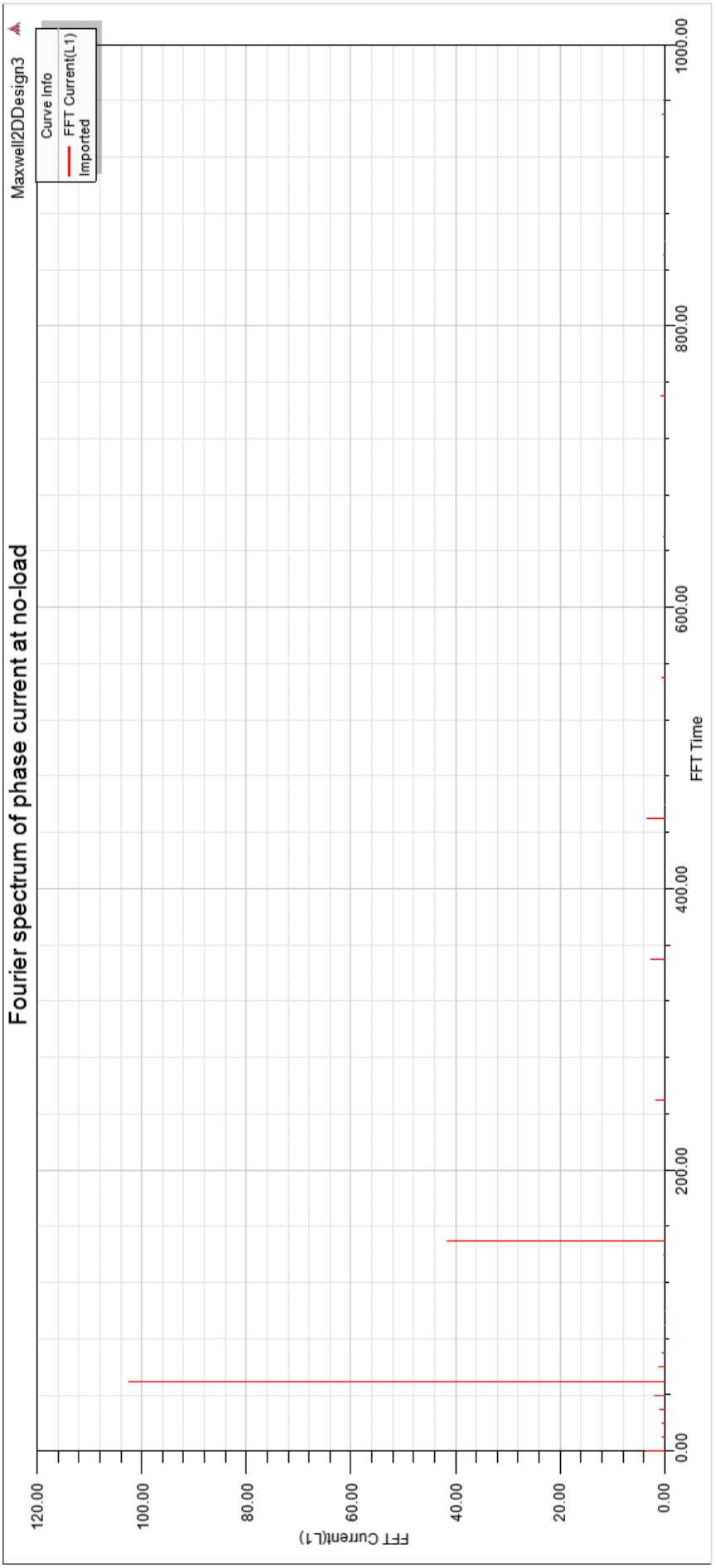

Figure 6: FFT of phase current at no-load

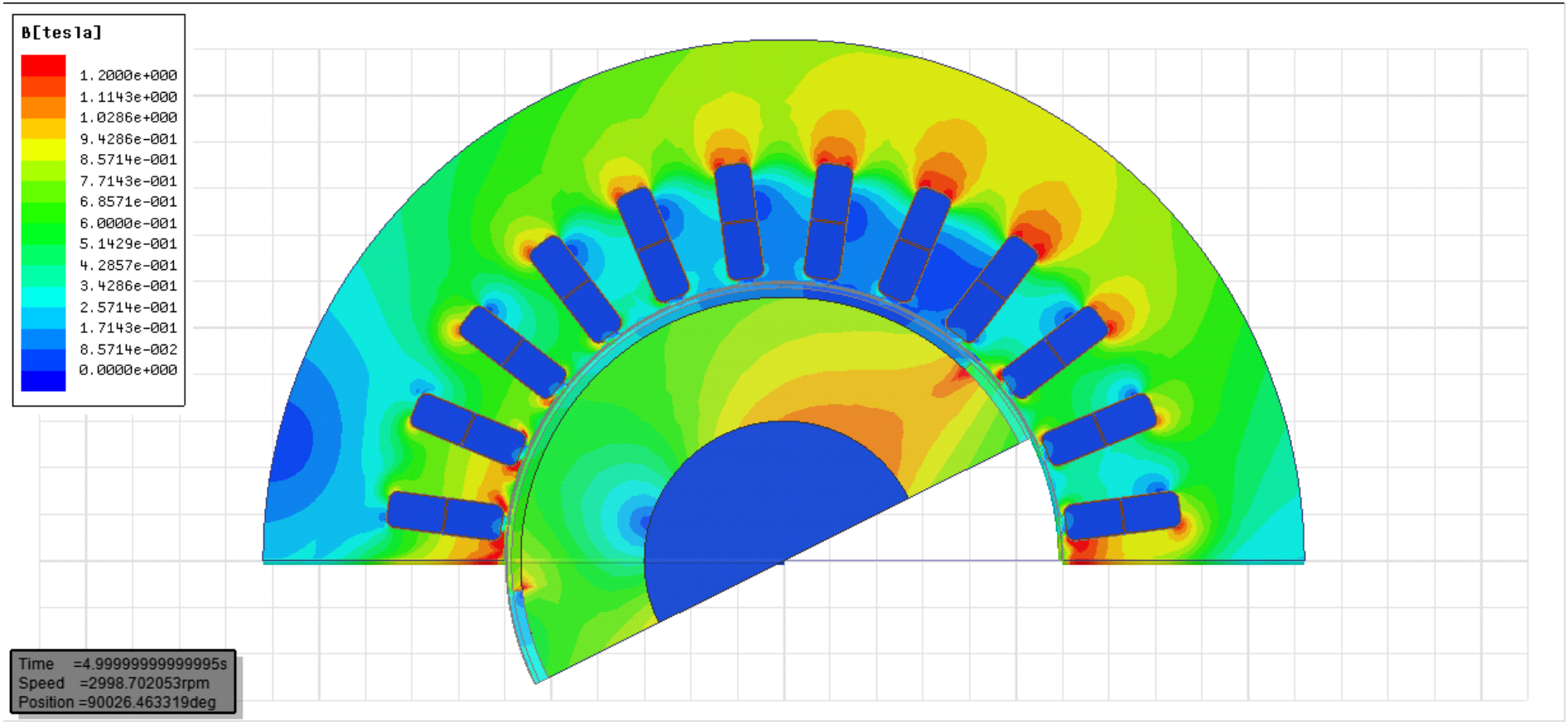

Figure 7: Flux density at full-load

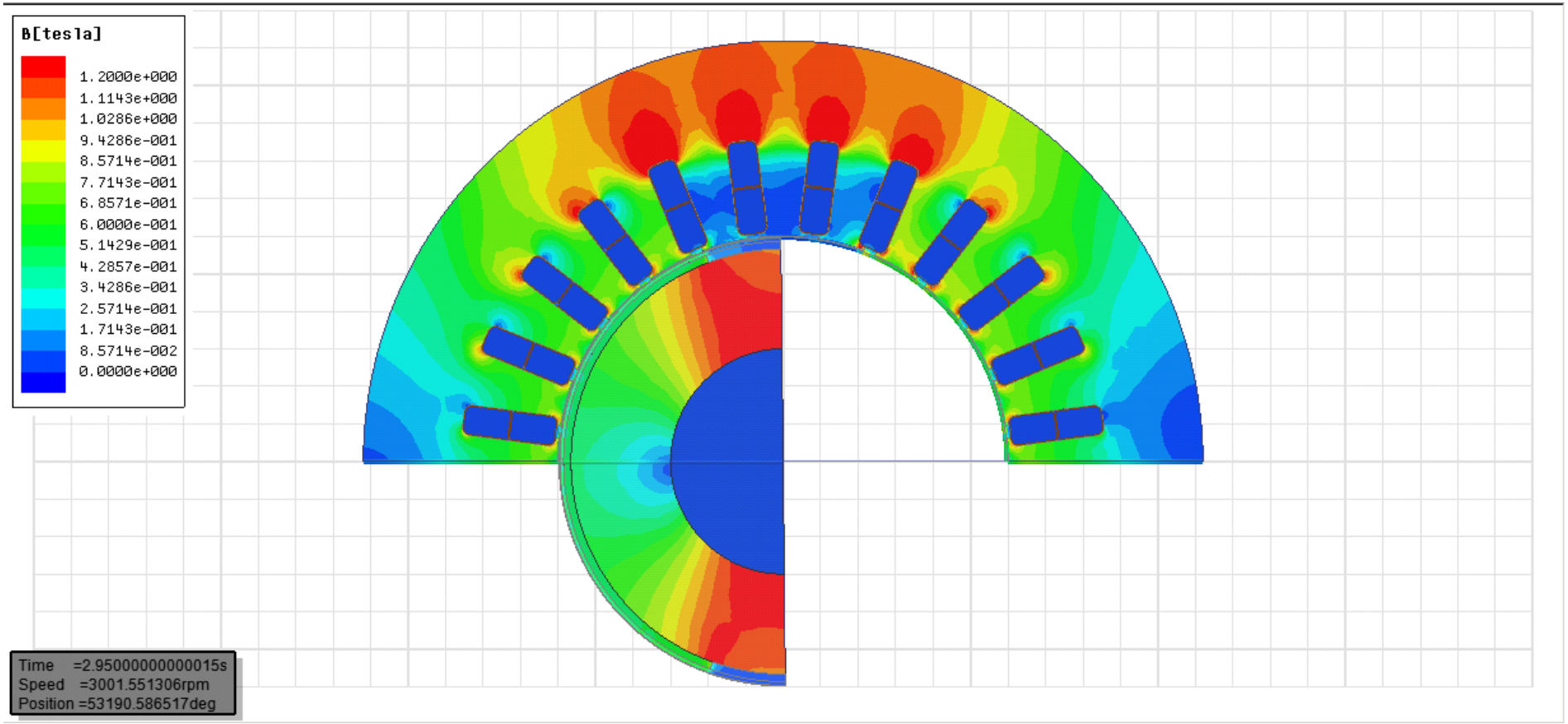

Figure 9: Flux density at no-load

Appendix D; A brief study of the currents in damper windings

Figures 1 to 8 show the current densities in the damper windings and permanent magnets for the saved time-step with the lowest and highest damper winding current. Note that all figures have the same colourscale, from $-5\frac{A}{mm^2}$ to $5\frac{A}{mm^2}$.

We can see that there is a pattern of current density being highest around the stator slots. This suggests that slot harmonics have quite a substantial impact on the induced currents in the. damper windings.

Figures are presented on the following pages.

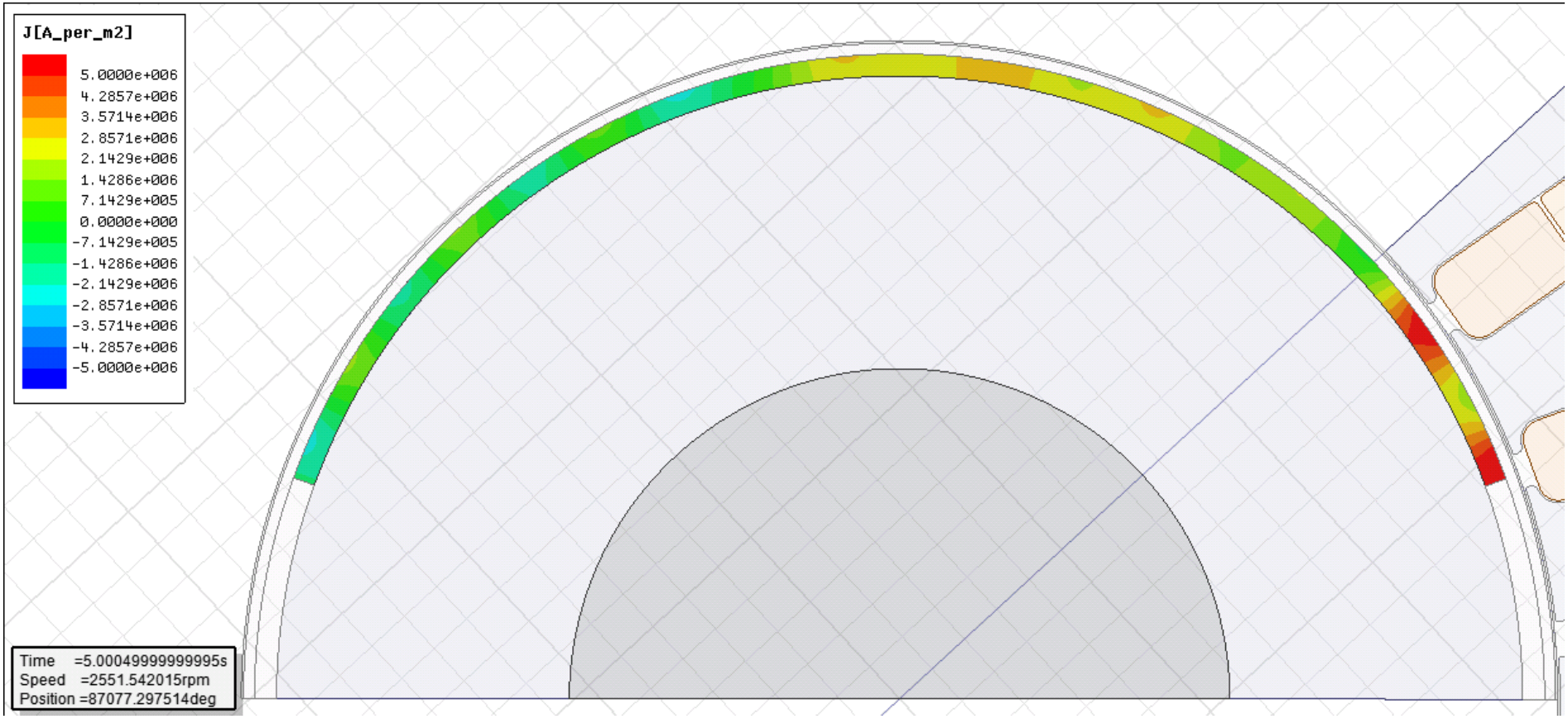

Figure 1: Case A: Max damper current with only PM.

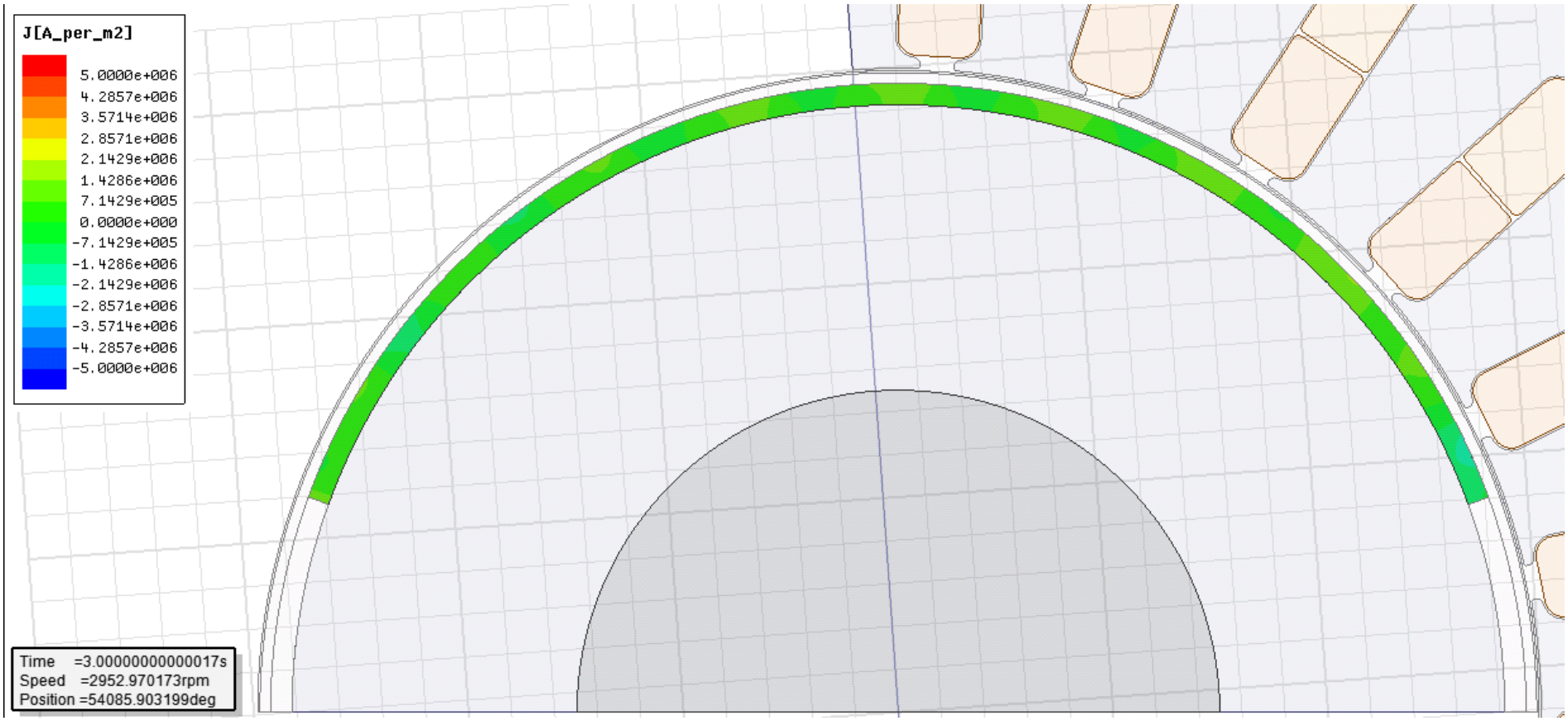

Figure 2: Case A: Minimum damper current with only PM.

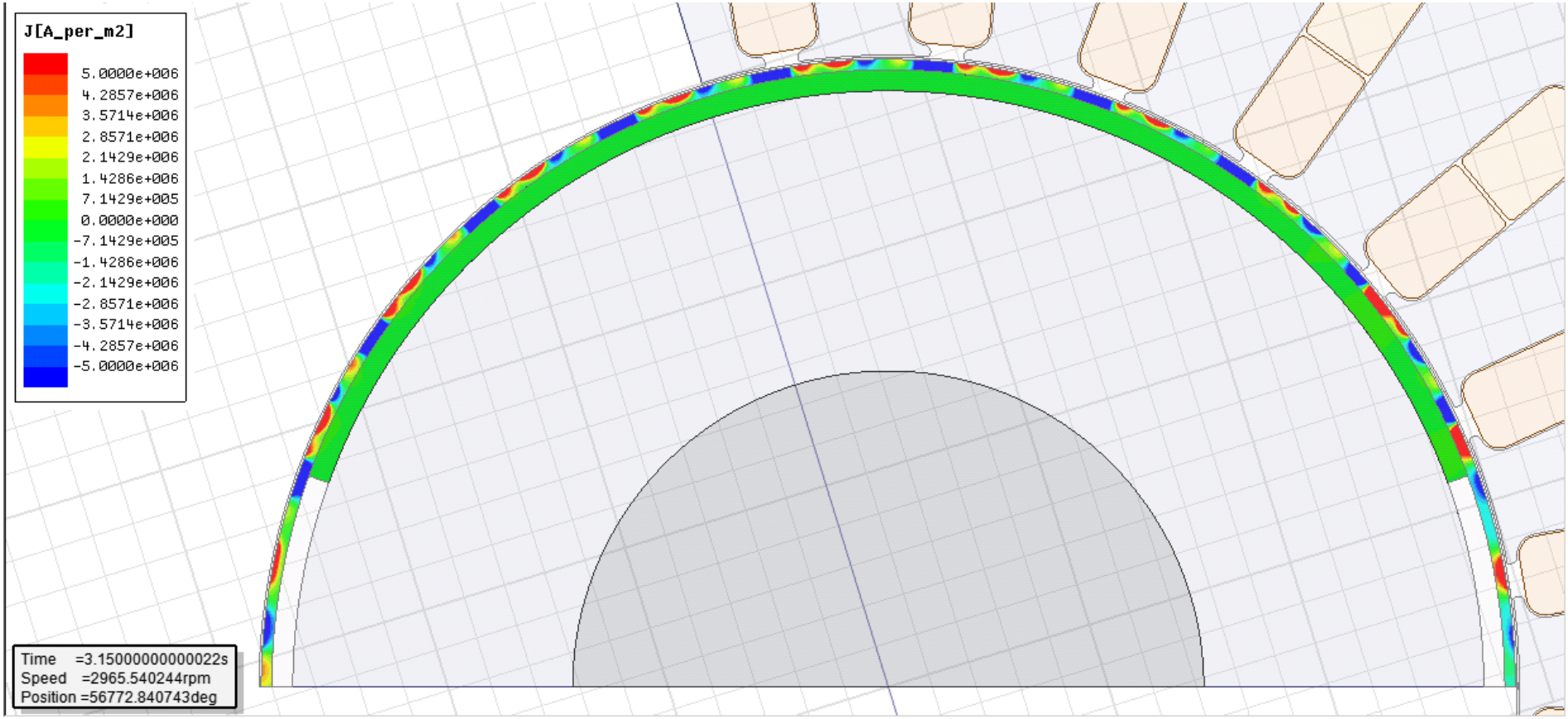

Figure 3: Case B: Max damper current with reduced copper damper winding

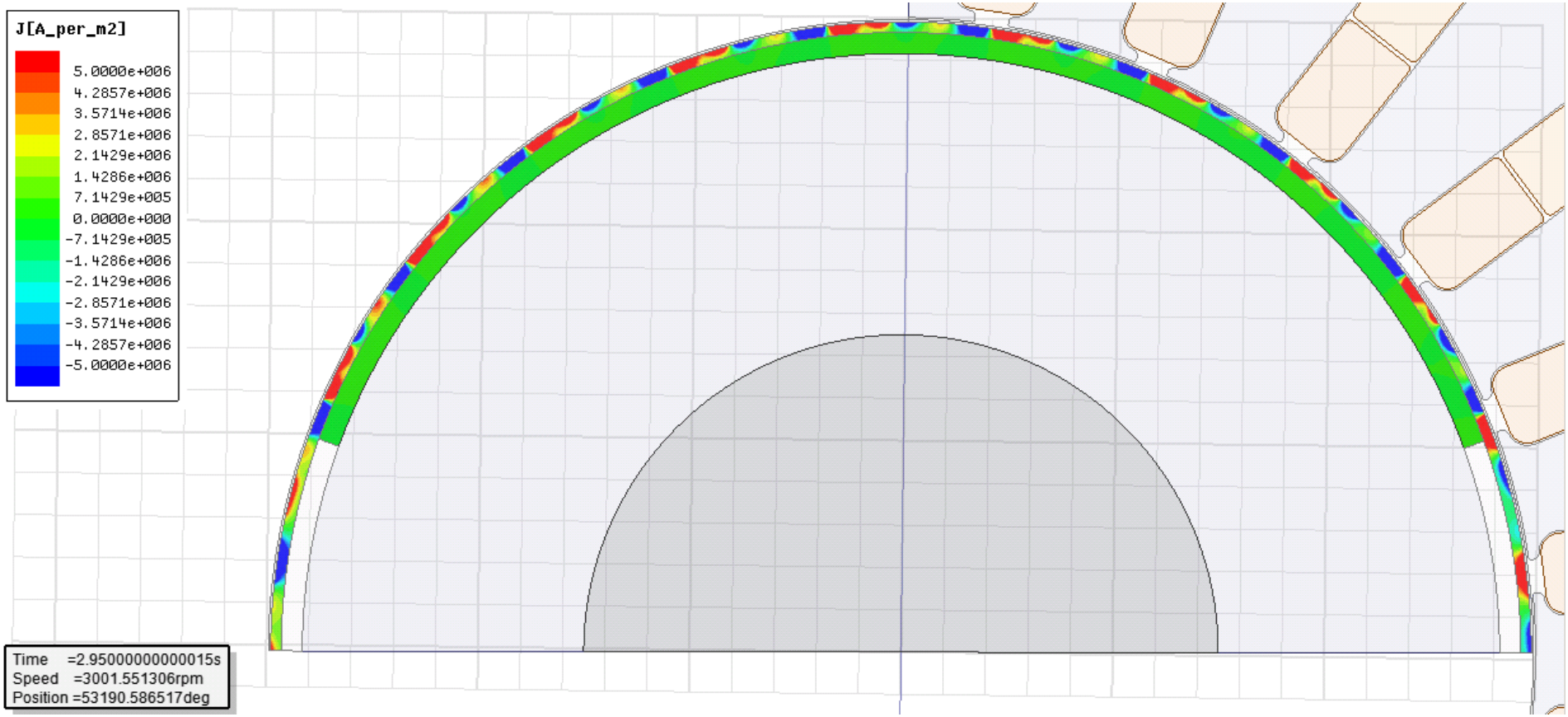

Figure 4: Case B: Minimum damper current with reduced copper damper winding

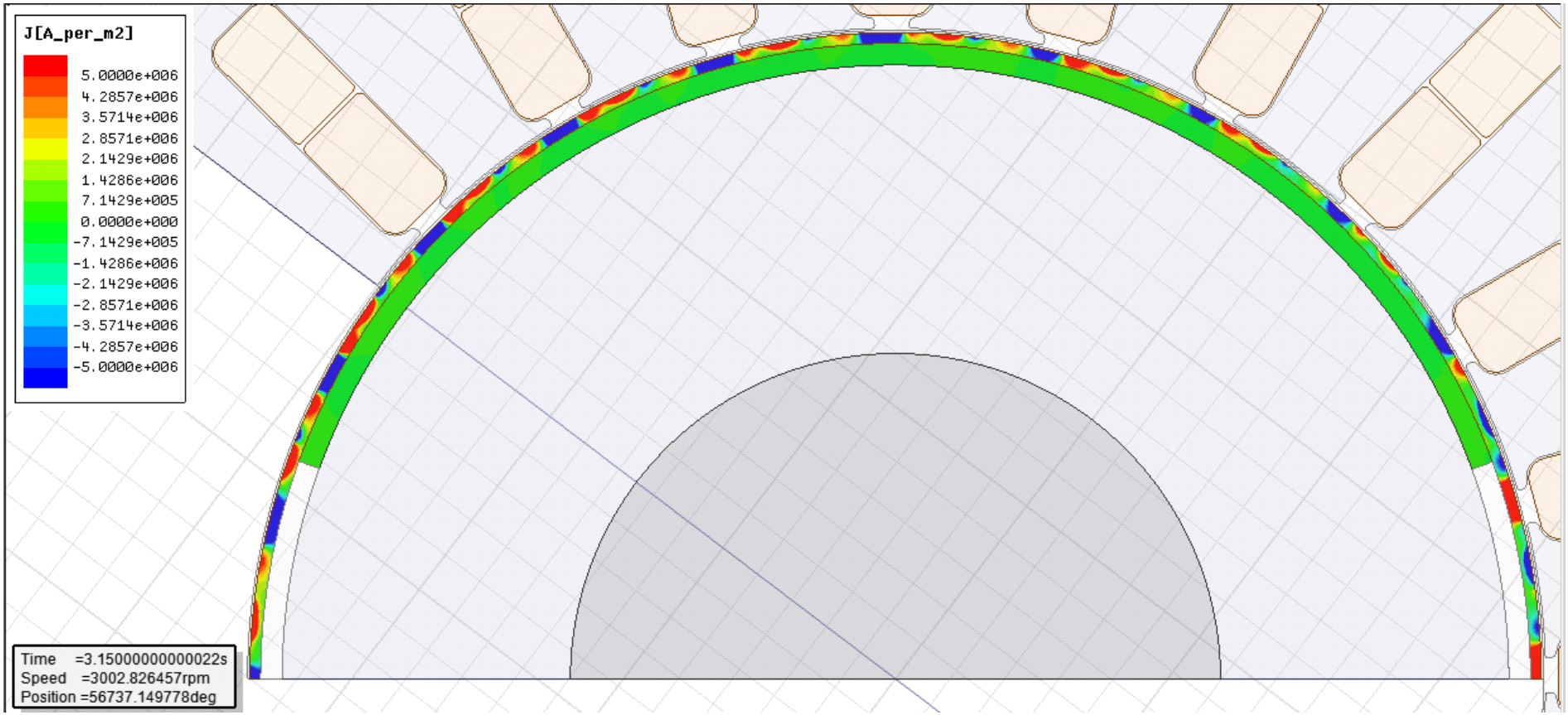

Figure 5: Case C: Max damper current with aluminium damper winding

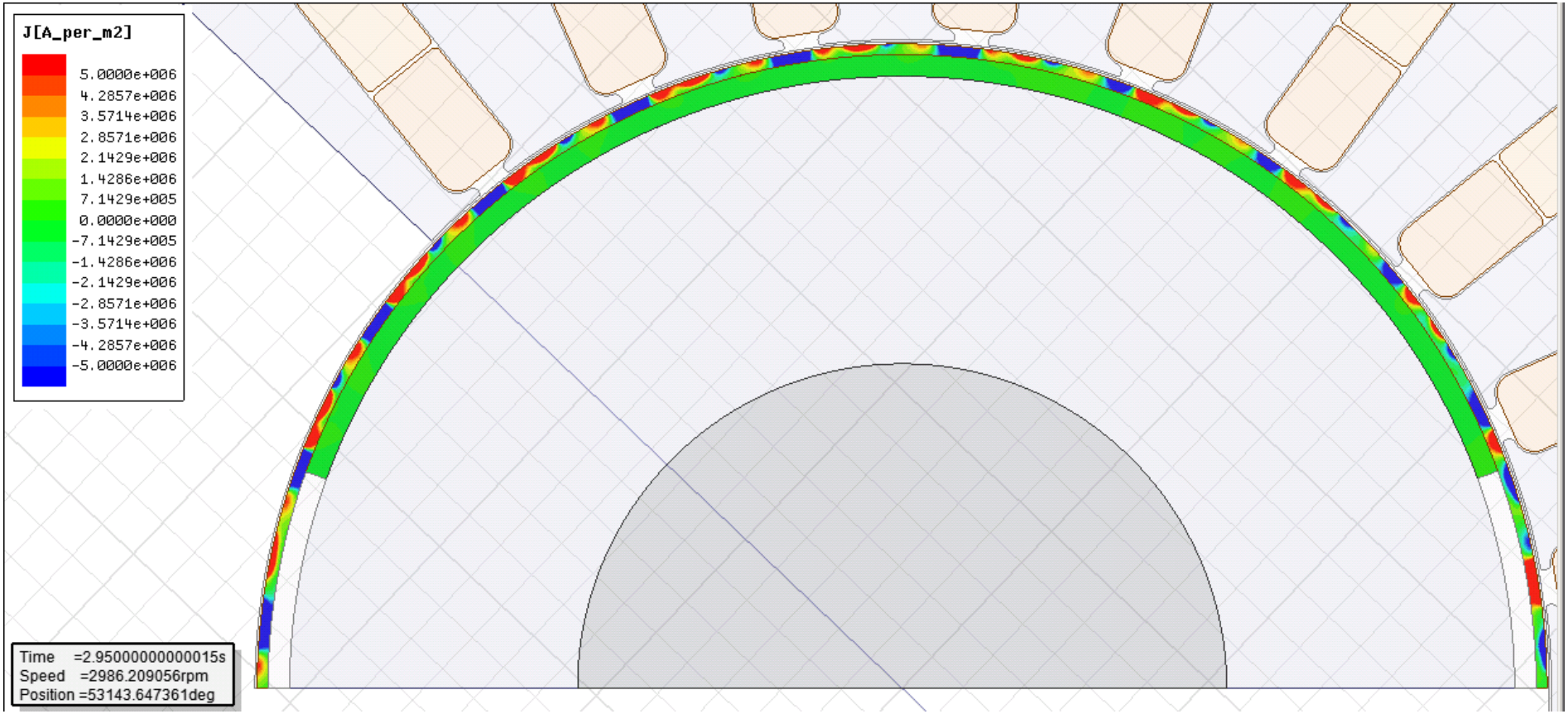

Figure 6: Case C: Minimum damper current with aluminium damper winding

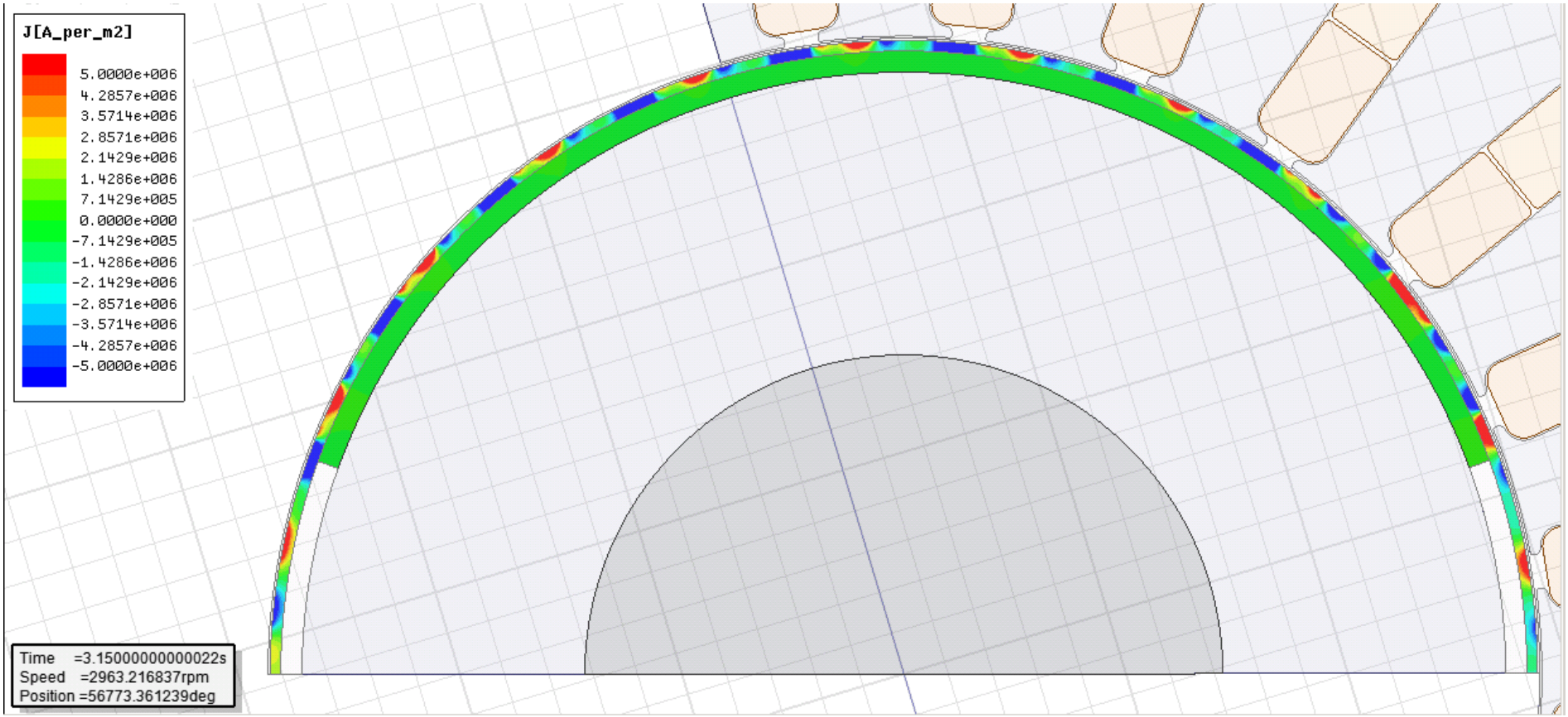

Figure 7: Case D: Max damper current with brass damper winding

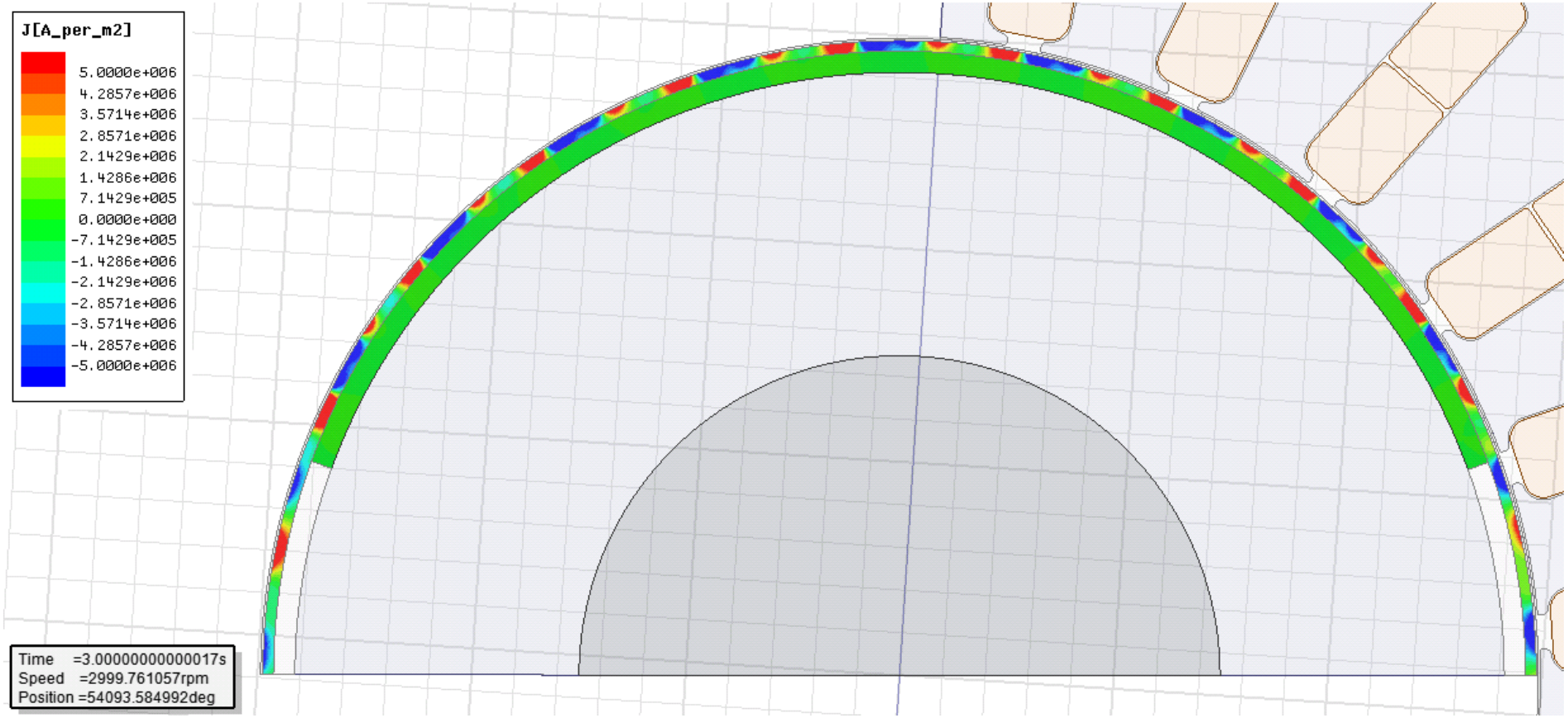

Figure 8: Case D: Minimum damper current with brass damper winding